An Investigation of Millerite (beta-NiS) Flotation Behaviour in Alkaline Solutions in Cu-Ni Sulphide Mineral Flotation Separation

by

Han Wang

A thesis submitted in partial fulfillment of the requirements for the degree of

Master of Science

in

Chemical Engineering

Department of Chemicals and Materials Engineering

University of Alberta

Abstract

In the Sudbury Basin nickel deposit, the presence of a less common nickel sulphide mineral – millerite (β-NiS) has a substantial impact on the Cu/Ni flotation separation efficiency. In this study, the flotation chemistry of millerite in alkaline solutions was investigated with pure minerals using potassium ethyl xanthate (KEX) as the collector. From the perspectives of surface and colloidal chemistry, the selective depression of millerite by natural polysaccharide in Cu-Ni sulphides flotation separation and the activation of millerite flotation by copper (II) ions were fundamentally studied.

Polysaccharides have been applied widely in the sulphide mineral flotation as depressants. In this study, the feasibility of using corn dextrin as a representative of polysaccharides to depress millerite in the differential Cu-Ni flotation at an alkaline environment was examined. Micro-flotation tests showed that adding corn dextrin after KEX can depress xanthate-treated millerite without deteriorating chalcopyrite ($CuFeS_2$) recovery, resulting in an efficient Cu/Ni flotation separation at both pH 9 and pH 12. The underlying interaction mechanism was investigated by static contact angle measurement, X-ray photoelectron spectroscopy (XPS) analysis, mineral dissolution and ethylenediaminetetraacetic acid (EDTA) extraction tests, atomic force microscopy (AFM) imaging, bulk adsorption tests, electrokinetic study and quartz crystal microbalance with dissipation (QCM-D). In the presence of xanthate, dextrin can lower the surface hydrophobicity of millerite but not chalcopyrite. Dextrin adsorption on millerite at alkaline pH was a chemisorption process, for which dextrin's hydroxyl functional group interacted with the nickel hydroxide on millerite surface. Dextrin adsorbed less on xanthate-treated millerite surface, indicating dextrin and xanthate adsorbed through different surface sites. As pH was increased, the nickel hydroxide passivation layer gradually inhibited

xanthate adsorption on millerite, which favoured dextrin adsorption. Comparing with chalcopyrite, dextrin displayed a higher affinity toward millerite accompanied with a higher free energy of adsorption. At pH 12, dextrin can adsorb on xanthate-treated millerite while negligible adsorption was observed on xanthate-treated chalcopyrite. The preferential adsorption of dextrin on millerite over chalcopyrite might be associated with the predominant passivation layer of nickel hydroxide on millerite surface at alkaline pH even in the presence of xanthate, while chalcopyrite was less prone to surface oxidation.

Furthermore, the effect of copper (II) ions on the millerite flotation was studied. Millerite flotation can be activated by conditioning with copper ions prior to KEX at both pH 9 and pH 12. The surface chemistry of millerite in the presence of Cu was studied by mineral dissolution and EDTA extraction tests as well as XPS analysis. At alkaline pH, the main copper species on millerite surface was Cu (I) sulphide with minor Cu (II) sulphide and Cu (II) oxide/hydroxide. The Cu (I) sulphide arose from the adsorption and reduction of Cu (II) species. In the meantime, sulphur oxidation was affected upon the reduction of Cu (II) to Cu (I). Monosulphide species (S^{2-}) at the surface was oxidized into disulphide species (S_2^{2-}), resulting in less sulphoxy species ($S_xO_y^{2-}$). There was no remarkable increase in nickel dissolution and growth in nickel hydroxide passivation layer upon the adsorption of Cu. In essence, copper ion activated millerite flotation under alkaline pH through affecting millerite surface oxidation.

Preface

A part of Chapter 4 has been submitted to Minerals Engineering for publication as Han Wang, Liyuan Feng, Rogerio Manica, Qingxia Liu, "Selective depression of millerite (β-NiS) by polysaccharides in alkaline solutions in Cu-Ni sulphides flotation separation." I was responsible for methodology, formal analysis, investigation, data curation, writing the original draft, reviewing and editing the manuscript, and data curation. Liyuan Feng is responsible for investigation, reviewing and editing the manuscript. Rogerio Manica is responsible for reviewing and editing the manuscript. Qingxia Liu is responsible for recourses, methodology, supervision, reviewing and editing the manuscript, and funding acquisition.

Acknowledgement

First of all, I would like to express my sincere gratitude and appreciation to my supervisor, Dr. Qingxia Liu, for giving me an opportunity to thrive with an exciting research project. Your guidance and support always motivate me to become a better researcher and help me to plan for my future career path throughout my M.Sc. program.

I would also like to thank all the members in my research group, especially my colleagues in the Nickel project. Special thanks to Ms. Liyuan Feng, Ms. Jean Han, Ms. Caroline da Costa Goncalves, Dr. Chao Qi, Dr. Rogerio Manica, Dr. Jing Liu and Mr. Evans Kwak, who have been constantly helping me with the experiment and giving me advice regarding my research, it was always a pleasure to work with you. I am also grateful to Ms. Laurie Kachmaryk for all the help with the paperwork.

I want to thank Dr. Yi Lu and Ms. Jie Ru for the equipment trainings, and I want to thank Dr. Shihong Xu and Dr. Nancy Zhang in Nanofab for helping me on the XPS analysis, XRF and XRD trainings. Thank you Dr. Mingli Cao, Mr. Darren Molinaro and Mr. Mark Labbe for all the help with my mineral samples. I also want to thank Ms. Ni Yang, Dr. Deepak Padasainee, Mr. Daniel Dixon, and Mr. Shiraz Merali for helping me analyzing the samples.

I also want to acknowledge the financial support from XPS – Expert Process Solutions, a Glencore company and National Sciences and Engineering Research Council of Canada (NSERC).

Finally, I want to thank my family and all my close friends for your care and support along the way.

Table of Contents

List of Figures

List of Tables

List of Symbols

C_e	Dextrin concentration at equilibrium ($mg\ L^{-1}$)
D, ΔD	Energy dissipation factor, shift in energy dissipation factor
f, Δf	Frequency, shift in frequency (Hz)
ΔG°_{abs}	Free energy of adsorption ($kJ\ mol^{-1}$)
K_a	Dimensionless thermodynamic equilibrium constant
K_f	Stability (formation) constant
K_F	Freundlich capacity factor ($mg^{1-\frac{1}{n}}\ L^{\frac{1}{n}}\ m^{-2}$)
K_L	Langmuir equilibrium constant ($L\ m^{-1}$)
K_{sp}	Solubility product constant
$\bar{M}_n$	Number average molecular weight ($g\ mol^{-1}$)
$\bar{M}_w$	Weight average molecular weight ($g\ mol^{-1}$)
n	Freundlich intensity parameter
pK_{sp}	The negative logarithm of solubility product constant K_{sp}
q_e	Amount of dextrin adsorbed ($mg\ m^{-2}$)
q_{max}	Saturation amount of dextrin adsorbed ($mg\ m^{-2}$)
R	Gas constant R = 8.314 ($J\ mol^{-1}\ K^{-1}$)
T	Absolute temperature (K)
θ	Contact angle (°)

List of Abbreviations

AFM	Atomic force microscopy
BET	Brunauer – Emmett – Teller
BSE	Back-scattered electron
Cp	Chalcopyrite
DRIFT	Diffuse reflectance infrared Fourier transform
EDS	Energy dispersive X-ray spectroscopy
EDTA	Ethylenediaminetetraacetic acid
FWHM	Full width at half maximum
GPC	Gel permeation chromatography
ICP-MS	Inductively coupled plasma mass spectroscopy
ICP-OES	Inductively coupled plasma optical emission spectroscopy
KEX	Potassium ethyl xanthate
Mi	Millerite
PDF	Powder diffraction file
PDI	Polydispersity index
QCM-D	Quartz crystal microbalance with dissipation
SEM	Scanning electron microscopy
SSA	Specific surface area
UV-Vis	Ultraviolet – visible
XPS	X-ray photoelectron spectroscopy
XRD	X-ray diffraction
XRF	X-ray fluorescence

Chapter 1 Introduction

1.1 Background and Problem Statement

The Sudbury Basin located in Ontario, Canada is the largest nickel deposit in North America. The main assemblages in the ore are chalcopyrite ($CuFeS_2$), pentlandite ($(Ni,Fe)_9S_8$) and pyrrhotite ($Fe_{(1-x)}S$, $0 < x \leq 0.125$), where sulphide minerals of significant economic interest are chalcopyrite and pentlandite that are used for copper and nickel metal production (Kerr, 2002; Qi, Liu, et al., 2019). In addition to pentlandite, *millerite* is also present in the Sudbury Basin as a less common type of nickel sulphide mineral. With a nickel content of 64.7% that is higher than other nickel-bearing minerals, millerite is an important resource for the production of nickel along with pentlandite (Haldar, 2017).

Nickel sulphide formed in ambient conditions, also known as millerite (β-NiS) has a rhombohedral lattice where Ni is in five-fold coordination with S (Rajamani & Prewitt, 1974; Shombe et al., 2020). The inversion between β-NiS and its high temperature polymorph α-NiS happens at a temperature of 397 ℃. Alpha-NiS has a hexagonal lattice and a niccolite (NiAs) type structure (Kullerud & Yund, 1962; Shombe et al., 2020; Sowa et al., 2010). Alpha-NiS is often obtained through synthesis and is widely used as a catalyst in the production of hydrogen by water splitting and manufacture of lithium/sodium ion batteries (Fan et al., 2016; Jiang et al., 2016). Recently, naturally formed α-NiS mineral crowningshieldite was found in diamond from the Letseng Mine, Lesotho (E. M. Smith et al., 2021).

Strathcona Mill, located in the north of the Sudbury Basin, processes ore from Nickel Rim South and Fraser Mines as well as a third-party custom feed (Glencore, n.d.; Kerr, 2002; Lotter et al., 2011). The simplified flotation circuit of the Strathcona Mill is shown in Figure 1.1. The feed ores are first ground with the addition of lime and xanthate, and the pulp pH is maintained around pH 9.2. The pulp is first fed into the primary nickel rougher, where Cu and Ni sulphide minerals are separated from gangue minerals such as pyrrhotite. Downstream of primary nickel rougher are secondary nickel rougher, scavengers and pyrrhotite rejection units, which are used to extract remaining valuable minerals. The bulk concentrate consisting of copper and nickel sulphide minerals goes into the Cu/Ni separation, producing a copper concentrate and a nickel concentrate, respectively. The copper – nickel separation is accomplished by

conditioning in a saturated lime environment around pH 12 and depressants is also added in order to depress nickel content in the Cu/Ni separation unit (Kerr, 2002; Qi, Liu, et al., 2019).

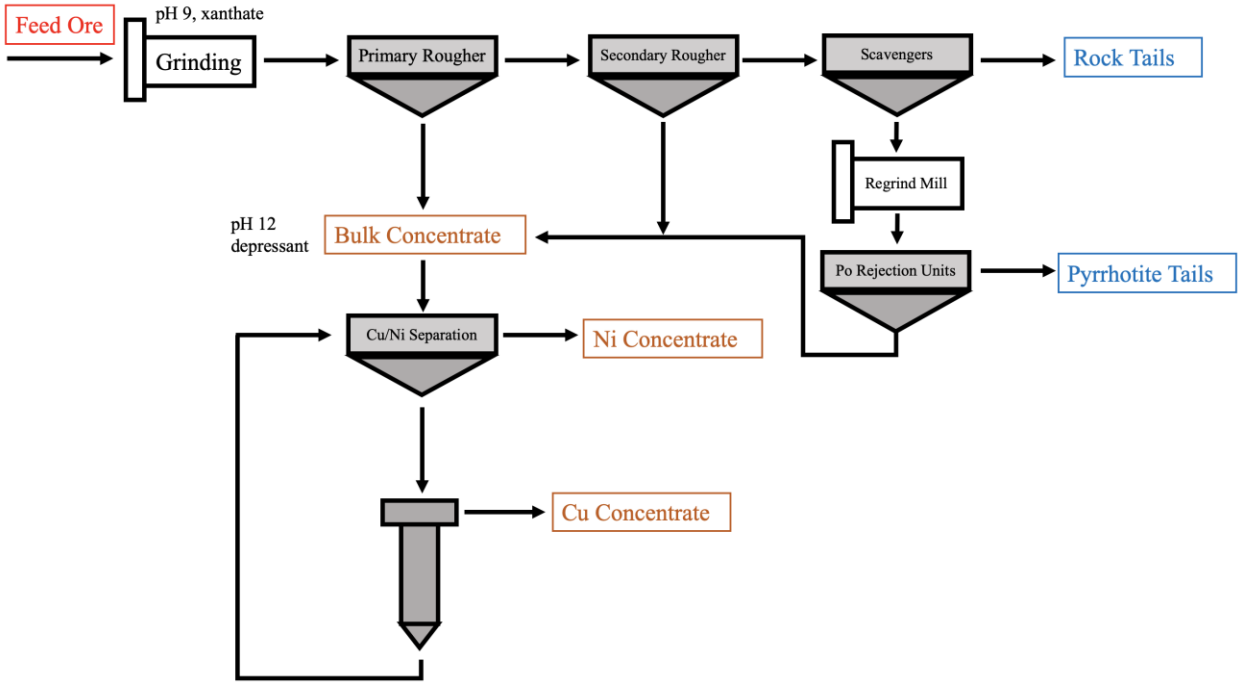

Figure 1.1 Simplified Strathcona Mill flotation circuit.

Millerite is much more abundant in copper – rich ore associated with Cu-bearing minerals such as chalcopyrite ($CuFeS_2$) and bornite (Cu_5FeS_4) (Bulatovic, 2007; Xu et al., 2011). Mineral liberation analysis (MLA) was carried out by Xu et al. (2011) for a specific Cu-rich ore samples with 3% Cu. It was discovered that portion of millerite reported to Cu concentrate was much higher than that of pentlandite when processing a Cu-rich ore. As millerite is more abundant in a copper – rich ore compared with a typical ore with only 1.4% Cu, it was found that approximately 70% of total Ni content in the copper concentrate came from millerite when processing Cu-rich ore while only 13% came from millerite for a typical ore. In the last decade, occasional high nickel contents in copper concentrate were observed. The nickel content in copper concentrate is required to be less than 0.5% or the economic value of copper concentrate would be reduced and causes penalty in the downstream smelting and refining operations (Zhao, 2019). Therefore, it was concluded that millerite is the major responsible species for the high nickel content in the copper concentrate. In order to maintain the economic value of both the

copper and nickel concentrates, a depression strategy for millerite needs to be developed to enhance Cu/Ni separation.

Due to the rarity of millerite in the Sudbury ore system, its flotation was seldomly investigated and not fully understood. Previous investigation on millerite flotation indicated that millerite is more floatable at pH 9 than pentlandite and cyanide is less efficient in depressing millerite, a higher dosage usually is required compared with pentlandite (L. K. Smith et al., 2011). In the past few decades, macromolecular polysaccharides such as starch, dextrin, guar gum, carboxymethyl cellulose and chitosan have been applied in sulphide mineral flotation as organic depressants at laboratory-scale studies, bench tests, pilot plants as well as industrial scale operations. Compared with inorganic depressants, polysaccharides have the advantages of being cost effective, bio-degradable and nontoxic. Preliminary laboratory flotation tests using Cu-rich ore carried out by Xu et al. (2011) showed promising results of using starch and dextrin to reduce the nickel content in copper concentrate; yet Cu-rich ore samples instead of pure millerite samples were used and the underlying mechanism was still not clear. It is vital to elucidate the depression mechanism of polysaccharide in order to achieve a better performance for the application in plant operations.

The existence of metal ions such as copper ions is inevitable in the plant process water. Copper ion was found capable of activating the flotation of pyrite (Ejtemaei & Nguyen, 2017b, 2017a; Leppinen, 1990; Leppinen et al., 1995; Voigt et al., 1994; Weisener & Gerson, 2000a, 2000b; Bo Yang et al., 2016), pyrrhotite (Allison & O'Connor, 2011; Gerson & Jasieniak, 2008; Nicol, 1984; Senior et al., 1994), and pentlandite (Malysiak et al., 2002). The plant surveys conducted at Strathcona Mill indicated the Ni content in Cu concentrate decreased from 0.60% to 0.51% if a pre-float circuit was introduced for feed ores with high Cu grade, where the tails combines with the rest of the feed ores to the primary nickel rougher. This suggested that presence of Cu might have an impact on Cu/Ni separation. To date, study on the effect of copper ions on millerite flotation have not been reported and copper ions activation on millerite's flotation is undesired. Hence, it is imperative to understand the role of copper ions in millerite flotation in order to obtain a better approach to reduce millerite's misreporting to copper concentrate.

1.2 Research Objectives

This study will examine millerite's flotation behaviour under alkaline environment in the presence of flotation reagents such as collector, depressant and activator with a special focus on copper-nickel separation. The research objectives are:

- To examine the feasibility of using natural polysaccharide such as dextrin to depress millerite at alkaline environment in Cu-Ni differential flotation with potassium ethyl xanthate (KEX) as the collector. Chalcopyrite will be used as the copper-containing sulphide mineral.
- To probe the underlying interaction mechanism for dextrin – mineral systems from perspectives of colloid and surface chemistry. The adsorption behaviour will be studied and the impact of dextrin adsorption on millerite surface wettability will be examined.
- To investigate the impact of copper ions on millerite's floatability at pH 9 and pH 12, the underlying activation mechanism will be studied from the perspective of millerite surface oxidation. The effect of dextrin on Cu-treated millerite will also be tested.

1.3 Thesis Structure and Organization

Chapter 1 provides a major scope of the thesis, including the background, motivations, and objectives of the study and the thesis structure and organization.

Chapter 2 is the literature review on sulphide mineral flotation, copper ion activation and application of polysaccharide in sulphide mineral flotation.

Chapter 3 discusses the experimental methodology in detail including mineral samples preparation, chemicals, reagents, and major techniques used in this study.

Chapter 4 examines the feasibility of using dextrin to enhance selectivity in millerite – chalcopyrite flotation. The adsorption behaviour of dextrin and the underlying interaction mechanism between mineral and dextrin from the perspectives of colloidal and surface chemistry are investigated.

Chapter 5 studies the effect of copper ions on the millerite's flotation at pH 9 and pH 12. The surface oxidation of millerite upon the addition of copper is probed.

Chapter 6 concludes the study with major findings related to research objectives, and suggestions on future work are discussed.

Chapter 2 Literature Review

2.1 Froth Flotation of Sulphide Minerals

Froth flotation is the most fundamental physical separation process utilized in mineral processing industry to obtain valuable minerals with economic interests. Mineral particles can be separated based on the difference in surface hydrophobicity. Minerals with a hydrophobic surface are able to attach to air bubbles and be recovered as concentrate, while hydrophilic minerals will be left in the tailings (Wills & Finch, 2016). In order to achieve an efficient recovery of valuable minerals, minerals' surface properties can be altered after the adsorption of highly hydrophobic surfactants known as collectors so that it is easier for the mineral particles to attach to the air bubbles. Collector is a kind of flotation reagent that has a polar ionizable group that can adsorb onto the mineral surface with a hydrocarbon tail facing outward which can alter mineral surface hydrophobicity (Wills & Finch, 2016). For sulfide minerals, typical collectors that are widely used are anionic, sulfhydryl type, among which the most common used one is called alkyl dithiocarbonate – "xanthate" (Avotins et al., 1994). In addition to collectors, flotation regulators are also employed to intervene xanthate adsorption on minerals in order to control the floatability of minerals to achieve efficient separations. The most important regulators are pH modifiers, activators and depressants (Bulatovic, 2007). As collector adsorption is usually dependent on the pulp pH for sulphide mineral, pH modifiers such as acid and alkaline are used to modify the pulp pH so that collector adsorption can be controlled. Activators such as copper ions are used to modify mineral surface to promote collector adsorption, flotation recovery is then increased as a result. Depressants are used to render surface more hydrophilic so that floatability can be decreased. Depressants used in sulphide mineral flotation usually function in the following ways:

(1) Depressants can react with mineral surface directly, alter the surface property and inhibit collector adsorption. For sulphide minerals, depressants can affect the mineral surface electrochemically to prevent xanthate adsorption and xanthate oxidation.
(2) Depressants can remove the adsorbed collector from the mineral surface, thus render the mineral surface less hydrophobic.
(3) With collector adsorbed, depressants can still adsorb on mineral surface to form hydrophilic patches, resulting in less floatability.

Inorganic depressants usually function through mechanisms described in (1) and (2) above, while organic depressants usually function through the mechanism depicted in (3) above, which will be further discussed in detail in Section 2.3.

2.1.1 Flotation Separation of Chalcopyrite and Pentlandite

The common plant practice for processing Cu-Ni ores usually involves rejection of gangue mineral and pyrrhotite ($Fe_{(1-x)}S$) in the rougher stage first to yield bulk concentrate of Cu and Ni sulphides. Usually, copper sulphides float well at this stage and the Cu recovery exceeds 90%. Then the bulk concentrate goes through Cu-Ni separation to yield Cu concentrate and Ni concentrate. For Cu-Ni separation, pentlandite usually is depressed while chalcopyrite is floated (Bulatovic, 2007; Kerr, 2002). Chalcopyrite's collectorless floatability have been extensively studied, a metal-deficient sulphur-rich surface due to metal ion dissociation is responsible for the surface hydrophobicity (Chander, 1991; Fairthorne et al., 1997; Gardner & Woods, 1979; Luttrell & Yoon, 1984). Upon the addition of ethyl xanthate, it was discovered that xanthate was first chemisorbed through sulfur in the xanthate and copper ion on the mineral surface to form copper (I) ethyl xanthate complex with a few monolayers. Subsequently, dixanthogen was formed with the copper (I) xanthate already adsorbed on the surface (Kalegowda et al., 2015; Leppinen, 1990; Leppinen et al., 1989; J. A. Mielczarski et al., 1998). For xanthate adsorption on pentlandite, it was concluded that free xanthate first chemisorbed on pentlandite surface through nickel site, then another free xanthate reacts with the chemisorbed xanthate to form dixanthogen through oxidation, as shown in Equations (2.1) and (2.2) (Bozkurt et al., 1998; Hodgson & Agar, 1989; Mendiratta, 2000). In addition, xanthate can form nickel (II) xanthate with Ni site on pentlandite and co-adsorb on pentlandite with dixanthogen (McNeil et al., 1994).

$$\mathrm{Ni_{surface}} + \mathrm{X^-} \rightarrow \mathrm{NiX} + \mathrm{e^-} \tag{2.1}$$

$$\mathrm{NiX} + \mathrm{X^-} \rightarrow \mathrm{NiX_2} + \mathrm{e^-} \tag{2.2}$$

Inorganic depressants have been widely used during Cu/Ni separation process. Cyanide has been used for pentlandite and pyrrhotite depression (Xu et al., 2011). The depression mechanism of cyanide is to form metal cyanide complex on mineral surface which inhibits xanthate adsorption; free cyanide can also reduce pulp potential which prevent chemisorption of xanthate and the oxidation of xanthate to metal xanthate and dixanthogen (de Wet et al., 1997; Guo et al., 2014). Cyanide can also react with elemental sulphur, polysulphide and thiosulfate to

form thiocyanate, thus rendering the mineral surface less hydrophobic (X. H. Wang & Forssberg, 1996). Although cyanide can also be used as copper sulphide depressant by reducing the pulp potential, it has been found that upon slight oxidation conditioning, the pulp potential increased allowing chalcopyrite to float while still depressing pentlandite and pyrrhotite (Agar, 1991). Therefore, aeration sometimes is introduced prior to Cu/Ni separation to induce oxidation.

Polyamines such as diethylenetriamine (DETA) and triethylenetetramine (TETA) have been used extensively in the pyrrhotite depression (Kelebek et al., 1996; Kelebek & Tukel, 1999; Nagaraj & Ravishankar, 2007). DETA can chelate with Cu or Ni ions to form complex. However, the use of DETA can also compromise pentlandite recovery (Kelebek et al., 1995). Polyamines are usually used in combination with sulphur dioxide or sulphoxy species such as sulfite and metabisuphite (MBS) to enhance selectivity (Kelebek et al., 1996; Kelebek & Tukel, 1999; Tukel & Kelebek, 2010). The combination usage of DETA and sodium sulfite (Na_2SO_3) to efficiently depress pentlandite and pyrrhotite while not impacting Cu recovery has been reported, where the depression of pentlandite might be because the majority of pentlandite was locked in pyrrhotite (Lawson et al., 2005). Introduction of sulphoxy species can decompose xanthate to carbon disulphide; the pulp potential and dissolved oxygen content can be reduced which inhibit dixanthogen formation (Bozkurt et al., 1999). The sulphoxy species can also remove hydrophobic species on the surface such as elemental sulphur and polysulphide and yield hydrophilic products (Mendiratta, 2000). Some studies revealed that sulphoxy species can form hydrophilic complex with metal ion-DETA complex. The example reaction between sulphoxy species and Ni-DETA complex is shown in Equation (2.3) (Kelebek et al., 1996).

$$S_2O_6^{2-} + Ni(DETA)_2^{2+} \rightarrow [Ni(DETA)_2]S_2O_6 \quad (2.3)$$

The combination use of DETA/Na_2SO_3 was also discovered to be able to depress Ni content in the Cu/Ni separation with little pyrrhotite. The result showed that Ni content was reduced in the copper concentrate, yet whether pentlandite was responsible for the reduced Ni content was not known (Xu et al., 2011).

2.1.2 Studies on Millerite Flotation

Flotation studies on millerite were rarely reported in the literature due to the difficulty to obtain pure pristine millerite samples. Under acidic environment, the recovery of collectorless flotation of millerite reached 95% when using methyl isobutyl carbinol (MIBC) as the frother at pH 2 (Nagaoka et al., 1999). A preliminary study on the millerite single mineral flotation was

carried out using a millerite sample with 77% purity with the rest being dolomite (L. K. Smith et al., 2011). It has been discovered that millerite was very floatable from pH 9 to pH 10.5 using potassium ethyl xanthate (KEX) as the collector, and as pH was increased, the recovery dropped. This study also investigated electrochemical flotation of millerite as shown in Figure 2.1 (A). The limiting threshold potential for millerite at pH 9 was at -100 mV which was much lower than that of pentlandite (200 mV). However, this pulp potential was lower than the potential for the formation of nickel ethyl xanthate and dixanthogen at the concentration of KEX studied. The effect of using cyanide to depress millerite at pH 9 was also studied. As shown in Figure 2.1 (B), millerite was not depressed until 400 g/t dosage of cyanide. It was found that at 200 g/t cyanide dosage, millerite was not depressed at all but pentlandite's recovery dropped from 90% to 67%. L. K. Smith et al. (2011) did not further probe the reason that cyanide was less efficient in depressing millerite's flotation than pentlandite. As discussed earlier, cyanide depresses sulphide flotation by suppressing electrochemical reactions and reducing the pulp potential so that xanthate oxidation on mineral surface is inhibited. A hypothesis might be that since the flotation edge of pentlandite was 300 mV higher than millerite in the presence of KEX, adding a same concentration of cyanide can reduce the pulp potential to below the flotation edge of pentlandite but not millerite.

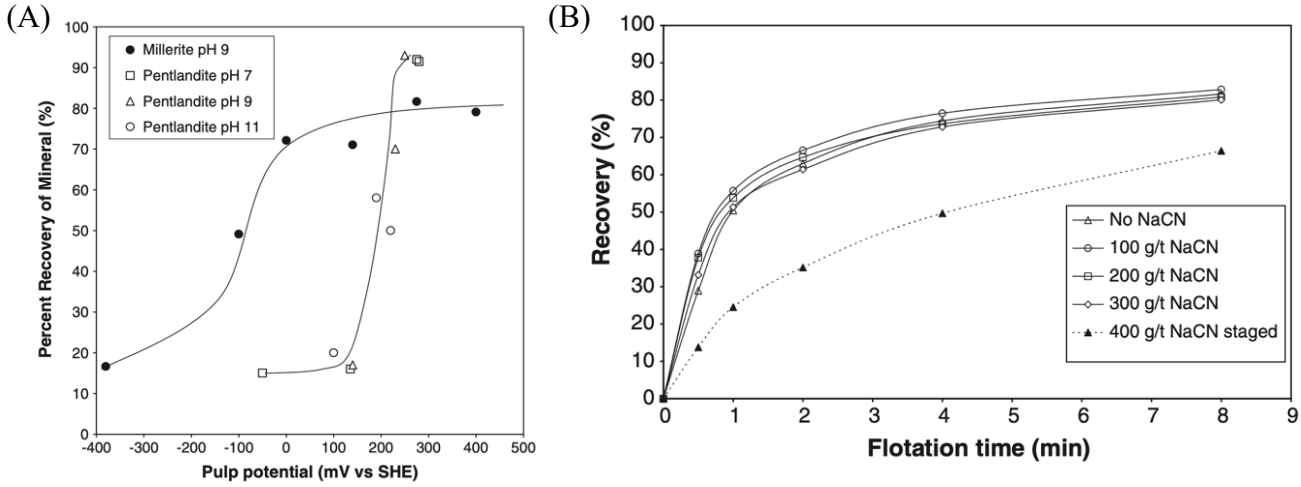

Figure 2.1 (A) Electrochemical flotation recovery of millerite and pentlandite as a function of pulp potential after 8 minutes of flotation and (B) The effect of cyanide addition on the flotation of millerite at pH 9 ([KEX]=1.4 × 10^{-4} M). Adapted from L. K. Smith et al. (2011) with permission from Elsevier.

Some flotation studies used synthetic millerite, which may not be representative of the real mineral flotation behavior. Lekki & Drzymala (1990) investigated collectorless flotation of synthetic millerite at pH 7.5. The recovery for 8 minutes flotation reaches 40% for a particle size of +40-45 μm. Furthermore, Stamboliadis (1978) examined pulp pH's effect on synthetic millerite flotation using dialkyl-dithiophosphate as the collector. It was found millerite was not floatable when pH was equal or greater than pH 12.

2.2 Copper Activation Mechanism of Iron and Nickel Sulphide Mineral

Activation of sulphide mineral by copper ion is a process in which copper ion can promote sulphide mineral floatability by rendering a stronger interaction with xanthate, or by affecting surface oxidation to preserve surface hydrophobicity, making it easier for the mineral particles to attach to the air bubbles during flotation. Activation of sulphide minerals by copper ion sometimes is desirable, for example, for sphalerite, or undesirable, such as for pyrite and pyrrhotite, depending on whether the activated mineral is valuable or is a gangue mineral. The source of copper ions in the flotation process can be either a deliberate addition into the process water in order to activate the mineral with economic interest such as sphalerite, or an inevitable presence due to mineral dissolution or chemical residuals. The copper ions in the latter case usually activate gangue minerals such as pyrite or pyrrhotite that need to be depressed, which is disadvantageous as the selectivity for valuable minerals can be reduced. As gangue minerals are associated with copper sulphide minerals in the orebody, removal of copper ions in the process water would be extremely challenging due to the copper sulphide dissolution. Therefore, it is vital to understand the activation mechanism of copper ions in order to better control or depress the undesired activation of gangue minerals.

2.2.1 Pyrite

Copper activation of pyrite (FeS_2) has been well studied in the literature. Early studies proposed a simple ion exchange model between Cu^{2+} and Fe^{2+} and resulted in the formation of CuS and elemental sulphur on pyrite surface as depicted in Equation (2.4) (X. Wang et al., 1989a).

$$FeS_2 + Cu^{2+} \rightarrow CuS + S^o + Fe^{2+} \quad (2.4)$$

Another ion exchange model suggested that activation of pyrite by Cu (II) is likely to be an electrochemical process where Cu (II) is reduced to Cu (I) and form Cu_2S through Equation (2.5) (Allison, 1982).

$$FeS_2 + 4Cu^{2+} + 6e^- \rightarrow Fe^{2+} + Cu_2S \quad (2.5)$$

Later, surface analysis by XPS suggested that Cu (II) can react with disulphide species (S_2^{2-}) at the surface to form a CuS_2 layer with Cu being in Cu (I) oxidation state regardless of the solution pH. The reaction is depicted in Equation (2.6) (Voigt et al., 1994).

$$Cu^{2+}_{ads} + {S_2^{2-}}_{surface} \rightarrow [Cu^+S_2^-]_{ads} \quad (2.6)$$

At alkaline pH, Voigt et al. (1994) proposed a two-step adsorption mechanism for Cu adsorption on pyrite. The first step is rapid adsorption and stabilization of Cu (I) that is achieved by the reduction from Cu (II), which is followed by precipitation of Cu (II) hydroxyl species that also gives rise to the increase in Cu (I) on the mineral surface. This mechanism was confirmed by Bo Yang et al. (2016), who used first principle calculations and showed that in addition to the interaction between Cu and S, a strong bond between oxygen in $Cu(OH)_2$ and Fe also exists; and the coexistence of both Cu (I) and Cu (II) species was confirmed by XPS analysis. Surface analysis techniques such as secondary ion mass spectroscopy (SIMS) and X-ray absorption fine structure spectroscopy (XAFS) were used to study Cu activation on pyrite (Weisener & Gerson, 2000a, 2000b). Their study suggested that Cu (II) is reduced to Cu (I) and S^{2-} is oxidized to S_2^{2-}, which is confirmed by the increasing sulphur oxidation. At alkaline pH, SIMS confirmed the existence of Cu (II) in addition to Cu (I) on the surface. At higher Cu concentrations, reduction of Cu (II) to Cu (I) species is followed by precipitation of $Cu(OH)_2$. Moreover, the solution and EDTA analysis indicated no obvious increase in iron dissolution and iron oxide/hydroxide species upon the addition of Cu, which ruled out the simple ion exchange mechanism for the interaction between copper and pyrite. Shen et al. (2001) proposed another mechanism regarding the existence of $Cu(OH)_2$ on Cu-activated pyrite at alkaline pH. The $Cu(OH)_2$ may come from both the direct precipitation from the bulk and the oxidation of the copper sulphide on pyrite, where the oxidation of copper sulphide on pyrite might be due to the galvanic interaction between copper sulphide on pyrite and the inactivated pyrite. Ejtemaei & Nguyen (2017a, 2017b) suggested a layer resembles chalcopyrite formed on pyrite upon the addition of Cu. This two-step electrochemical process is illustrated in Figure 2.2. The first step is the reduction of Cu (II) to Cu (I) accompanied by the oxidation of S^{2-} to S^-, then Fe^{2+} was also oxidized to Fe^{3+}, resulting in the formation of a layer with a structure of $CuFeS_2$ on pyrite surface. Zeta potential results also supported this mechanism by showing that at neutral pH, zeta potential of Cu-activated pyrite was similar to that of chalcopyrite.

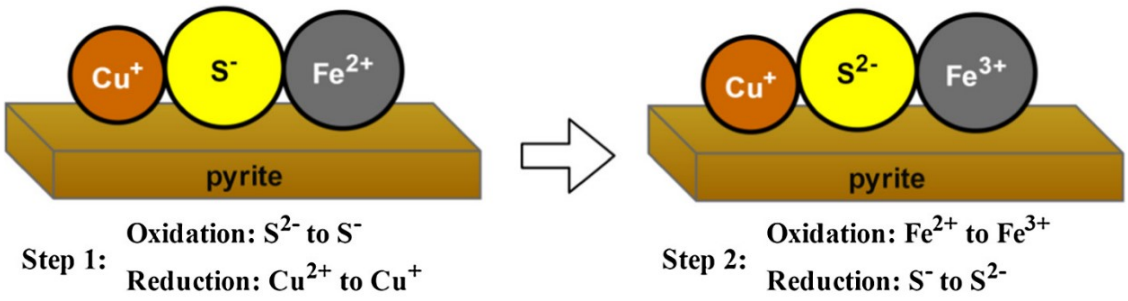

Figure 2.2 Schematic of $CuFeS_2$ type layer formation on pyrite upon the adsorption of Cu (II). Adapted from Ejtemaei & Nguyen (2017a) with permission from Elsevier.

The xanthate product formed on pyrite upon the adsorption of Cu was also examined. Copper (I) xanthate was suggested to be the main product formed on Cu-activated pyrite (Leppinen, 1990; Leppinen et al., 1995; Voigt et al., 1994). However, dixanthogen can still be detected and can coexist with Cu (I) xanthate. The ratio of Cu (I) xanthate to dixanthogen is dependent on Cu concentration: if Cu concentration is less than xanthate concentration, then dixanthogen will be the predominant species; if Cu concentration is equal to xanthate concentration, then Cu (I) xanthate will be the sole species formed on Cu-activated pyrite. Ejtemaei & Nguyen (2017b) suggested that only a small amount of Cu (I) xanthate can be detected with the majority being dixanthogen. Voigt et al. (1994) suggested that between pH 6 and pH 9, both Cu (I) and Cu (II) can lead to the formation of Cu (I) xanthate. Xanthate ion can adsorb on CuS_2 layer, which leads to the formation of Cu (I) xanthate as shown in Equation (2.7).

$$Cu^{+} + X^{-} \rightarrow CuX_{ads} \tag{2.7}$$

Also, Cu (II) precipitated as hydroxyl species on pyrite can react with xanthate ion to form both Cu (I) xanthate and dixanthogen, as shown in Equation (2.8).

$$Cu^{2+} + 2X^{-} \rightarrow CuX_{(s)} + \frac{1}{2} X_2 \tag{2.8}$$

2.2.2 Pyrrhotite and Pentlandite

Compared with pyrite, copper activation study on pyrrhotite and pentlandite is less well-understood. The presence of Cu can significantly enhance pyrrhotite's floatability for particle with particle size range of +10-100 μm (Senior et al., 1994). Gerson & Jasieniak (2008) carried out a comprehensive study to probe Cu activation on polymorphic (monoclinic and hexagonal)

pyrrhotite and pentlandite at alkaline pH. The study suggested that copper activation process on pyrrhotite and pentlandite is similar to pyrite, the copper activation is an adsorption process instead of an ion exchange process. Both Cu (I) species and Cu (II) precipitates exist on the surface, the majority is Cu (I) species and might be overlaid by Cu (II) precipitates. Copper activation was found to stabilize the mineral surface, making it less prone to oxidation. However, increasing the conditioning time will increase O/S ratio and decrease Cu/Fe ratio, indicating a passivation layer of Fe (III)-O-OH formed on the mineral surface. The study also investigated the impact of surface oxidation on the copper activation. It was found that Cu activation is compromised if the surface is pre-oxidised before introducing Cu ions. Nicol (1984) conducted electrochemical study and suggested that the rest potential of Cu-activated pyrrhotite was similar to that of covellite, which confirmed Cu (I) species formed on pyrrhotite. Regarding the role of Cu (II) species on mineral surface, Gerson & Jasieniak (2008) proposed that Cu (II) precipitates may reduce minerals' recoveries by rendering the surface hydrophilic non-selectively and reduce metal grades by reacting with xanthate and promoting surface hydrophobicity non-selectively thus promoting all mineral's recoveries. Allison & O'Connor (2011) also confirmed that pre-treatment of pyrrhotite with copper can promote xanthate adsorption. For the interaction with xanthate, $Cu(OH)_2$ would be the main adsorption species instead of Cu^{2+} directly interact with xanthate. Copper (II) xanthate (CuX_2) is formed by reacting with $Cu(OH)_2$ first, the unstable CuX_2 was then converted to both dixanthogen and copper (I) xanthate (CuX), as shown in Equation (2.9).

$$2CuX_2 \rightarrow 2CuX + X_2 \quad (2.9)$$

Flotation studies of Cu activation on pentlandite are limited. Malysiak et al. (2002) and Shackleton et al. (2003) confirmed that pentlandite's floatability was increased in the presence of Cu and xanthate at pH 9, while ToF-SIMS analysis confirmed the presence of Cu (II) species on pentlandite. Copper was found to be able to activate pentlandite flotation for particles with size ranges of +4 -10 μm and +100-200 μm in both single mineral flotation and mixed mineral flotation with pyrrhotite (Senior et al., 1994).

2.2.3 Hypothesis on Millerite Activation by Copper Ions

Discussions and hypotheses regarding the interaction between millerite and copper ions were also found in the literature. Acar & Somasundaran (1992) conducted an electrokinetic study on synthetic millerite, and they proposed that millerite surface was converted to covellite upon

the adsorption of Cu (II) as the IEP of oxidized millerite shifted towards that of oxidized covellite. Plant practice in Mt Keith Mill in Western Australia deliberately add copper sulphate to activate millerite flotation when the ore contained little copper, that is there is no Cu activation if no copper sulphate is added. The hypothetical reaction is illustrated in Equation (2.10), where Ni and Cu get exchanged and copper sulphide is formed (Crundwell et al., 2011; Kerr, 2002) .

$$CuSO_{4\,(aq)} + NiS_{(S)} \rightarrow CuS_{(S)} + NiSO_{4\,(aq)} \quad (2.10)$$

Another hypothesis is that fletcherite ($CuNi_2S_4$) and Cu_2S can form upon the reaction of copper sulphate and millerite without the oxidation of sulphur, the reaction is shown in Equation (2.11) (Bryson et al., 2008).

$$3CuSO_{4\,(aq)} + 5NiS_{(S)} \rightarrow Cu_2S_{(S)} + CuNi_2S_{4_{(S)}} + 3NiSO_{4\,(aq)} \quad (2.11)$$

2.3 Application of Natural Polysaccharides in Sulphide Mineral Flotation

The most common natural polysaccharides that have been used in sulfide mineral flotation are cellulose, guar gum, starch and dextrin, which are primarily composed of D-glucose as the monomer (Laskowski et al., 2007; Q. Liu et al., 2000; Pugh, 1989). For starch and dextrin, the monomer is α-D-glucose as shown in Figure 2.3 (A), for which the hydroxyl group at C1 extends below the ring, forming "axial" position. Dextrin is an intermediate product of enzymatic hydrolysis of starch to fermentable sugar, produced through liquefaction process using α-amylase or β-amylase. Dextrin's nature depends, to a great extent, on the starch source from which they are derived (Power, 2003). Starch contains two components: amylose is a linear chain connected by α-(1-4) linkage and amylopectin has a branched structure and the branch point is linked by α-(1-6) linkage (Laskowski et al., 2007; Ma & Deng, 2017; Power, 2003). Figure 2.3 (B) shows the branched structure of dextrin. During liquefaction process, as amylase can only cleave α-(1-4) linkage and bypass α-(1-6) linkage, dextrin has a highly branched structure that contains both amylose and amylopectin, yet the molecular weight of dextrin is significantly smaller than amylopectin. Compared with starch, dextrin has a much smaller molecular weight that ranges from 800 to 79,000; thus, dextrin can be visualized as the "fragments" of the original starch (Kandil, 2016; Q. Liu & Laskowski, 1989b). In addition, dextrin has a higher solubility in water which can easily provide a stable stock solution ready for flotation process. The large molecular weight of starch usually makes it a better flocculant rather than a good depressant (Q. Liu & Laskowski, 2006). Iwasaki & Lai (1965) showed that through heating and causticizing-

homogenization, the starch molecular weight could be reduced; as a result, the adsorption of starch on quartz and hematite dropped while the settling rate of hematite particles decreased as well. Therefore, lowering the molecular weight of starch can increase its performance as a depressant.

(A)

(B)

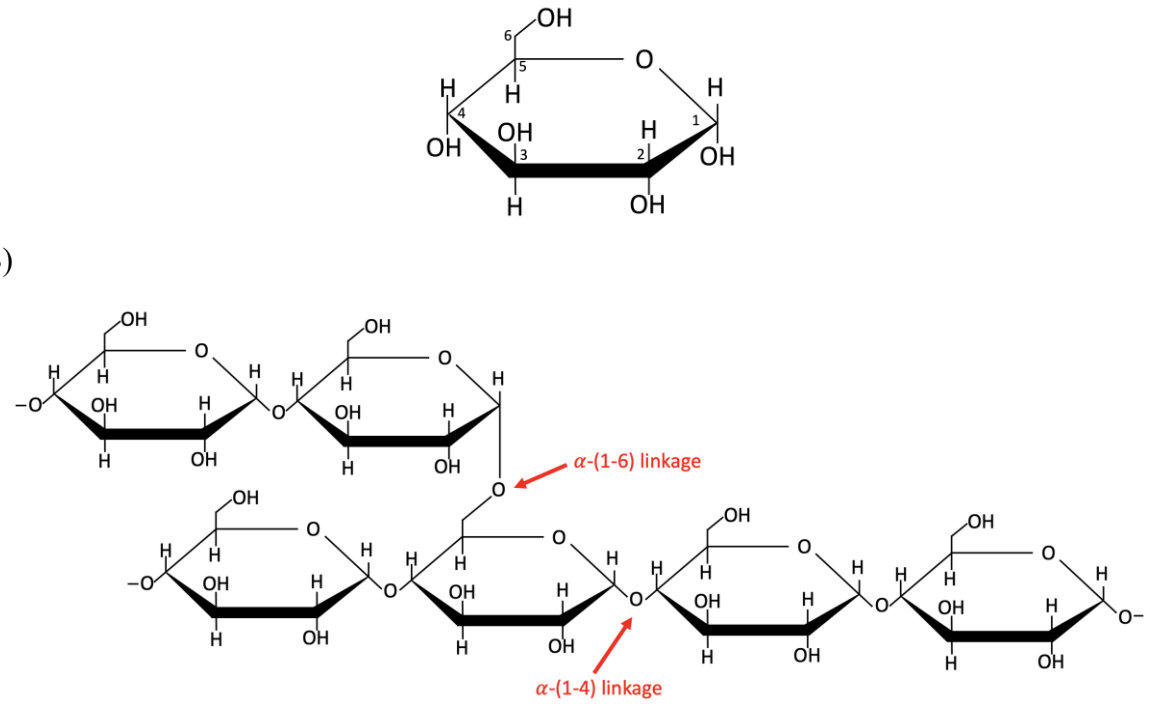

Figure 2.3 Structures of (A) α-D-glucose and (B) dextrin. Adapted from Laskowski et al. (2007) with permission from Elsevier.

In contrast to α-D-glucose, if the hydroxyl group at C1 extends above the ring and forms an "equatorial" position, the structure represents the β-D-glucose which is the monomer of cellulose, as shown in Figure 2.4 (A) (Q. Liu et al., 2000). Unlike starch and dextrin, cellulose has a linear structure as shown in Figure 2.4 (B). Cellulose's monomer β-D-glucose is connected through (1-4) linkage but in β configuration instead of α configuration. The molecular weight of cellulose is significantly larger than dextrin, usually composed of 10,000 or more glucose units. The most common derivative of cellulose used as flotation depressant is carboxymethyl cellulose (CMC), where the carboxymethyl group react with hydroxyl groups and replace the proton in the hydroxyl groups, as shown in Figure 2.4 (C) (Power, 2003; Pugh, 1989). CMC has been used most extensively in depressing naturally hydrophobic gangue minerals such as graphite and talc;

it has been used to depress minerals floated by fatty acid as well (Rhodes, 1979; Solari et al., 1986; Steenberg & Harris, 1984).

(A)

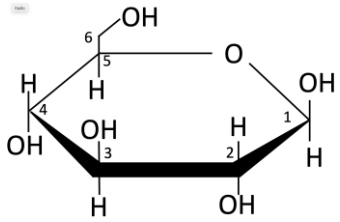

(B)

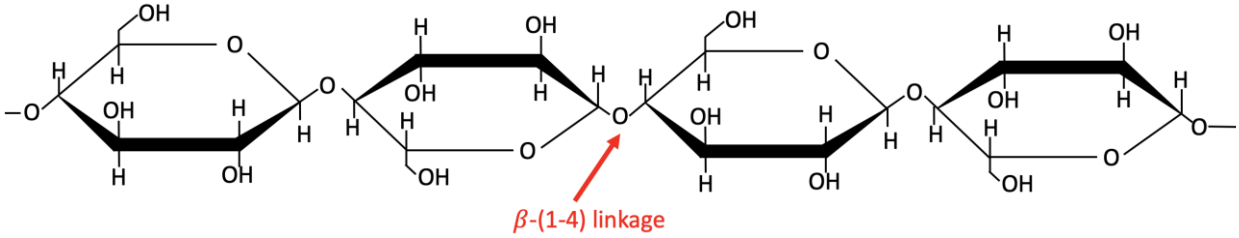

(C)

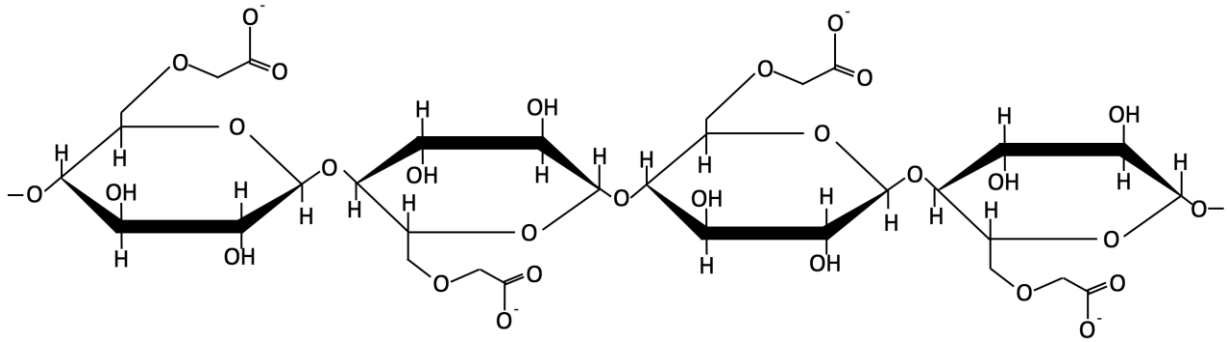

Figure 2.4 Structures of (A) β-D-glucose, (B) cellulose, and (C) carboxymethyl cellulose (CMC). Adapted from Laskowski et al. (2007) with permission from Elsevier.

2.3.1 Use of Dextrin in Sulphide Mineral Flotation

An extensive range of applications of dextrin as an organic depressant to increase the selectivity in sulphide mineral flotation can be found in the literature. Dextrin was reported as a pyrite depressant. In pyrite-sphalerite mixed flotation, dextrin is able to depress pyrite while copper-activated sphalerite is floated (Kydros et al., 1994). In addition, dextrin was able to depress pyrite while not affecting chalcopyrite's recovery at pH 8 when the pulp was aerated (López-Valdivieso et al., 2007). Also, dextrin was used together with calcium hypochlorite to

depress pyrite while floating galena in the differential pyrite-galena flotation at pH 10 (C. Wang et al., 2020). In the Cu-Pb or Zn-Pb differential flotation, dextrin was found to primarily depress galena. Dextrin was used with SO_2 to depress galena in a galena-chalcopyrite system in Brunswick Mines in Canada (Neumann & Schnarr, 1971). At alkaline pH environment, galena was depressed by dextrin while chalcopyrite was floated with or without calcium ion present (Q. Liu & Laskowski, 1989c; Q. Liu & Zhang, 2000). Bolin & Laskowski (1991) showed that combining dextrin with caustic depressed galena in bench and pilot tests. It was also reported that dextrin can depress chalcopyrite while not affecting galena's floatability under weak acidic to neutral pH (Q. Liu & Laskowski, 1989c). In Zn-Pb differential flotation, dextrin was found to depress galena recovery to less than 10% while floating copper-activated sphalerite at pH 12 using potassium ethyl xanthate or sodium isopropyl xanthate as the collector. It was found that the addition order for KEX and dextrin did not have an impact on the selectivity (Rath & Subramanian, 1999). Furthermore, dextrin was also used in Cu-Ni differential flotation in both industry scale and laboratory tests. Dextrin was reported to be used in the selective flotation of Cu-Ni concentrate in the presence of lime at pH 12 at Kotalahti mine in Finland, pentlandite was depressed while chalcocite was floated (Laskowski & Nyamekye, 1994). Similarly, Nyamekye & Laskowski (1991) used tapioca dextrin as the depressant with amyl xanthate as the collector in the differential flotation of chalcocite-heazlewoodite. It was found that heazlewoodite could be depressed while chalcocite was floated at pH 11.7 – pH 12. Recently, Xu et al. (2011) used starch and dextrin as depressants to reject Ni content in Cu-rich ore with aeration stage added at pH 11.8. It was found dextrin was the most promising depressant to reject nickel content than starch. However, the Cu recovery was also compromised slightly.

It can be concluded that when using dextrin as the depressant, the selectivity of differential sulphide mineral flotation is greatly dependent on pulp pH, and most separation windows were found at alkaline pH. The pulp pH at which a given sulphide mineral can be depressed varies case by case. It is well known that pulp pH has a significant impact on sulphide mineral's floatability, thus it is vital to understand the adsorption mechanism of dextrin and the relationship between pulp pH and dextrin adsorption.

2.3.2 Investigation of Adsorption Mechanism

Several mechanisms have been proposed for the polysaccharide adsorption on mineral surface in aqueous solutions. The adsorption mechanisms are usually derived based on one or more specific mineral systems studied.

It has been well discussed in the literature that the adsorption of dextrin on mineral surface is a chemisorption process. The binding between polysaccharide and metal species was first proposed through the study of starch and CMC adsorption on oxide and sulphide minerals. It was postulated that polysaccharide adsorbs on mineral surface through forming complex with metal cations such as Fe^{3+}, Ca^{2+} and Mg^{2+} (Khosla et al., 1984; Pugh, 1989; Solari et al., 1986; Somasundaran, 1969; Subramanian & Natarajan, 1988).

In recent years, more experimental evidence suggested that polysaccharide can form ring complex with metal hydroxide on mineral surface through the hydroxyl functional group, which was embodied by the pH-dependence of polysaccharide adsorption (Q. Liu & Laskowski, 1989b, 1989c, 1989a; Nyamekye & Laskowski, 1993; Rath & Subramanian, 1999; Subramanian & Natarajan, 1988). The reaction schematic is shown in Figure 2.5.

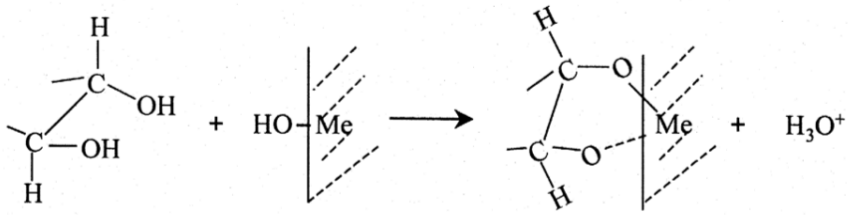

Figure 2.5 Schematic reaction of formation of chemical complexes on mineral surfaces. Adapted from Q. Liu et al. (2000) with permission from Elsevier.

Q. Liu & Laskowski (1989b) studied dextrin's adsorption on quartz surface with and without lead coating. It was found that the lead-coated quartz was able to adsorb more dextrin compared with the bare quartz, and the adsorption was strongly pH-dependent, the maximum adsorption occurs at the pH where lead hydroxide formed. A more general study was carried out to investigate the interaction between dextrin and various metal ions (Fe^{3+}, Cu^{2+} and Pb^{2+}). It was found that the dextrin only co-precipitated with metal ions at the pH where metal hydroxide formed. Infrared spectroscopy results showed the disappearance of peaks at 930 cm^{-1} and 760 cm^{-1} due to the interaction between dextrin and lead hydroxide. These peaks represented the

glucopyranose ring vibration and the disappearance of these peaks might be due to lead hydroxide forming a complex with the hydroxyl groups located at C2 and C3 of the glucopyranose ring, as the substitution of hydroxyl groups exerts stain on the glucopyranose ring which limited ring vibration (Q. Liu & Laskowski, 1989a).

Oxidation of sulphide mineral leads to dissociation of metal ions, formation of metal oxide/hydroxide and precipitation of metal oxide/hydroxide on the mineral surface, as depicted in Equation (2.12) (Fullston et al., 1999; Gardner & Woods, 1979; Smart et al., 2003).

$$MS + \frac{1}{2}nO_2 + nH_2O \rightarrow M_{1-n}S + nM(OH)_2 \quad (2.12)$$

Under this circumstance, isoelectric points (IEPs) will be observed as the surface is covered by metal oxide/hydroxide. An IEP is the pH at which the surface charge is zero and surface charge is reversed at IEP. Usually for oxide or hydroxide, when the pH is smaller than IEP, surface carries positive charge; when pH is greater than IEP, surface carries negative charge. As a result, the dissociation or adsorption of hydrogen ions will account for the sign of surface charge, as shown in Equations (2.13) and (2.14); and hydrogen and hydroxyl ions are considered as potential-determining ions (D. W. Fuerstenau & Pradip, 2005).

$$MOH_{surface} \rightarrow MO^-_{surface} + H^+ \quad (2.13)$$

$$MOH_{surface} + H^+ \rightarrow MOH^+_{2\,surface} \quad (2.14)$$

Hence, for oxidized sulphide minerals with metal hydroxide on the surface, there are usually two IEPs, where the IEP at the lower pH resembles the start of nucleation of metal hydroxide on mineral surface while the IEP at higher pH resembles the IEP of the metal hydroxide, which indicates the coverage of that metal hydroxide on the mineral surface (X. Wang et al., 1989b).

It was found that polysaccharide's adsorption was strongly pH-dependent. The pH at which the polysaccharide adsorption reached its maximum was usually close or similar to the isoelectric point (IEP) of the oxidised sulphide mineral surface or oxide mineral surface, which again confirms the chemical interaction between dextrin and metal hydroxide (Q. Liu et al., 2000). Based on the evidence for chemical complex formation, an acid-base model was proposed. Essentially, the hydroxyl group in polysaccharide acts like Brønsted acid to donate protons and the surface metal hydroxide act as Brønsted base in order to form a complex. Hence, a more basic mineral surface results in a stronger interaction between hydroxyl group and the

surface metal hydroxide (Laskowski et al., 2007; Q. Liu et al., 2000). The IEP of a specific metal oxide or hydroxide is an indication of basicity. For example, lead and nickel hydroxide have an IEP between pH 10 and pH 12, this means the galena and heazlewoodite surfaces covered by lead and nickel hydroxide show strong basicity. Therefore, this model can be used to explain why the maximum amount of dextrin adsorbed varies for different minerals. Figure 2.6 shows the relationship between the maximum amount of dextrin adsorbed and the IEPs of some oxide and sulphide minerals. Note that the IEPs of sulphide minerals here are actually the IEPs of the metal oxide/hydroxide on the mineral surface due to oxidation. It can be found that dextrin can adsorb more on galena and heazlewoodite than chalcopyrite and chalcocite due to the difference in IEPs of lead/nickel hydroxide and cupric hydroxide. As lead and nickel hydroxide are more basic than cupric hydroxide, oxidised galena and heazlewoodite would be more basic than oxidised chalcopyrite and chalcocite. As a result, the dextrin adsorption on galena and heazlewoodite would be stronger than that on chalcopyrite and chalcocite.

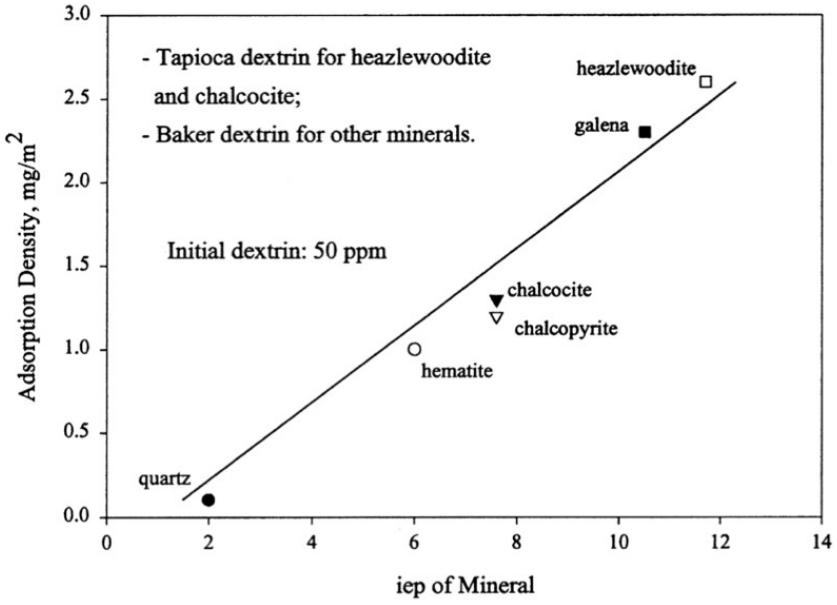

Figure 2.6 Maximum adsorption densities of dextrin on different mineral surfaces versus IEPs of minerals. Adapted from Q. Liu et al. (2000) with permission from Elsevier.

In addition to chemical complex formation, hydrogen bonding was also proposed to be the key interaction between dextrin and mineral surface. Balajee & Iwasaki (1969) studied adsorption of corn starch on hematite and quartz surface and hydrogen bonding was assumed to

be the primary adsorption process. The study proposed the alcohol group at C6 can form strong O-H⋯O bond with the oxygen on the surface. However, most studies in the literature suggested that the interaction mechanism involves both formation of chemical complex and hydrogen bonding (Rath & Subramanian, 1999; Santhiya et al., 2002; Subramanian & Natarajan, 1988; C. Wang et al., 2020; Weissenborn et al., 1995). As hydrogen bonding is a strong type of directional dipole – dipole attraction instead of a covalent bond, the bond strength would be much weaker compared with the formation of complex. In fact, the acid/base model argues that for weak acid/base interaction, only hydrogen bond can form, which can gradually transfer to a chemical complexation as the acid/base interaction gets stronger (Q. Liu et al., 2000).

Physisorption processes such as electrostatic interaction and hydrophobic interaction are also proposed to model the dextrin adsorption on the mineral surface. A solid surface in aqueous solution could be charged due to ionization of surface functional group, preferential ionic solubility or adsorption of chemicals. The excess of surface charge generates an electric field which is balanced by ions that carry opposite charge (counterions). The electric double layer is defined as the layer of surface charges with the layer of counter ions (M. C. Fuerstenau et al., 2007). A well-accepted Stern model was proposed to illustrate electric double layer, which is shown in Figure 2.7 (Masliyah & Bhattacharjee, 2005).

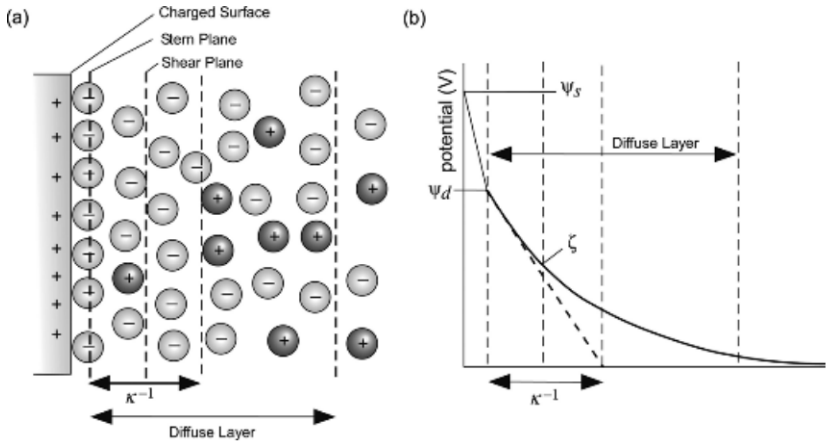

Figure 2.7 Schematic of Stern model for electric double layer (A) and the corresponding potential profile over the electric double layer (B). Adapted from Masliyah & Bhattacharjee (2005) with permission from John Wiley and Sons.

The Stern plane is defined as the inner boundary for a layer of immobile counterions adsorbed on the surface. The potential at the Stern layer is called Stern potential (ψ_d) and the layer between the Stern plane and the charged surface is called Stern layer. Ions that are in mobile state located beyond Stern layer in the surroundings compose the diffuse layer. Shear plane in the diffuse layer is defined with no-slipping boundary conditions applied. The potential at the shear plane is defined as zeta-potential (ζ). Attractive or repulsive electrostatic interaction arises due to the charged solid surface and the adsorbed species carry the same or different signs. Usually for non-ionic polysaccharide such as starch and dextrin, electrostatic interaction is possible as starch and dextrin are slightly negatively charged in water, especially at alkaline pH, which is due to the dissociation of protons from hydroxyl functional group (Moreira et al., 2017; Tang & Liu, 2012). For example, Somasundaran (1969) studied the mechanism of starch adsorption onto calcite and concluded that the negatively charged starch interacts with positively charged calcite surface via electrostatic attraction.

Hydrophobic interaction originates from adhesion of two non-polar groups in polar medium such as aqueous solution. The proposed mechanism was derived based on indifferent dextrin adsorption on naturally hydrophobic minerals such as coal, molybdenite and talc, for which the adsorption is independent of mineral's chemical composition and pH (Beattie et al., 2006; Haung et al., 1978; Miller et al., 1983). Wie & Fuerstenau (1974) studied the adsorption of dextrin onto molybdenite and quartz surfaces, and they found that the adsorption density of dextrin onto molybdenite is much higher than that of quartz and was independent of pH. The free energy of adsorption for dextrin on molybdenite was calculated to be -5.4 kCal/mol monomer. This value is similar to that of dextrin adsorption on coal, which was calculated to be -5.5 kCal/mol monomer (Miller et al., 1983; Wie & Fuerstenau, 1974). Beaussart et al. (2009) investigated dextrin's adsorption on three naturally hydrophobic minerals – graphite, talc and molybdenite. A correlation between the amount of dextrin adsorbed and the hydrophobicity reduction was discovered. The initial surface hydrophobicity of the mineral has a significant impact on the flotation response on the premise that the adsorbed layer of dextrin is similar.

Collectors or surfactants are usually present in the pulp to render the mineral surface hydrophobic, yet the co-adsorption of collectors and polysaccharides is usually observed. Thus, the impact of collector on the interaction between polysaccharide and mineral surface were also studied. Somasundaran (1969) observed mutual enhancement in the adsorptions of starch and

oleate ions on calcite. The suggested mechanism was that oleate ions occupy a position inside the helix formed by the interior of the adsorbed starch chain, resulting in a non-polar bonding between oleate and adsorbed starch, which explained that calcite surface still remained hydrophilic with the xanthate adsorbed on the surface. Q. Liu et al. (1994) studied the adsorption of dextrin and fatty acids on oxide and fluoride minerals. The study showed that addition of moderate amount of fatty acids prior to dextrin was able to increase dextrin's adsorption. The hydroxyl functional groups of the dextrin monomer can rotate to one side of the glucopyranose ring rendering that side hydrophilic, which leaves the opposite side hydrophobic with the exposure of -CH group on the glucopyranose ring. This kind of rotation results in a helical form for the long chain, for which the inner side is hydrophobic while the outer shell is hydrophilic. Therefore, in addition to the chemical interaction, the "loop" of unattached hydrophobic side of dextrin helix is capable of interacting with surface hydrophobic species, wrapped the hydrocarbon chain of the collector in the "loop", which well explained the enhanced adsorption of dextrin with collector pre-adsorbed on the mineral surface. The study also suggested that if the collector concentration was in excess or the hydrocarbon chain of the collector was too long, dextrin adsorption was compromised. Eirich (1977) illustrated two possible adsorption modes for polymer – forming chemical complex and hydrophobic bonding. The example is the adsorption of polystyrene sulfonate on charcoal as shown in Figure 2.8. Both strong ionic interaction between the functional group and the surface cations and the weak hydrophobic interaction between the backbone of the polymer and the surface are possible.

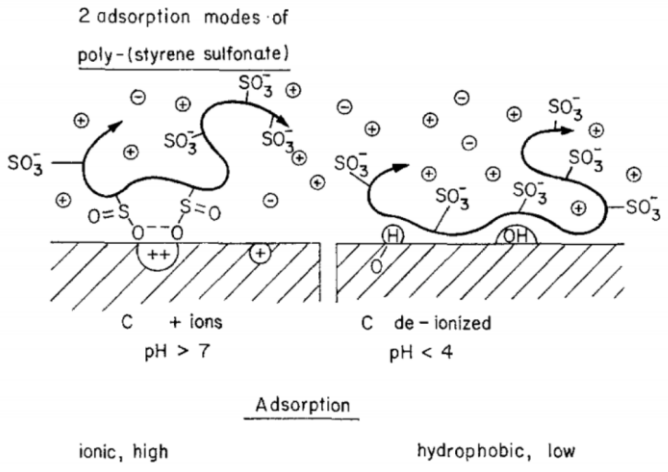

Figure 2.8 Schematic of two mechanisms of polystyrene sulfonate adsorption on charcoal surface. Adapted from Eirich (1977) with permission from Elsevier.

For sulphide minerals, similar enhanced adsorption of polysaccharide due to collector was also observed. López-Valdivieso et al. (2004) studied xanthate and dextrin adsorptions on pyrite. Xanthate can still adsorb on pyrite surface with dextrin already adsorbed on pyrite, yet the adsorption of xanthate cannot render pyrite surface hydrophobic. Similarly, Rath et al. (2001) observed a mutually enhanced adsorptions of xanthate and guar gum on chalcopyrite at a certain concentration of xanthate; and the enhanced adsorption of xanthate due to guar gum's presence did not render surface more hydrophobic.

Chapter 3 Materials and Methods

3.1 Mineral Samples

Ore samples with massive millerite and chalcopyrite originated from Sudbury, ON, Canada were purchased from Kaygeedee Minerals. The surface oxidation of base metal sulphide minerals was considered and minimized during the preparation of the mineral samples. The ore samples were first crushed by a jaw crusher (BB200, Retsch, Germany) and then hand-sorted to remove gangue minerals and impurities. After that, the pure mineral samples were ground in a mortar grinder mill (Retsch, Germany) and dry screened with 38 μm and 75 μm sieves using a Ro-Tap sieve shaker (W.S. Tyler, Canada). The -75+38 μm fraction of mineral particles was cleaned ultrasonically in Milli-Q water to remove fines and surface oxidation (Clarke et al., 1995; Multani et al., 2018). Ultrasonication was found to be able to reduce mineral surface oxidation verified by the XPS analysis of an oxidized millerite sample with and without 5 minutes sonication, details can be found in Appendix E. Milli-Q water was added to the mineral in a beaker, and the mineral was cleaned ultrasonically for 1-minute using an ultrasonic bath followed by another 1-minute settling, the supernatant was then decanted. This procedure was repeated until the supernatant was clear. After that, the mineral samples were frozen and then transferred to a freeze dryer (FreeZone 4.5, Labconco, USA) to be vacuum dried. The dried mineral samples were then stored in polyethylene bags and vacuum-sealed. All mineral samples were stored in a vacuum desiccator to prevent oxidation.

The prepared mineral samples were characterized by X-ray powder diffraction (XRD) and X-ray fluorescence (XRF) techniques. Figure 3.1 shows the XRD spectra of millerite and chalcopyrite against the reference peaks analyzed by a Rigaku Ultima IV X-ray Diffractometer. Based on the XRD spectrum and comparison with the reference peaks, the millerite sample was confirmed as β-NiS (Shombe et al., 2020). For millerite XRD spectrum, the peak at $2\theta = 29.3°$ might characterize chalcopyrite, and the peak at $2\theta = 51.4°$ might characterize pentlandite (PDF# 00-008-0090), indicating the millerite sample contained some impurities. Chemical assays of millerite and chalcopyrite samples were analyzed by XRF (Orbis PC Micro-EDXRF Elemental analyzer) and the results are shown in Table 3.1. Based on XRD and XRF analyses, millerite contained 58.3% Ni which yielded a purity of 90.1%; while chalcopyrite contained 33.0% Cu which yielded a purity of 96.6%. The -75+38 μm size fraction was used for micro-

flotation tests and XPS analysis while the -38 µm size fraction was used for the mineral dissolution tests, adsorption tests, and zeta potential tests. The specific surface area (SSA) of the -38 µm size fraction was analyzed using Brunauer-Emmett-Teller (BET) method by a surface area analyzer (Autosorb – iQ, Quantachrome), which were 0.500 m^2/g and 0.849 m^2/g for millerite and chalcopyrite, respectively. Bulk mineral samples were used in AFM imaging and contact angle measurement. The bulk mineral samples were characterized by scanning electron microscopy (SEM) and details can be found in Appendix C.

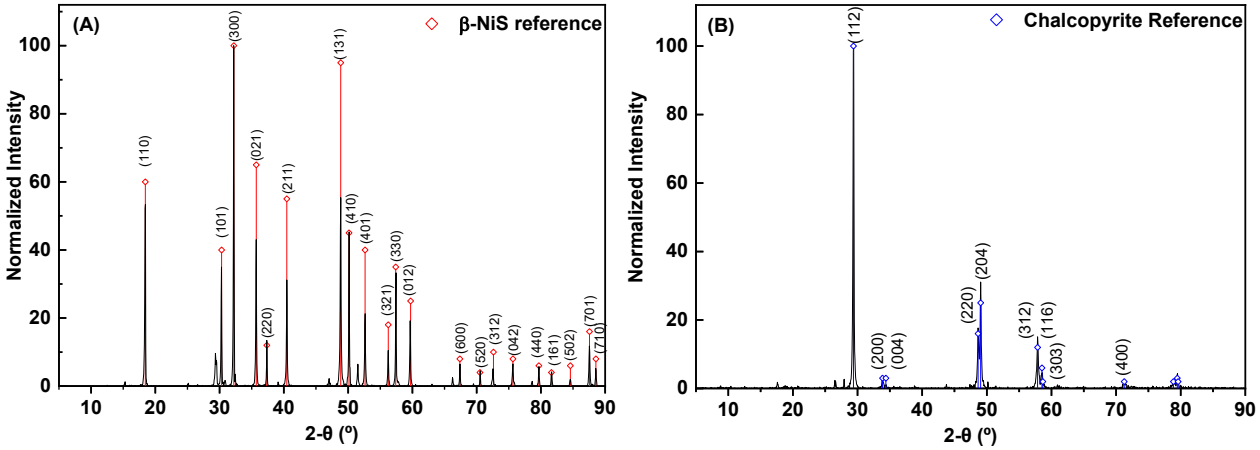

Figure 3.1 XRD spectra of powder samples of (A) millerite against the reference from the JCPDS Powder Diffraction File (PDF) database (PDF# 00-012-0041) and (B) chalcopyrite against the reference from the JCPDS PDF database (PDF# 00-037-0471)

Table 3.1 Chemical assay of millerite and chalcopyrite samples.

Element	Composition (wt%)					
	S	Fe	Co	Ni	Cu	Zn
Millerite	35.0	3.62	0.25	58.3	2.82	-
Chalcopyrite	35.8	30.6	-	0.23	33.0	0.38

3.2 Chemicals and Reagents

Copper (II) nitrate trihydrate ($Cu(NO_3)_2 \cdot 3H_2O$, 99%, ACROS Organics) was used as the source of the copper (II) ions. Potassium ethyl xanthate (KEX, $C_3H_5OS_2K$, 98%, Fisher Scientific), corn dextrin ($(C_6H_{10}O_5)_n$, analysis grade, Millipore Sigma), potassium chloride (KCl, ACS reagent grade, Fisher Scientific), hydrochloric acid (HCl, ACS reagent grade, Fisher Scientific), sodium hydroxide (NaOH, ACS reagent grade, Fisher Scientific), nickel hydroxide ($Ni(OH)_2$, analysis grade, Acros Organics), sulfuric acid (H_2SO_4, ACS reagent grade, Fisher Scientific), phenol (C_6H_6O, ACS reagent grade, Fisher Scientific), octadecyl trichlorosilane (OTS, $C_{18}H_{37}Cl_3Si$, 95%, Millipore Sigma), ethylenediaminetetraacetic acid disodium salt dihydrate (Na_2EDTA, $C_{10}H_{14}N_2Na_2O_8 \cdot 2H_2O$, ACS reagent grade, Fisher Scientific), acetone (C_3H_6O, ACS reagent grade, Fisher Scientific), toluene (C_7H_8, ACS reagent grade, Fisher Scientific), sodium nitrate ($NaNO_3$, ACS reagent grade, Fisher Scientific), sodium dodecyl sulfate (SDS, $NaC_{12}H_{25}O_4S$, 99%, Millipore Sigma) were all used as received without any modifications. All pH values of aqueous solutions were measured using a Fisherbrand accumet XL 150 pH meter with a Fisherbrand accuTupH Rugged bulb pH combination electrode. The pH meter was calibrated daily using Thermo Scientific Orion buffers. Pulp potential was measured using an Orion Star A221 portable pH meter (Thermo Scientific) with an Orion Redox/ORP electrode, and a 90-FLT meter (TPS) with an ORP probe (EOREA5W-111259). All experiments were conducted using Milli-Q water with a resistivity of 18.2 $m\Omega \cdot cm$ (Millipore Elix Essential 3 UV and Milli-Q Gradient A10 water purification systems) at room temperature unless stated otherwise. The dissolved oxygen (DO) content of Milli-Q water was measured using a polarographic dissolved oxygen probe (Orion 083005MD) with an Orion Versa Star Pro Benchtop meter. The DO content of Milli-Q water was consistent, which was around 3 to 4 ppm.

3.3 Experimental Techniques

3.3.1 Modified Hallimond Tube

In this study, micro-flotation tests were conducted using a custom built modified Hallimond tube (University of Alberta glass shop). Figure 3.2 shows the schematic of a modified Hallimond tube. Nitrogen gas that entered the Hallimond tube was filtered by the glass frit. A magnetic stirrer was placed on top of the glass frit to agitate pulp during flotation. The narrow connection between the flotation tube and the concentrate bulb allowed only one bubble going through at a time when no frother was used, aimed to minimize the inconsistency due to

mechanical entrainment (Cao & Liu, 2006; Chachula & Liu, 2003). After the flotation, the concentrate was collected in the concentrate bulb while the tailing was left over on top of the glass frit. Hallimond tube is suitable for studying the flotation behavior of pure minerals that only requires a small amount of sample, usually 1 to 2 grams.

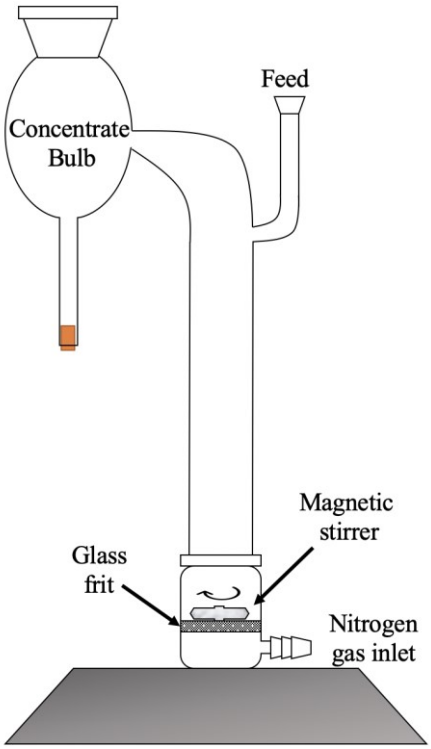

Figure 3.2 Schematic of a modified Hallimond tube.

3.3.2 X-ray Fluorescence (XRF)

X-ray fluorescence (XRF) is a non-destructive technique that provide elemental analysis for solid or liquid samples. High energy X-rays is bombarded to excite the sample surface by ionizing the atom, which results in emission of radiation with a different characteristic energy. The characteristic energy can then be used to identify the corresponding element. The intensity of each characteristic energy can be correlated to the proportion of each element in the sample (Bertin, 1975). The advantage of XRF is efficient when analyzing plenty samples.

In this study, an Orbis PC Micro-EDXRF Elemental analyzer was used, and a rhodium source was used as the primary radiation source. Mineral powder samples with size fractions of -75+38 μm and -38 μm was used. During data acquisition, at least three different spots on each sample were measured and the average was calculated.

3.3.3 X-ray Diffraction (XRD)

X-ray diffraction (XRD) is a non-destructive surface characterization technique that identifies crystal structure of solids such as salts, metals, minerals. X-ray radiation onto the crystal will cause the beam to diffract. This phenomenon can be explained by Bragg's Law, as shown in Equation (3.1), where λ is the wavelength of the incident X-ray source, n is an integer, θ is the incident angle and d is the distance between the atomic layers in a crystal.

$$n\lambda = 2d\sin\theta \tag{3.1}$$

By measuring the intensities of the diffracted beams at different angles, a unique spectrum will be obtained to identify the crystal structure for an unknown mineral.

In this study, a Rigaku Ultima IV X-ray Diffractometer was used to qualitatively identify the crystal structure of powder mineral samples with size fraction of -38 μm. The spectrum was then analyzed by MDI Jade software and compared against the reference powder diffraction files (PDF) in International Centre for Diffraction Data (ICDD).

3.3.4 X-ray Photoelectron Spectroscopy (XPS)

X-ray photoelectron spectroscopy (XPS) is widely used as a non-destructive surface characterization technique to analyze the surface chemistry of solid surface within 10 nm below the surface under ultra-high vacuum. XPS can be used either qualitatively or quantitively to provide elemental composition through survey scan as well as chemical species compositions based on fitting of high-resolution narrow scan. The working mechanism of XPS is based on photoelectric effect: the incident X-ray source stimulates the sample surface through the adsorption of photon by the atom, which results in the electron emission from the atom to the electron energy analyzer. Each emitted electron has a unique binding energy which can then be calculated using Equation (3.2), where $h\upsilon$ is the energy of X-ray photon source, KE is the kinetic energy of the emitted electron and BE is the binding energy of electrons rejected. The number of electrons detected versus binding energy is obtained as an XPS spectrum (Kibel, 2003).

$$BE = h\upsilon - KE \tag{3.2}$$

In this study, an AIXS Ultra XPS spectrometer (Kratos Analytical Ltd., Manchester, UK) with a monochromatic Al-Kα photon source (hυ=1486.6 eV) was used. The test was conducted in an ultra-high vacuum chamber. The spectra were analyzed using software CasaXPS. Binding energy shift of spectra due to charge neutralization was calibrated using C 1s at 284.8 eV. Shirley background was used and the high resolution spectra were fitted using Gaussian (70%)-

Lorentzian (30%) line shape (Legrand et al., 1998; Nesbitt, Legrand, et al., 2000; Nesbitt & Reinke, 1999).

3.3.5 Ultraviolet-Visible (UV-Vis) Spectroscopy

Ultraviolet-Visible (UV-Vis) spectroscopy is a spectroscopic technique that uses visible-ultraviolet light to pass through the sample to measure the amount of light being absorbed. The technique can be applied to colored solution containing transition metal ions, organic compound and macromolecule. Absorbance of radiation excites the electron within the molecule and results in an increase in the energy levels. The absorbance versus wavelength can be obtained as the UV-Vis spectrum. This technique can be used to quantitively determine concentration of the absorbing species using Beer-Lambert law, which is depicted in Equation (3.3):

$$\mathrm{A} = -\mathrm{Log}\left(\frac{\mathrm{I}}{\mathrm{I_o}}\right) = \varepsilon \mathrm{cL} \tag{3.3}$$

where A is the measured absorbance, I_o is the intensity of the incident light source, I is the intensity of the light after passing through the sample, and the ratio of $\frac{I}{I_o}$ is called the transmittance, terms ε, c and L represent molar absorptivity, concentration of the absorbing species and the path length of sample, respectively (Perkampus, 1992). For a typical test, samples with known concentrations are tested first to obtain a linear calibration curve of absorbance versus concentrations. In this study, UV-Vis Spectroscopy was used to measure the concentrations of dextrin and KEX in aqueous solutions. A Shimadzu UV-3600 UV-Vis-NIR Spectrophotometer was used in this study.

3.3.6 Atomic Force Microscopy (AFM)

Atomic force microscopy (AFM) was used to conduct topographical characterizations of mineral surface in this study. Figure 3.3 depicts the schematic of an AFM. The AFM tip is connected to a cantilever spring, which is deflected toward or away from the substrate during scanning due to the interaction force between the AFM tip and the surface. The deflection of the cantilever spring at certain location is measured and the topographical imaging of the substrate is then accomplished. In addition, when the AFM tip approaches the substrate, the position of the tip and the deflection of the cantilever are measured and can be converted to “force-distance curves” that can be used to probe the interaction force between the tip and the substrate (Butt et al., 2005).

In this study, an MFP-3D AFM system (Asylum Research, Santa Barbara, CA) with a ScanAsyst-Fluid + probe (Bruker) was used for the surface topography images obtained by AFM tapping mode. The root-mean-square (RMS) roughness and peak-to-valley (PTV) value were analyzed by Asylum Research Igor Pro-based software.

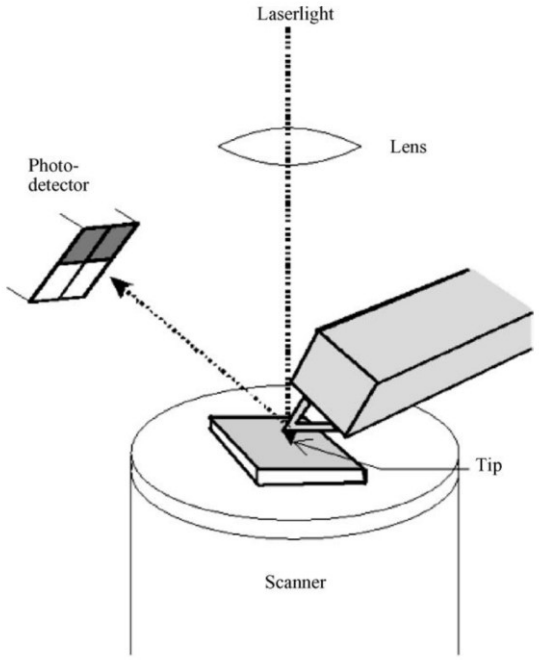

Figure 3.3 Schematic of AFM. Adapted from Butt et al. (2005) with permission from Elsevier.

3.3.7 Zeta Potential Measurement

Zeta potential of particles can be determined by electrophoresis measurement, where an electric field (E_x) is applied and particle velocity (v_p) is measured. As a result, the electrophoretic mobility of the particle (U_E) can be obtained using Equation (3.4).

$$\mathrm{U_E} = \frac{\mathrm{v_p}}{\mathrm{E_x}} \tag{3.4}$$

Consequently, the electrophoretic mobility can be converted into zeta potential using Helmholtz-Smoluchowski Equation as shown in Equation (3.5),

$$\zeta = \frac{\mathrm{U_E}\eta}{\varepsilon\varepsilon_0} \tag{3.5}$$

where ζ is the zeta potential, U_E is the motility, η is the dynamic viscosity of fluid, ε is the dielectric constant of the fluid and ε_0 is the vacuum permittivity (Berg, 2009). The Helmholtz-

Smoluchowski Equation is generally valid for particle size greater than 1 micron. A Brookhaven ZetaPALS zeta potential analyzer was used in this study. For a typical measurement, 10 runs of zeta potential measurement were obtained. For each run, 10 cycles of mobility measurement were obtained to obtain a stable mobility. The measured mobility was then converted to zeta potential using Helmholtz-Smoluchowski Equation. The highest and lowest values in the 10 runs were neglected when calculating the average value and the error.

3.3.8 Inductively Coupled Plasma (ICP) Spectroscopy

Inductively coupled plasma spectroscopy (ICPS) is a destructive technique used to analyze concentrations of chemical elements in aqueous samples. The plasma discharge is usually the result of argon gas being heated inductively and ionized by an intense electromagnetic field within the coil. The plasma discharge has a very high temperature and contains sufficient high concentration of electrons. There are two types of ICPS – mass spectroscopy (MS) and optical emission spectroscopy (OES), both techniques were used in this research.

For analysis using ICP-OES, the atoms/ions were excited in the plasma through collision with electrons, which then emit light with different wavelengths for different elements when transitioning to a lower energy level. The emitted light was divided into different lines based on wavelength and analyzed in the optical chamber. The light intensities of different wavelengths were quantified in the detector array to yield concentrations for each element in the sample. On the other hand, for ICP-MS, the atoms in the sample were ionized into cations and anions. Then the cations were divided based on their mass to charge ratio (m/z) in a quadrupole mass filter, only one m/z will be allowed to pass through the mass spectrometer. After going through the mass filter, the cations strike the electron multiplier detector in a sequence to yield a mass spectrum, where the intensity of the detected cations are plotted against the m/z ratios. The intensity of the given mass is proportional to the concentrations of isotopes at that mass (Singh, 2016; Thompson & Walsh, 1989).

In this study, ICP-MS was used to measure transition metal ion concentrations such as nickel, copper and iron as ICP-MS is more sensitive and has a lower detection limit compared with ICP-OES. Total dissolved sulphur content in aqueous samples was measured using ICP-OES instead of ICP-MS as the determination of sulphur isotopes by ICP-MS can be severely interfered by the presence of polyatomic ions such as $O_2{}^+$ and $(OH)_2{}^+$ which shares the same

molecular weight as sulphur. In addition, ICP-MS may be insensitive for sulphur measurement as sulphur requires a relatively high ionization potential, which results in inefficient ionization in the plasma. (Amais et al., 2012). For ICP-MS analysis, a Thermo Scientific iCAP-Q quadrupole mass spectrometer was used; for ICP-OES, a Thermo iCAP6300 Duo inductively coupled plasma – optical emission spectrometer was used.

3.3.9 Contact Angle Measurement

Contact angle θ is defined as the wettability of a solid surface by a liquid, which can be represented by the Young equation, as shown in Equation (3.6).

$$\cos\theta = \frac{\gamma_{sv} - \gamma_{sl}}{\gamma_{lv}} \tag{3.6}$$

Contact angle can be calculated by knowing the surface tensions of solid in vapor (γ_{sv}) and liquid in vapor (γ_{lv}), as well as the interfacial tension between solid and liquid (γ_{sl}) (Masliyah et al., 2011). Contact angle measurement of a water droplet on a solid surface can be used to characterize the hydrophobicity of a surface. Figure 3.4 shows the schematic of contact angle in a vapor-water-solid system.

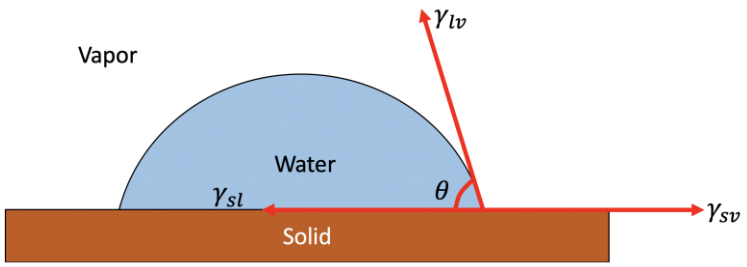

Figure 3.4 Schematic of contact angle in a vapor-water-solid system.

In this study, the static water contact angle was measured by an Attension Theta Optical Tensiometer T200 (Biolin Scientific, Stockholm, Sweden) using the sessile drop method. An approximately 6 µL water droplet was dropped on the mineral surface through a syringe, and the contact angle was calculated by analyzing the droplet shape using the Biolin software.

3.3.10 Quartz Crystal Microbalance with Dissipation (QCM-D)

Quartz crystal microbalance with dissipation (QCM-D) is an in-situ technique that allows real-time monitoring of changes in frequency and dissipation of a QCM-D sensor made of quartz crystal. This technique is widely used in studying adsorption/desorption processes, biomaterials characterization as well as cellulose nanocrystals applications (Dixon, 2008; Keleşoğlu et al.,

2012; X. Sun et al., 2014). The working principle of QCM-D was well described in many studies (Chen et al., 2016; Krasowska et al., 2018; Sedeva et al., 2010; Shrimali et al., 2017). Due to the piezoelectric effect, the quartz crystal deforms and oscillates with an alternating potential. As a result, the crystal oscillates in a resonance frequency that directly reflects the thickness of the sensor, which can be related to the mass of the sensor. In many cases, the oscillation of crystal decays or the energy of the oscillation dissipates due to soft material or water adsorbed on the sensor, an energy dissipation factor is also considered. The dissipation factor D is defined by Equation (3.7), where $E_{dissipated}$ is the energy dissipated during oscillation while E_{stored} is the energy stored during oscillation (Rodahl et al., 1995).

$$\mathrm{D} = \frac{\mathrm{E_{dissipated}}}{2\pi \mathrm{E_{stored}}} \tag{3.7}$$

The relative change in dissipation ΔD can be used to evaluate the viscoelastic characteristic and the structure property of the adsorbed layer. A large ΔD implies the adsorbed layer has a soft and loose structure while a small ΔD indicates the adsorbed layer is rigid and compact.

Therefore, QCM-D allows for both quantitative investigations on adsorption kinetics of polymers and qualitative study on the conformation of polymers through examining frequency and dissipation changes. If the sensor surface is relatively rigid and thin after the adsorption or deposition, that is the change in dissipation is less than 10^{-6} for a 10 Hz frequency change, Sauerbrey Equation can be applied to calculated the mass changed based on the changed in frequency (Sauerbrey, 1959). As shown in Equation (3.8), a linear relationship exists between the change in mass Δm and the change in frequency Δf, where *C* is the constant with a value of 17.7 ng cm^{-2} Hz^{-1}, and *n* is the harmonic overtone number (n= 1, 3, 5, …)

$$\Delta \mathrm{m} = -\frac{\mathrm{C}\Delta \mathrm{f}}{\mathrm{n}} \tag{3.8}$$

If the adsorbed layer is non-rigid and formed a viscoelastic film on the sensor surface, the change in dissipation would be significant, Voigt model can be used to describe the shift in frequency and dissipation (Voinova et al., 1999).

In this study, a Q-sense Analyzer (E4, Biolin Scientific, Gothenburg, Sweden) was employed to investigate the surface evolution of millerite-coated sensor at pH 12. The experiment was performed at room temperature ($\mathrm{T} = 22℃$). The frequency and dissipation change were collected by software Q-sense Qsoft 401. After experiments, the data analysis was carried out using Q-sense Qtools 3.0.

Chapter 4 Selective Depression of Millerite by Polysaccharides in Alkaline Solutions in Cu-Ni Sulphides Flotation Separation

4.1 Introduction

Natural polysaccharides have been applied as depressants in mineral industry for decades, studies on the specific application of polysaccharide as depressant in the Cu-Ni sulphide mineral flotation were rarely reported in the literature (Laskowski & Nyamekye, 1994; Nyamekye & Laskowski, 1991). Xu et al. (2011) carried out a preliminary laboratory flotation study using a copper-rich ore samples with 0.23% millerite and 1.14% pentlandite, and the results showed that dextrin and starch had a better ability to depress nickel content in copper concentrate than cyanide, yet the interaction mechanism was not fully understood, which might require more study using pure mineral samples (Xu et al., 2011).

In this chapter, micro-flotation tests using pure mineral were carried out to examine the feasibility of using dextrin to separate xanthate-treated millerite from chalcopyrite in an alkaline environment. The impact of dextrin and xanthate adsorption on the surface hydrophobicity of millerite and chalcopyrite was studied by static contact angle measurement. The surface chemistry of millerite and chalcopyrite with and without dextrin was studied by X-ray photoelectron spectroscopy (XPS) to understand the interaction mechanism between dextrin and mineral surface. The surface oxidation of millerite and chalcopyrite was quantified by mineral dissolution and EDTA extraction tests. The adsorption behaviour of dextrin was also visually inspected by atomic force microscopy (AFM) topography imaging to complement the flotation results. Furthermore, the adsorption behavior of dextrin on millerite and chalcopyrite with and without the presence of potassium ethyl xanthate (KEX) at alkaline pH was characterized through bulk adsorption tests and electrokinetic study. A preliminary dextrin adsorption study using a millerite-coated sensor by quartz crystal microbalance with dissipation (QCM-D) was carried out. This study provides a viable and feasible depression strategy for millerite while floating chalcopyrite using dextrin as a representative of polysaccharide. The goal of this chapter is to elucidate the interaction mechanism between dextrin and millerite in the presence of xanthate, in order to pave the way for the potential application of other novel organic depressants to enhance Cu/Ni separation.

4.2 Experimental

4.2.1 Micro-flotation Test

Prior to each test, approximately 1.5 g of -75+38 μm fraction millerite or chalcopyrite was cleaned ultrasonically using ultrasonic bathing in Milli-Q water for 5 minutes to reduce surface oxidation. For mixed flotation, an artificial mixture of chalcopyrite and millerite with a weight ratio of 1:1 was used, millerite and chalcopyrite were cleaned separately by sonication to avoid interaction at this stage. The sample was decanted and 150 mL pH-adjusted water with a KEX concentration of 10^{-5} M was added to the mineral sample. For the mixed mineral flotation, millerite and chalcopyrite were added together and the pulp was gently smeared by pestle in a mortar to ensure proper mixing and contact in the presence of KEX. The conditioning time with KEX was 5 minutes. After conditioning with KEX, dextrin was added to achieve the desired concentration and pulp was conditioned for another 5 minutes. The pulp pH was adjusted constantly by sodium hydroxide or hydrochloric acid to be maintained at pH 9 or pH 12 during the conditioning stage. The flotation lasted for 5 minutes, and ultra-high purity nitrogen (99.998%, Praxair Inc.) was used to generate bubbles in the Hallimond tube with a flowrate of 30 standard cubic centimetres per minute (sccm). The nitrogen flow rate was controlled by a gas mass flowmeter (Cole – Parmer). Each condition was repeated at least three times.

For the single mineral flotation, the recovery was calculated using Equation (4.1).

$$\text{Recovery}(\%) = \frac{\text{Mass of concentrate}}{\text{Mass of concentrate} + \text{Mass of tailing}} * 100\% \quad (4.1)$$

For mixed flotation, the Cu and Ni grades were calculated using Equations (4.2) and (4.3), where millerite and chalcopyrite compositions in the concentrate were obtained by analyzing the chemical compositions of concentrates using XRF.

$$\text{Cu grade in concentrate } (\%) = \text{Cu wt\% in chalcopyrite} * \text{Chalcopyrite \% in concentrate} * 100\% \quad (4.2)$$

$$\text{Ni grade in concentrate } (\%) = \text{Ni wt\% in millerite} * \text{Millerite \% in concentrate} * 100\% \quad (4.3)$$

Subsequently, the Cu and Ni recoveries were calculated using Equations (4.4) and (4.5) and the separation efficiency on the Cu/Ni flotation was obtained using Equation (4.6).

$$\text{Cu recovery } (\%) = \frac{\text{Mass of conc} * \text{Cu grade in conc}}{\text{Mass of conc} * \text{Cu grade in conc} + \text{Mass of tail} * \text{Cu grade in tail}} * 100\% \quad (4.4)$$

$$\text{Ni recovery (\%)} = \frac{\text{Mass of conc} * \text{Ni grade in conc}}{\text{Mass of conc} * \text{Ni grade in conc} + \text{Mass of tail} * \text{Ni grade in tail}} * 100\% \quad (4.5)$$

$$\text{Separation Efficiency (\%)} = \text{Cu recovery to concentrate} - \text{Ni recovery to concentrate} \quad (4.6)$$

4.2.2 Contact Angle Measurement

Pieces of high purity millerite and chalcopyrite samples were embedded in non-conductive epoxy resins (West System) in a circular mould with a diameter of 30 mm. For millerite, the cleaved surface was exposed. Prior to each test, the mineral sample in the resin was polished sequentially using 600, 800, and 1200 grits silicon carbide (SiC) sandpapers (Buehler), followed by the polishing cloth with 9 μm and 3 μm diamond suspensions, and 0.05 μm alumina suspension (Buehler) to obtain a fresh and smooth surface. After polishing, the mineral surface was cleaned by sonication for 5 minutes to remove polishing suspensions and was rinsed thoroughly using Milli-Q water. The mineral was then immersed in pH 9 or pH 12 solution with 10^{-4} M KEX and/or 1 ppm dextrin for 5 minutes or 30 minutes. For mineral conditioned with both KEX and dextrin, the mineral was first exposed to KEX solution for 5 minutes then conditioned with dextrin for another 5 minutes. After conditioning, the mineral surface was rinsed by Milli-Q water and dried by high purity nitrogen before measuring the contact angle. At least five measurements were obtained for each condition, and the average was reported.

4.2.3 X-ray Photoelectron Spectroscopy (XPS) Analysis

For each test, approximately 1 g of +38-75 μm mineral sample was cleaned by sonication for 5 minutes and then conditioned in 150 mL solution with desired dextrin concentration for 1 hour. For the mineral conditioned with both KEX and dextrin, the mineral was first conditioned with 100 μM KEX for 30 minutes and then conditioned with dextrin for another 1 hour. After conditioning, the mineral particles were washed by Milli-Q water thoroughly to remove any residual dextrin or KEX that was loosely attached to the mineral surface due to settlement. The water was decanted, and the mineral particles were vacuum dried in the freeze-dryer until the test in order to prevent oxidation. For the nickel hydroxide and dextrin complex, 0.5 g of nickel hydroxide was mixed with 500 mL 1000 ppm dextrin solution and was conditioned for 1 hour. After conditioning, the nickel hydroxide power was thoroughly washed by water and vacuum dried until the test.

4.2.4 Mineral Dissolution Test and EDTA Extraction Analysis

For each test, approximately 1 g of -38 μm mineral particles were mixed with 50 mL solution with desired pH and KEX concentration, the pulp was then conditioned in an incubator shaker (Eppendorf New Brunswick Innova 42) for 1 hour at 300 rpm, 22 ℃. The particles and water were then separated by a 0.22 μm membrane filter. The filtrate was then analyzed for mineral dissolution. The metal concentration was analyzed by ICP-MS and the sulfate concentration was analyzed using barium chloride turbidimetric method (Thermo Gallery Plus Beermaster Autoanalyzer). The filtered mineral particles were freeze-dried and analyzed by ethylenediaminetetraacetic acid (EDTA) extraction method to quantify oxidised species on the mineral surface following a procedure well described in Rumball & Richmond (1996). For the EDTA extraction, 3% w/w EDTA solution was adjusted pH 9 by NaOH which was then purged with nitrogen for at least two hours to ensure no dissolved oxygen in the solution. The filtered mineral particle was then added to the 250 mL purged EDTA solution. The EDTA extraction lasted for three hours to ensure all metal hydroxide species were extracted from the surface, and the EDTA solution was constantly purged by nitrogen during the extraction stage to prevent mineral oxidation. After extraction, the EDTA solution was sent for ICP-MS analysis. All analysis results were normalized by the masses of the samples tested.

4.2.5 Atomic Force Microscope (AFM) Imaging

A freshly cleaved millerite surface was first glued onto a silicon wafer. Prior to each test, the mineral surface was cleaned by sonication for 5 minutes in Milli-Q water and dried with high purity nitrogen. After cleaning, the mineral surface was conditioned in the dextrin solution with a desired concentration for 20 minutes. A piece of high purity chalcopyrite sample was first embedded in epoxy resin. Prior to each test, the chalcopyrite surface was polished following the procedure described in Section 4.2.2. For chalcopyrite conditioned with 10^{-4} M KEX and 10 ppm dextrin, chalcopyrite was first conditioned in KEX solution for 5 minutes and then conditioned with dextrin for another 20 minutes. All conditionings were conducted at pH 12. After conditioning, the mineral surface was rinsed thoroughly by Milli-Q water and dried by high purity nitrogen before being transferred immediately to the AFM chamber for the experiment. The surface topography images of the mineral surface were acquired in Milli-Q water.

4.2.6 Bulk Adsorption Test

For each test, approximately 1 g of -38 μm mineral particles were mixed with 50 mL solution with desired pH and 50 ppm dextrin, the pulp was then conditioned in an incubator shaker (Eppendorf New Brunswick Innova 42) for 1 hour at 300 rpm at the room temperature. For mineral conditioned with KEX only, the conditioning time was 30 minutes. For the mineral conditioned with both KEX and dextrin, the mineral was first conditioned with 100 ppm KEX for 30 minutes and then conditioned with 50 ppm dextrin for another 1 hour. After conditioning, the pulp was taken out and the final pH was measured and recorded as the pH reported. The mineral particle and the supernatant were then separated using a centrifuge (Sorvall WX80) at 10,000 rpm for 10 minutes. The supernatant was then assayed for residual dextrin and/or KEX concentrations using the UV-Vis-NIR spectrophotometer (Shimadzu UV-3600). For measuring dextrin concentrations, the supernatant was digested to an orange color solution using sulfuric acid-phenol method, and then the absorbance was measured at 490 nm (Dubois et al., 1956). For the sulfuric acid-phenol method, 4 mL supernatant was mixed with 1.5 mL of 5% w/w phenol solution and 10 mL sulphuric acid. While for residual KEX concentration, the supernatant was diluted 10 times with Milli-Q water and then the absorbance was measured at 301 nm (Pomianowski & Leja, 1963). Dilution can help eliminate the effect of dextrin's presence on measuring absorbance at 301 nm for xanthate for samples conditioned with both KEX and dextrin. On the other hand, impact of KEX was negligible on the measurement of dextrin's absorbance at 490 nm, thus the samples were not diluted when measuring dextrin's absorbance (Afenya, 1982; Nyamekye, 1993).

4.2.7 Zeta-potential Measurement

Electrokinetic study was employed to investigate dextrin's interaction with millerite and chalcopyrite by measuring the zeta potential of mineral particles with and without dextrin at room temperature. For each measurement, approximately 0.02 g -38 um mineral particle was ground with 5 mL of 0.01 M KCl with desired dextrin concentration and pH for 2 minutes. The ground particles were then mixed with another 15 mL 0.01 M KCl to form a 20 mL pulp sample. The pulp pH was then adjusted, and the sample was placed in the shaking incubator and conditioned for 30 minutes at 300 rpm, 22℃ to allow the adsorption of dextrin to reach equilibrium. After that, approximately a 4 mL aliquot was transferred into a glass cuvette for zeta-potential measurement.

4.2.8 Quartz Crystal Microbalance with Dissipation (QCM-D)

Prior to each experiment, the flow module and connection tubes were sonicated in 2 wt% sodium dodecyl sulfate (SDS) solution and Milli-Q water, each for 30 minutes to remove any contaminants, and blow-dried by high purity nitrogen. The millerite sensor was first sonicated in Milli-Q water for 5 minutes to remove any surface oxidations and then was blow-dried by nitrogen. The contact angle of the sensor was immediately measured right after the sonication. The sensor was then mounted in the QCM-D module and put in the chamber ready for the test. For a typical test, pH 12 Milli-Q water adjusted using sodium hydroxide was pumped into the chamber as the background solution using an IPC-N peristaltic pump (Ismatec, Switzerland) at a flow rate of 0.15 mL/min for at least 5 minutes; then 10^{-4} M KEX was injected first followed by 100 ppm dextrin. During the experiment, the pH of all solutions was constantly adjusted to maintain at pH 12. Whenever the solution needed to be changed the pump was stopped to prevent introducing air bubbles into the QCM-D module, and the sensor was always rinsed by the background solution for at least 10 minutes after KEX or dextrin solutions. After the experiment, the sensor was taken out and dried by nitrogen, contact angle of the sensor was measured again.

4.3 Results and Discussion

4.3.1 Dextrin Characterization

4.3.1.1 Molecular Weight Distribution of Dextrin

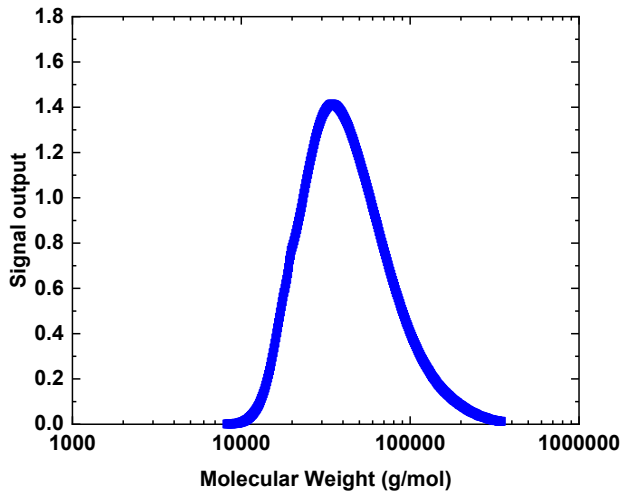

Figure 4.1 Molecular weight distribution of dextrin.

The molecular weight distribution of dextrin was obtained by using gel permeation chromatography (GPC), in which the detailed procedure is given in Appendix A. Figure 4.1 shows the molecular weight distribution of dextrin. The weight average molecular weight of dextrin was 45754 Da and the number average molecular weight was 28828 Da; the polydispersity index was 1.59. The GPC result revealed that dextrin is a relatively low molecular weight polysaccharide compared with starch or CMC.

4.3.1.2 Diffuse Reflectance Infrared Fourier Transform (DRIFT) Spectrum

Diffuse reflectance infrared Fourier transform (DRIFT) spectrum was used to identify dextrin's structure. Detailed procedure is described in Appendix A. Figure 4.2 shows the diffuse reflectance infrared Fourier transform (DRIFT) spectrum of the corn dextrin. The dextrin's monomer structure was identified by some important peaks. The hydroxyl functional group and C-H/C-H_2 stretchings were located at peaks above 3000 cm^{-1} and peaks above 2000 cm^{-1} respectively. The peak at 1150 cm^{-1} represents the C-O-C stretching of the glucopyranose ring and the peaks at 930 cm^{-1} and 765 cm^{-1} represent the glucopyranose ring vibration. Note that there is no peak around 1500 cm^{-1} which implies dextrin does not carry carboxylic acid functional group (Moreira et al., 2017; Tang & Liu, 2012).

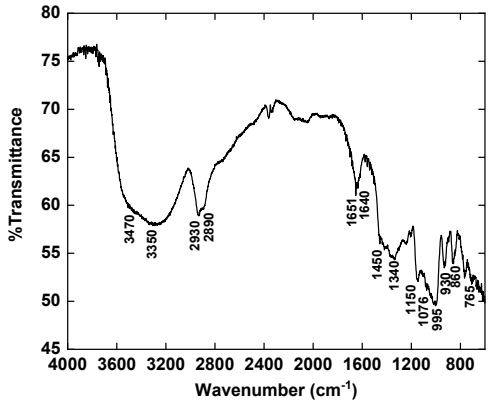

Figure 4.2 DRIFT spectrum of dextrin.

4.3.1.3 XPS Analysis

Figure 4.3 (A) shows the survey scan of the corn dextrin used in this study. Based on the survey scan, the C/O ratio was 1.58, indicating the carbon content was slightly higher while the

oxygen content was slightly lower compared with the theoretical value due to the inevitable adventitious carbon contamination during sample preparation and measurement (Stevens & Schroeder, 2009). Narrow scans of C 1s and O 1s were also decupled and analyzed. Detailed peak parameters including binding energy, full width at half maximum (FWHM), and the corresponding chemical state (peak assignment) can be found in Appendix B.

Figure 4.3 (B) shows the narrow scan of C 1s, where the most dominant peak at 286.3 eV was hydroxyl functional group (C-O), and the peak at 284.8 eV represented C-C, C-H bond. The peak with the highest binding energy at 287.7 eV represents the carbon bonded to the oxygen in the glucopyranose ring and to the oxygen in the glycosidic linkage (O-C-O). The ratio of C-O to O-C-O based on C 1s spectrum was 4.0 which was consistent with the theoretical value. (Beamson & Briggs, 1993; Stevens & Schroeder, 2009) Figure 4.3 (C) shows the O 1s spectrum with two bonds at 532.46 eV and 533.2 eV, which are C-O in the hydroxyl functional group and O-C-O bond, respectively (Amaral et al., 2005; Beamson & Briggs, 1993; S. Liu et al., 2017; Stevens & Schroeder, 2009). The XPS spectra of dextrin confirmed the monomer of dextrin has an α-D-glucose structure by identifying both the hydroxyl functional group as well as the glycosidic linkage.

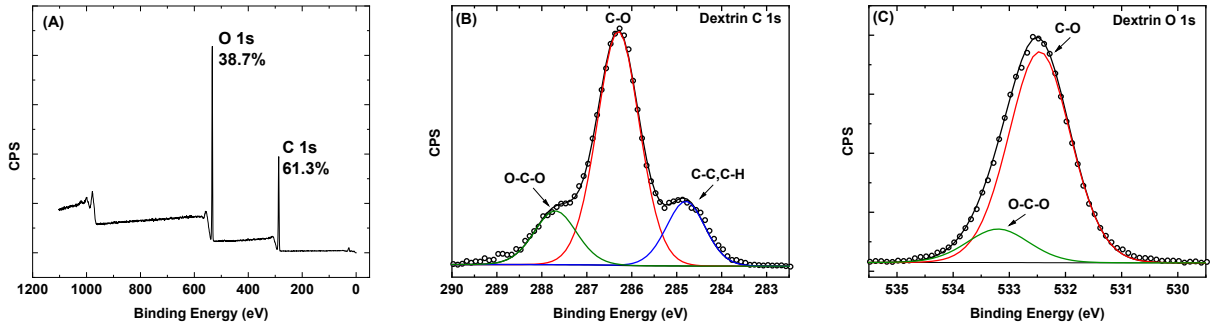

Figure 4.3 XPS spectra of (A) survey scan and narrow scans of (B) C 1s and (C) O 1s of dextrin.

4.3.2 Flotation with Xanthate and Dextrin

Figure 4.4 (A) shows the single mineral flotation recoveries of chalcopyrite and millerite as a function of pulp pH in the presence of 10^{-5} M KEX with and without 1 ppm dextrin. Chalcopyrite was very floatable with KEX from pH 4 to pH 12, which was consistent with previous studies (Q. Liu & Zhang, 2000; Zhang, 2015). Upon the addition of 1 ppm dextrin, chalcopyrite only responded slightly to dextrin at pH 9, where the recovery dropped from 97% to

82%. Millerite was floatable after being treated with xanthate from pH 4 to pH 9. Millerite was quite floatable from pH 4 to pH 9. Previous surface wettability study of millerite by AFM bubble probe technique concluded that bubble attachment to millerite was favored under acidic pH (L. Feng, 2019). Millerite's recovery was 84% at pH 9, which was similar to the value reported by Smith et al. (2011). Under acidic pH, dextrin had a limiting depressing effect on millerite flotation. However, millerite recoveries dropped from 84% to 23%, and from 48% to 16% at pH 9 and pH 12, indicating millerite was efficiently depressed by dextrin at alkaline pH. In addition to pulp pH, the effect of dextrin's concentrations on millerite and chalcopyrite recoveries at pH 9 and pH 12 was also studied, and the results are shown in Figure 4.4 (B). At pH 12, 0.5 ppm dextrin was sufficient to depress millerite flotation, where the recovery dropped to 20%. The depressing effect was similar as the concentration of dextrin was increased to 5 ppm. On the other hand, dextrin has a limiting depressing effect on chalcopyrite flotation, in the presence of 0.5 ppm dextrin, chalcopyrite's recovery was still 90%, implying xanthate-treated chalcopyrite did not interacted with dextrin. When the dextrin dosage was increased to 5 ppm, chalcopyrite's recovery only decreased to 77% and 82% at pH 9 and pH 12, respectively. Therefore, xanthate-treated millerite and chalcopyrite responded differently to dextrin, especially at alkaline pH. With a precise control in dextrin's dosage and pulp pH, it seemed promising to achieve selectivity in the mixed flotation with a precise control of the pulp pH and dextrin dosage.

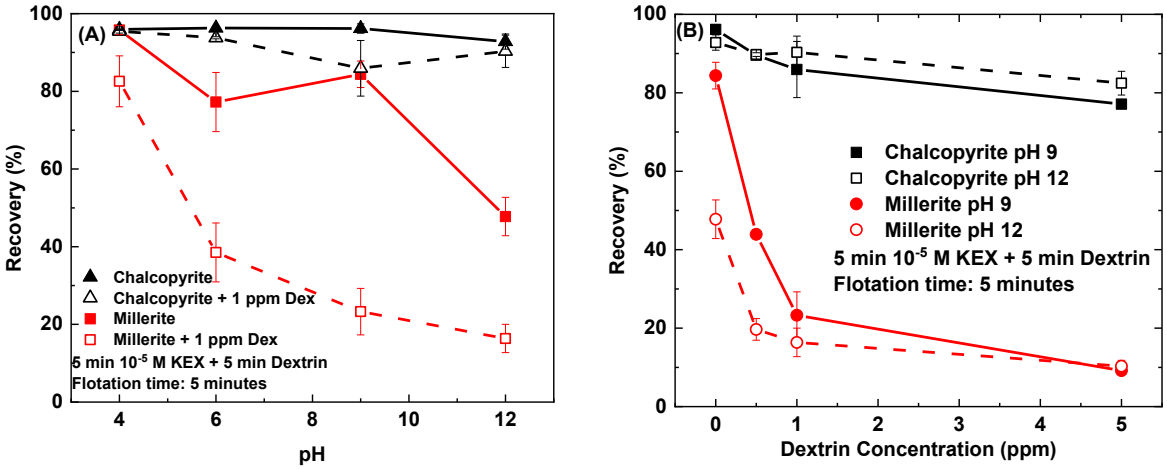

Figure 4.4 Single mineral flotation recoveries of chalcopyrite and millerite (A) as a function of pH in the presence of 10^{-5} M KEX with and without 1 ppm dextrin addition and (B) as a function of dextrin concentration at pH 9 and pH 12 with 10^{-5} M KEX.

Figure 4.5 (A) and (B) show the mixed flotation recoveries and metal grades of copper and nickel in the concentrate as a function of dextrin concentration at pH 9 and pH 12, respectively; where Figure 4.5 (C) depicts the Ni recovery versus Cu recovery that summarized the results at both pH 9 and pH 12. At pH 9, selectivity was enhanced with Ni recovery being depressed yet the copper recovery was also slightly compromised as the dextrin concentration was higher than 1.5 ppm. The optimum dosage of dextrin was 2 ppm where the separation efficiency increased to 63.6%, by a difference of 49.5% when comparing with no dextrin added. At pH 12, a separation window can be found at a dextrin dosage of 0.5 ppm without compromising Cu recovery. The Ni recovery was not depressed more as the dextrin concentration was higher than 0.5 ppm. With a dextrin dosage of 0.5 ppm, the separation efficiency was increased to 79.0% by a difference of 39.3% when compared with no dextrin added. In addition to the depression of Ni recovery, Ni grade in the Cu concentrate also reduced at both pH 9 and pH 12. Therefore, dextrin was a suitable depressant for millerite in Cu-Ni flotation, the selectivity between millerite and chalcopyrite was greatly dependent on the pulp pH and dextrin's dosages.

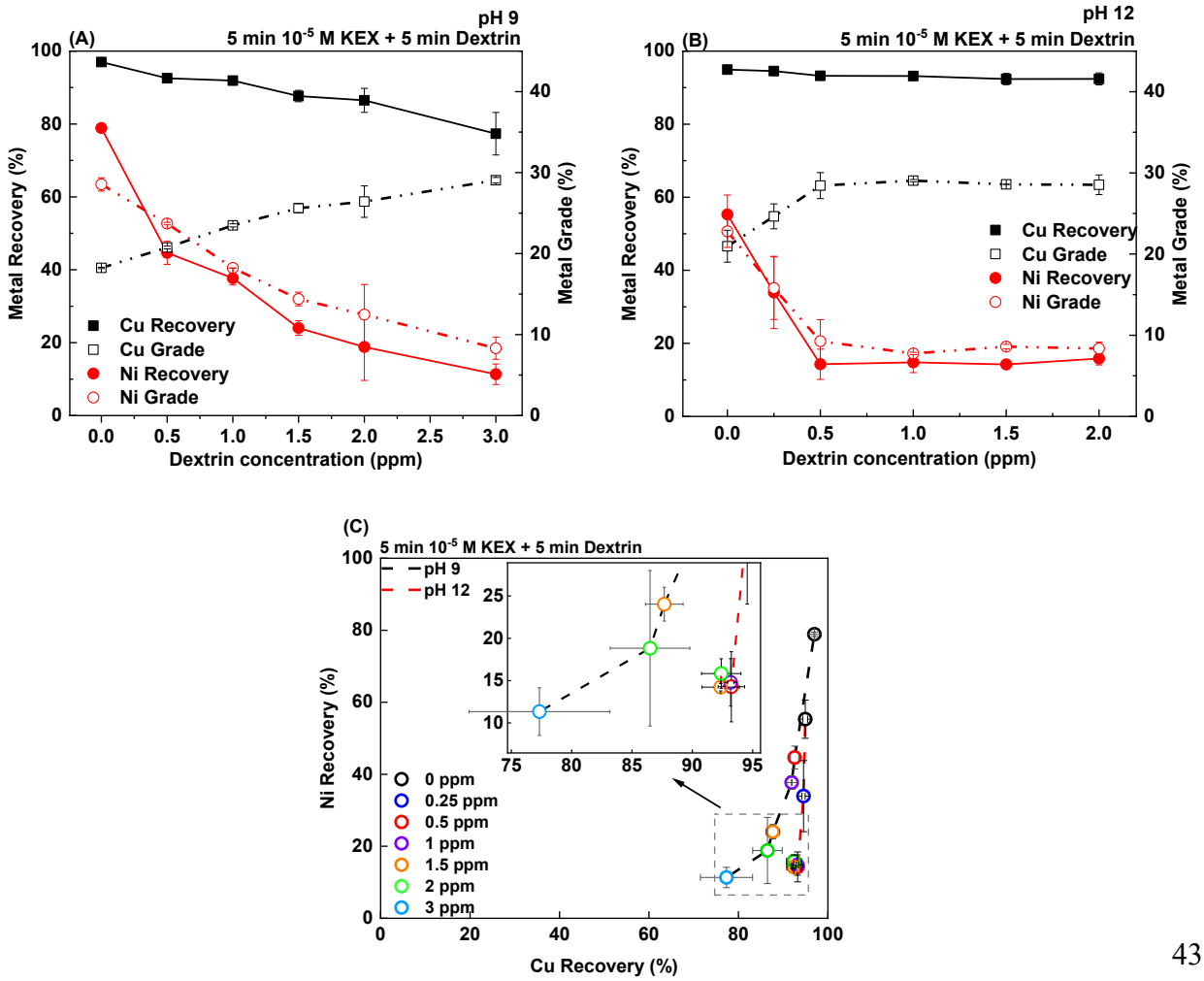

Figure 4.5 Copper and nickel recoveries and grades of mixed mineral flotation of chalcopyrite and millerite as a function of dextrin concentration at (A) pH 9 and (B) pH 12 with 10^{-5} M KEX; (C) Ni recovery vs. Cu recovery at different dextrin concentrations at pH 9 and pH 12.

4.3.3 Contact Angle Measurement

Contact angles of millerite and chalcopyrite were measured to examine the effects of pH, xanthate and dextrin on the surface hydrophobicity. Figure 4.6 shows the static contact angle in the presence of KEX and/or dextrin at pH 9 and pH 12, respectively. Millerite's surface hydrophobicity was more sensitive to pH and conditioning time than chalcopyrite. Increasing pH or the conditioning time lowered the hydrophobicity of millerite surface. An increase in contact angle was observed after conditioning the millerite surface with KEX while the contact angle dropped upon the addition of dextrin, this confirmed that both KEX and dextrin can adsorb on millerite surface, KEX can render millerite surface more hydrophobic while dextrin can render millerite surface more hydrophilic. If millerite was conditioned with KEX first then conditioned with dextrin, the contact angle was lower than that conditioned with KEX solely, especially at pH 12 where the contact angle was similar to that conditioned with dextrin only, implying dextrin can still adsorb on xanthate-treated millerite at both pH 9 and pH 12. Chalcopyrite also responded similarly to KEX and dextrin. However, when chalcopyrite was treated with KEX first then with dextrin, the contact angle remained similar to that conditioned with KEX solely, implying dextrin did not affect the surface hydrophobicity of xanthate-treated chalcopyrite. Therefore, the static contact angle measurement indicated that in the presence of xanthate, dextrin can lower the surface hydrophobicity of millerite but not chalcopyrite, which supported the micro-flotation test results.

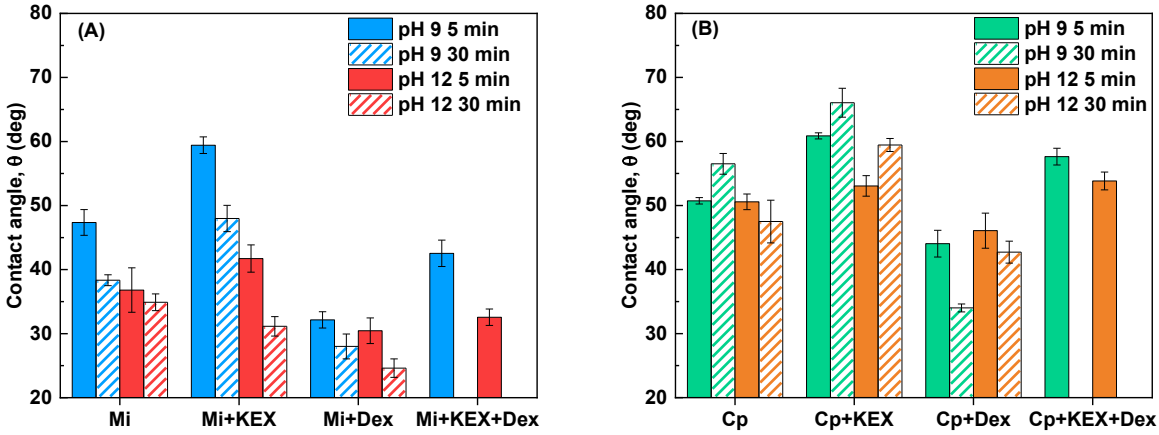

Figure 4.6 Static contact angles of (A) millerite and (B) chalcopyrite at pH 9 and pH 12 conditioned for 5 minutes and 30 minutes under conditions: Mi or Cp, Mi or Cp conditioned with KEX, Mi or Cp conditioned with dextrin, and Mi or Cp conditioned with KEX and dextrin (concentration of KEX was 10^{-4} M and concentration of dextrin was 1 ppm).

4.3.4 XPS Analysis

To further reveal the surface chemistry of millerite and chalcopyrite upon adsorption of dextrin, X-ray photoelectron spectroscopy (XPS) was used to analyze the surface chemistry of millerite and chalcopyrite upon the addition of dextrin at pH 12. Detailed peak fitting parameters including binding energy, full width at half maximum (FWHM), and the corresponding chemical state (peak assignment) of C 1s, O 1s and Ni $2p_{3/2}$ spectra are given in Appendix B.

4.3.4.1 Chalcopyrite

Three conditions were studied for chalcopyrite-dextrin interaction at pH 12: 0 ppm dextrin (baseline), 10 ppm dextrin, 10^{-4} M KEX and 10 ppm dextrin. Figure 4.7 shows the fitted spectra of C 1s and O 1s of chalcopyrite surfaces under three different conditions. For C 1s of chalcopyrite pH 12 baseline, the spectrum mainly represented the adventitious carbon, which was fitted into three different peaks. The peak at 284.8 eV represents C-C, the peak at 286.3 eV represents the alcohol group, and the peak at 288.4 eV was the carboxylic acid functional group (Yuan et al., 2019). Upon the addition of dextrin, a minor new peak at 287.7 eV appeared, which represented the O-C-O linkage in the dextrin. In addition, the intensity of the C-O bond at 286.3 eV increased slightly, confirming the presence of dextrin on chalcopyrite surface, yet the

spectrum was still dominated by the C-C peak at 284.8 eV, which indicated only a slight adsorption of dextrin. When chalcopyrite was conditioned with KEX and dextrin, the O-C-O linkage was not observed, and the C 1s spectrum still represented the adventitious carbon similar to the baseline, indicating negligible dextrin adsorption at pH 12.

Three peaks were found for the O 1s spectrum of the baseline, which were located at 530.0 eV, 531.6 eV and 533 eV; these three peaks are for oxide, hydroxide and adsorbed water, respectively (Acres et al., 2010; Fairthorne et al., 1997; Huang et al., 2012; Kalegowda et al., 2015; Moreira et al., 2017; Yin et al., 2000). When conditioned with dextrin, two more peaks appeared in addition to the adsorbed water, which were located at 532.7 eV and 533.5 eV, representing the oxygen in the hydroxyl group (C-O) and the oxygen in the glucopyranose ring and the glycosidic linkage (O-C-O). The intensity of C-O bond was lower than that of the adsorbed water, indicating that the proportion of dextrin adsorbed was insignificant compared with other species on chalcopyrite surface. When chalcopyrite was conditioned with KEX and dextrin, the spectrum was identical to the baseline, indicating negligible dextrin adsorption. It is well known that ethyl xanthate can have a strong chemical interaction with fresh chalcopyrite surface, resulting in the formation of both dixanthogen and cuprous ethyl xanthate that renders the surface hydrophobic (Kalegowda et al., 2015; Leppinen, 1990; Leppinen et al., 1989; J. A. Mielczarski et al., 1996, 1998). Hydrophilic oxide or hydroxide product such as iron hydroxide can be removed with the adsorption of xanthate, which can then prevent dextrin's adsorption by possibly eliminating the adsorption sites available for dextrin. Based on the XPS analysis, when chalcopyrite was conditioned with xanthate first then with dextrin at pH 12, no peaks of dextrin adsorption were observed, indicating that dextrin adsorption became negligible.

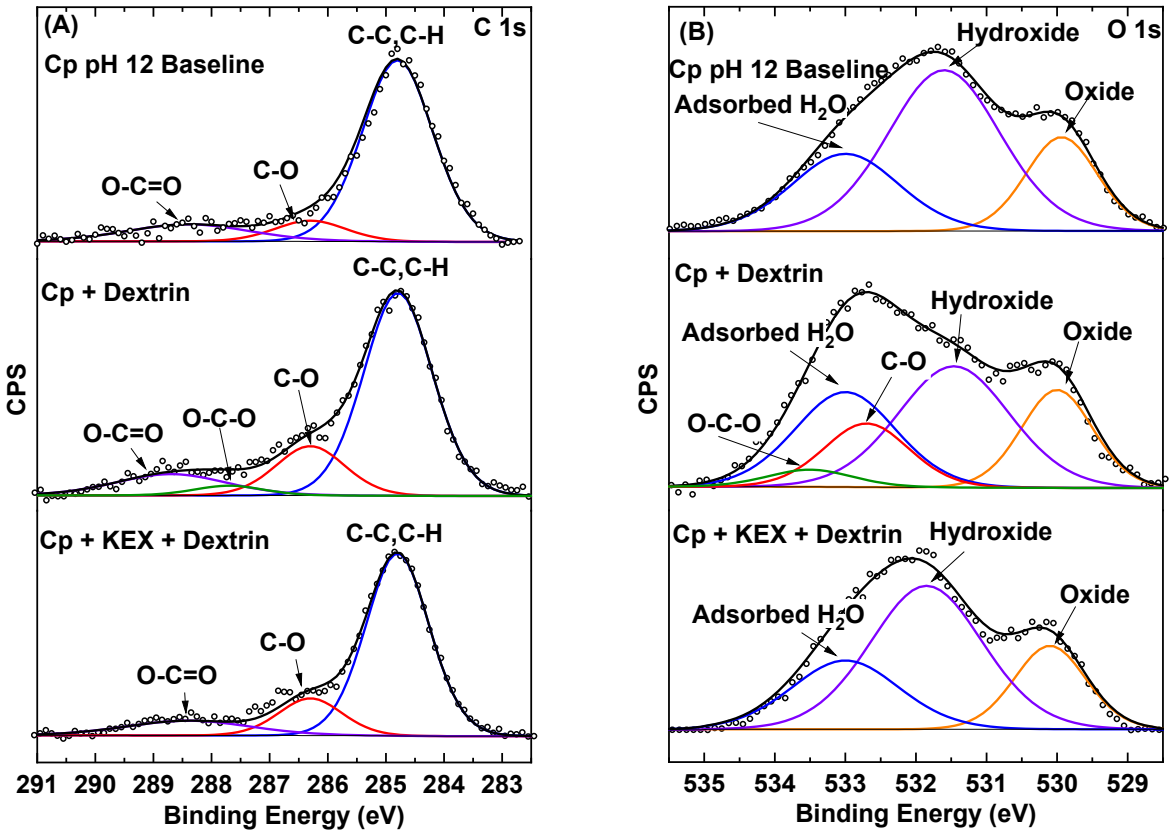

Figure 4.7 XPS narrow scans of (A) C 1s and (B) O 1s of chalcopyrite surface conditioned with (i) collectorless condition, (ii) 10 ppm dextrin and (iii) 10^{-4} M KEX first then 10 ppm dextrin at pH 12.

4.3.4.2 Millerite

Compared with chalcopyrite, millerite responded differently to dextrin at pH 12. Figure 4.8 shows the fitted C 1s, O 1s and Ni $2p_{3/2}$ spectra of millerite surfaces under three different conditions (baseline, 10 ppm dextrin, 10^{-4} M KEX and 10 ppm dextrin) as well as $Ni(OH)_2$-dextrin complex.

The C 1s spectrum of pH 12 baseline mainly exhibited the adventitious carbon. The fitting of adventitious carbon was discussed with chalcopyrite C 1s spectrum. Upon the addition of dextrin, the intensity of peak at 286.4 eV increased significantly, which represents C-O. The intensity of the peak located at 287.8 eV also increased, which represented the O-C-O linkage. The ratio of proportions of C-O to O-C-O here was 4.2, which was comparable to that of the dextrin. The carboxylic functional group was observed at 288.7 eV which might be due to the

adventitious carbon contamination. When KEX was introduced, the intensity of C-O bond decreased, which implied slightly less dextrin adsorption due to xanthate adsorption.

In addition, O 1s spectra were also analyzed and the deconvolution results are shown in Figure 6 (B). For the pH 12 baseline, the spectrum was deconvoluted into three peaks located at 531.1 eV, 532 eV and 533 eV, which represented hydroxide, sulphate and the adsorbed water (Biesinger et al., 2009, 2011; Legrand et al., 1998; Qi, Liu, et al., 2019; Richardson & Vaughan, 1989). As shown in the O 1s spectrum, the millerite surface was dominated by $Ni(OH)_2$ at pH 12. When millerite was conditioned with 10 ppm dextrin, the adsorbed water at 533 eV was replaced by two new peaks that appeared at 532.7 eV and 533.5 eV, representing the hydroxyl group and the O-C-O linkage, respectively; this implies that dextrin adsorbed on millerite surface through the hydroxyl functional group on millerite. When comparing the peak locations of the conditioned millerite against dextrin, energy shifts of 0.24 eV and 0.3 eV towards higher binding energy were observed for the C-O peak and O-C-O peak, respectively, which implies a chemisorption process. The O 1s spectrum of millerite surface conditioned with both KEX and dextrin was identical to the one that was only conditioned with dextrin, indicating dextrin can still adsorb on millerite with xanthate adsorbed on the surface at pH 12. Note that the intensity of the sulphate peak decreased with the addition of KEX, implying that the adsorption of KEX affected surface oxidation.

In order to verify millerite surface was dominated by $Ni(OH)_2$ at pH 12, the Ni $2p_{3/2}$ spectra were also analyzed and shown in Figure 4.8 (C). For Ni $2p_{3/2}$ spectrum, each main peak was accompanied by a satellite peak, but only the main peaks are discussed here (Biesinger et al., 2009, 2011; Legrand et al., 1998; Mansour, 1994b, 1994a; Mansour & Melendres, 1994; Richardson & Vaughan, 1989). The most intense peak at 855.4 eV represented $Ni(OH)_2$, indicating the millerite surface was dominated by $Ni(OH)_2$ at pH 12, which was consistent with the previous XPS analysis on the millerite (Zhao, 2019). The less-intense peak around 853.1 eV represented the bulk nickel monosulphide, while the peaks at 856.5 – 857.5 eV represented nickel sulphoxy species formed due to surface oxidation. When xanthate was present, the peak intensity of $Ni(OH)_2$ dropped slightly relative to the nickel monosulphide peak, indicating that the adsorption of xanthate reduced the amount of $Ni(OH)_2$ on the millerite surface, yet the passivation layer still dominated the surface at pH 12. Consequently, dextrin can still adsorb on the xanthate-treated millerite surface.

To further illustrate dextrin-millerite interaction at pH 12, $Ni(OH)_2$ – dextrin complex was prepared and examined by XPS analysis, and the C 1s, O 1s and Ni $2p_{3/2}$ spectra of $Ni(OH)_2$ – dextrin complex are shown in Figure 4.8. The C 1s spectrum was similar to that of the dextrin powder with the most intensive peak being C-O peak instead of C-C/C-H peak, implying that adventitious carbon became insignificant and a complex formed between $Ni(OH)_2$ and dextrin. The O 1s spectrum was similar to the mineral-dextrin one, the C-O peak became more intense relative to the peak for $Ni(OH)_2$. The same energy shift of 0.24 eV was observed for C-O peak, which was consistent with that of the mineral-dextrin system.

To summarize, XPS analysis depicts that dextrin adsorb on millerite surface by interacting with $Ni(OH)_2$ site on the millerite surface at pH 12, the energy shift of the hydroxyl group of dextrin implying dextrin adsorption on millerite was a chemisorption process. A chemical complex formation mechanism was proposed for such interaction between sulphide mineral and dextrin (Laskowski et al., 2007; Q. Liu et al., 2000; Q. Liu & Laskowski, 1989a; Nyamekye & Laskowski, 1993; Rath & Subramanian, 1999; Subramanian & Natarajan, 1988). By comparing the spectra of millerite and chalcopyrite with KEX adsorbed on surface, millerite can still adsorb a significant amount of dextrin, which was not observed for chalcopyrite. This is because millerite was dominated by the passivation layer composed of $Ni(OH)_2$ even in the presence of xanthate, where such site for dextrin adsorption was significantly reduced on xanthate-treated chalcopyrite surface.

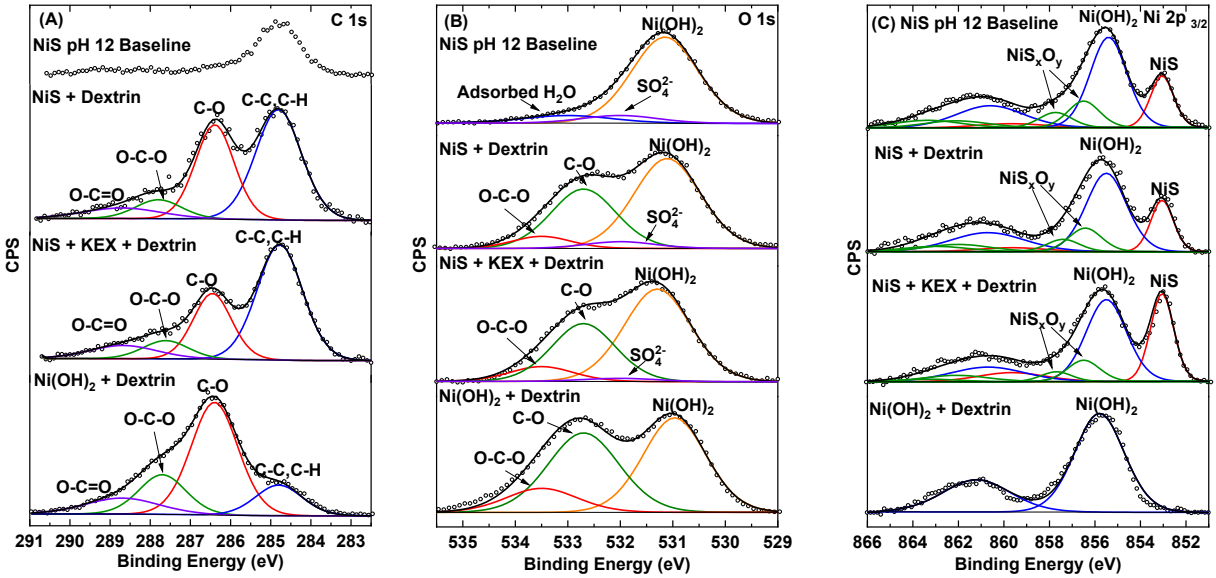

Figure 4.8 XPS narrow scans of (A) C 1s, (B) O 1s and (C) Ni 2p $_{3/2}$ of millerite surface conditioned with (i) collectorless condition, (ii) 10 ppm dextrin, (iii) 10^{-4} M KEX first then 10 ppm dextrin and the $Ni(OH)_2$-dextrin complex at pH 12.

4.3.5 Mineral Dissolution Test and EDTA Extraction Analysis

In aqueous solution, sulphide mineral usually undergoes surface oxidation as described in Equation (4.7),

$$MS + \frac{1}{2}nO_2 + nH_2O \rightarrow M_{1-n}S + nM(OH)_2 \tag{4.7}$$

which results in a metal-deficient, sulphur-rich surface and the formation of metal hydroxide. The metal hydroxide can precipitate and adsorb on mineral surface (Fullston et al., 1999; Gardner & Woods, 1979; Smart et al., 2003). Based on this, millerite and chalcopyrite oxidation were quantified through metal ion and sulphate dissolution as well as EDTA extraction test under alkaline pH with and without KEX to elucidate the enhanced selectivity between millerite and chalcopyrite in the presence of dextrin.

EDTA is a strong chelating reagent that can form complex with heavy metal ions, which can be used to extract metal hydroxides on sulphide minerals surface to quantitatively examine the oxidation species on mineral surface (Clarke et al., 1995; Rumball & Richmond, 1996). The mechanism is that EDTA can only dissolve metal hydroxide but not metal sulphide. Table 4.1 shows stability (formation) constants K_f of Ni (II) – EDTA and Cu (II) – EDTA complexes (Rumball & Richmond, 1996) as well as the solubility product constants pK_{sp} of millerite and various copper sulphide minerals (Shea & Helz, 1989; Speight, 2005; D. Wang & Hu, 1987). As the stability constants of Ni-EDTA and Cu-EDTA are larger than the solubility constants of millerite and chalcopyrite, indicating the dissolution of sulphide mineral by EDTA is strongly unfavoured.

Table 4.1 Stability constant K_f of Ni (II) – EDTA and Cu (II) – EDTA complexes at 20°C and 0.1 M ionic strength (Rumball & Richmond, 1996) and Solubility product constant pK_{sp} of millerite and various copper sulphide minerals at 25°C (Shea & Helz, 1989; Speight, 2005; D. Wang & Hu, 1987).

	Ni (II) - EDTA	Cu (II) - EDTA
K_f	18.62	18.8

Minerals	Millerite, β-NiS	Chalcopyrite, $CuFeS_2$	Cu_2S	Covellite, CuS*
pK_{sp}	24 – 24.9	61.5	47.6 – 48.5	22.27

*: This value was adapted from Shea & Helz (1989)

Table 4.2 shows the millerite dissolution as well as EDTA extraction as the pH was increased from pH 9 to pH 12 with and without the addition of KEX. The amount of nickel dissociated from millerite decreased dramatically as the pH was increased from pH 9 to pH 12 while nickel hydroxide species that formed on millerite surface increased. Under alkaline environment, nickel that dissociated from millerite might immediately adsorb back as $Ni(OH)_2$ on millerite surface to form a passivation layer. Hence, the millerite surface was dominated by such passivation layer at pH 12, which confirmed the XPS result. The sulphate concentration decreased as the pH was increased from pH 9 to pH 12, which might be due to the passivation layer of $Ni(OH)_2$ preventing the sulphur from oxidising into sulphate and be released into the solution as the pH is increased. Upon the addition of KEX, sulphate in the solution and Ni dissociated from lattice significantly decreased at pH 9. Previous studies suggested that ethyl xanthate can form complex with the dissociated nickel ion and adsorb on millerite surface via chemisorption (L. K. Smith et al., 2011; Zhao, 2019). As a result, the amount of nickel hydroxide species slightly decreased at both pH 9 and pH 12, indicating that KEX adsorption reduces the hydrophilic passivation layer. Table 4.3 shows the chalcopyrite dissolution as well as EDTA extraction of Cu and Fe oxide/hydroxide species at pH 9 and pH 12 with and without KEX. The sulphate concentration for chalcopyrite was lower than that of millerite. Also, both copper and iron oxide/hydroxide formation and precipitation were less than the $Ni(OH)_2$ formation and precipitation on millerite, which might be due to the solubility product constant for millerite was

much larger than chalcopyrite. Upon the addition of KEX, EDTA-extractable Cu and Fe further decreased. It can be seen that chalcopyrite is more "stable" and cannot be easily oxidized in aqueous solution (Fullston et al., 1999). Millerite is more prone to oxidation and dissolution than chalcopyrite under alkaline pH, a remarkable difference lied in the amount of metal hydroxide species between millerite and chalcopyrite. Millerite surface was dominated by the $Ni(OH)_2$ passivation layer. Therefore, it is hypothesized that dextrin adsorption on millerite is facilitated by the $Ni(OH)_2$ passivation layer, even for the xanthate-treated millerite; while much less metal hydroxide species on xanthate-treated chalcopyrite results in less adsorption of dextrin, thus less depression effect.

Table 4.2 Millerite dissolution (Ni, SO_4) and EDTA extractable nickel under alkaline pH with and without KEX. (KEX concentration: 100 ppm)

Condition	Mineral Dissolution (ppm)		EDTA Extraction - Ni ($\times 10^{-6}$ mol/m^2)
	Ni	SO_4	
pH 9	16.6	75.7	95.9
pH 11.6	0.04	67.8	111.5
pH 12	0.0009	62.9	116.2
pH 9 + KEX	0.04	50.4	72.2
pH 12 + KEX	0.0015	64.7	91.5

Table 4.3 Chalcopyrite dissolution (Cu, Fe and SO_4) and EDTA extractable copper and iron under alkaline pH with and without KEX. (KEX concentration: 100 ppm)

Condition	Mineral Dissolution (ppm)			EDTA Extraction ($\times 10^{-6}$ mol/m^2)	
	Cu	Fe	SO_4	Cu	Fe
pH 9	0.018	0.095	30.4	7.84	21.7
pH 12	0.024	0.540	31.6	5.73	22.4
pH 9 + KEX	0.007	0.200	24.2	2.10	25.1
pH 12 + KEX	0.010	0.278	49.4	2.72	26.9

4.3.6 AFM Imaging

Topography imaging by AFM was used to visually inspect the adsorption of dextrin on millerite and chalcopyrite at pH 12. Figure 4.9 shows the SEM images of a cleaved millerite surface under different magnifications. The cleaved surface was smooth and could be used to perform AFM imaging without further polishing.

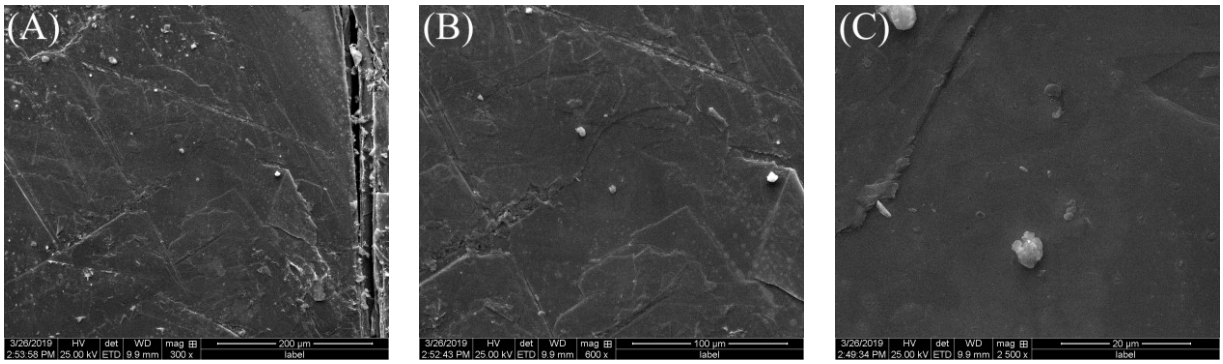

Figure 4.9 SEM images of a freshly cleaved millerite surface under (A) 300×, (B) 600× and (C) 2500× magnifications.

The AFM height and phase images of millerite surface conditioned with 0, 10, 50 and 100 ppm dextrin over an area of $2 \times 2\ \mu m^2$ are shown in Figure 4.10. Height image demonstrates the surface topography while phase image indicates whether the adsorbed material is hard or soft (Sedeva et al., 2010). The corresponding root-mean-square (RMS) roughness and the peak-to-valley (PTV) values are shown in Table 4.4. When no dextrin was added (Figure 4.10 (A)), the roughness was the lowest, showing a fairly smooth surface. Millerite treated with 10 ppm dextrin clearly showed a distinctive pattern (Figure 4.10 (B)). The adsorbed dextrin clearly formed randomly sized aggregates on the entire millerite surface examined, indicating a significant amount of dextrin adsorbed on the millerite surface. Both the surface roughness and PTV value increased significantly after conditioning with dextrin. When dextrin's concentration was increased to 50 ppm and 100 ppm (Figure 4.10 (C – D)), films of the adsorbed dextrin were observed as the size of the aggregates became more uniform. Meanwhile, both the roughness and the peak to valley value decreased compared with 10 ppm, implying that a more compacted and uniform film of adsorbed dextrin was detected on the millerite surface at a higher concentration of dextrin.

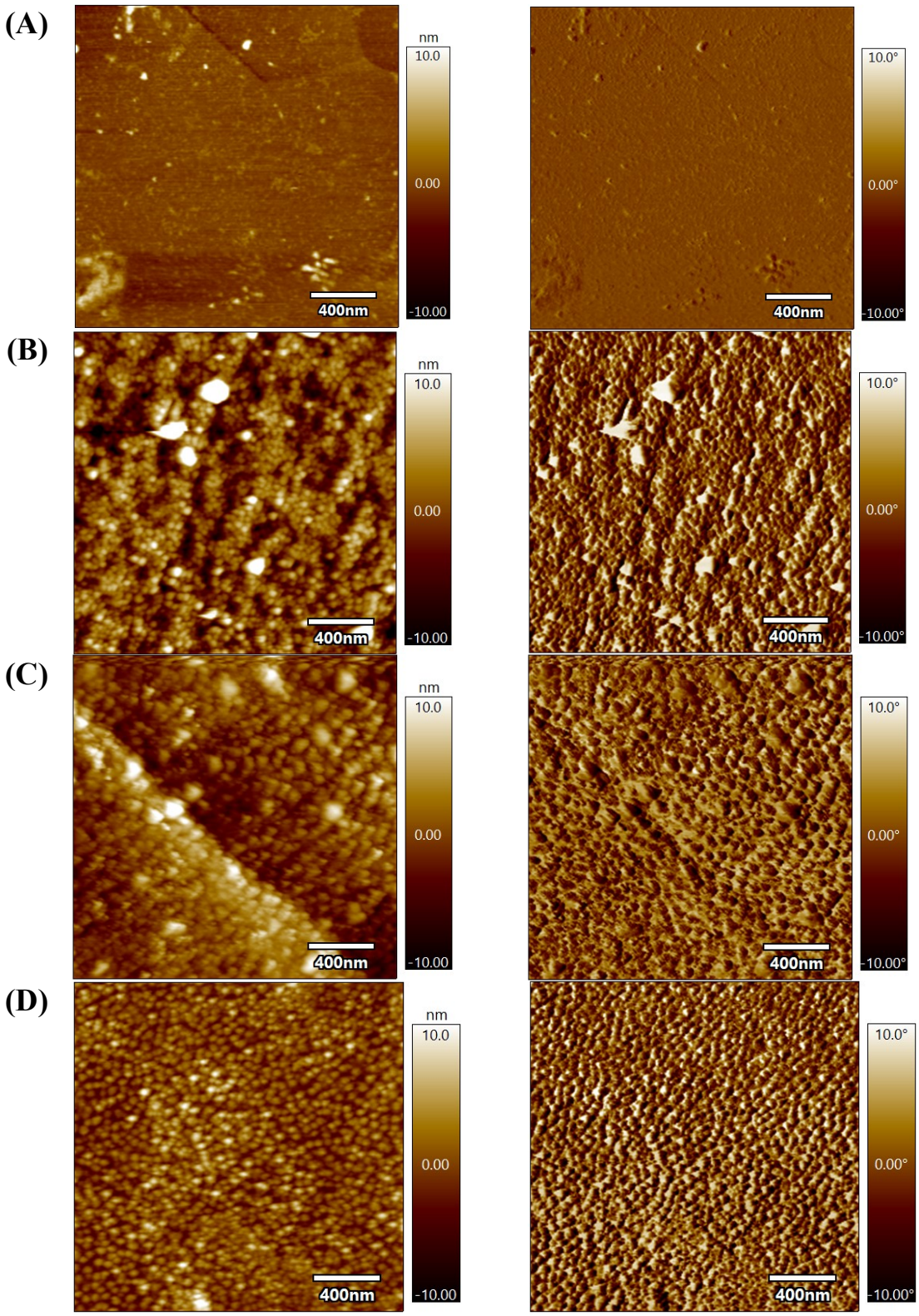

Figure 4.10 AFM height (left) and phase (right) images (2×2 μm^2) of millerite surface conditioned with (A) 0 ppm, (B) 10 ppm, (C) 50 ppm, and (D) 100 ppm dextrin, and

chalcopyrite surface conditioned with (E) 0 ppm dextrin and with (F) 10^{-4} M KEX and 10 ppm dextrin at pH 12.

Table 4.4 Roughness and peak-to-valley value for millerite surface conditioned with various dextrin concentrations at pH 12.

Dextrin Concentration (ppm)	RMS roughness (nm)	Peak-to-valley value (nm)
0	1.14	20.4
10	4.04	57.3
50	2.93	22.1
100	2.18	19.5

In order to verify the negligible adsorption of dextrin on xanthate-treated chalcopyrite at pH 12, both the unconditioned chalcopyrite surface and the chalcopyrite surface conditioned with 10^{-4} M KEX and 10 ppm dextrin were examined, and the results are shown in Figure 4.11. Based on both height and phase images, no significant adsorption of dextrin was observed for xanthate-dextrin-treated chalcopyrite. Similar surface roughness was obtained for the fresh and the conditioned chalcopyrite surfaces, which were 2.59 nm and 2.66 nm, respectively. Hence, the AFM imaging results demonstrated the insignificant dextrin adsorption for xanthate-treated chalcopyrite at pH 12, which supported the XPS result.

(A)

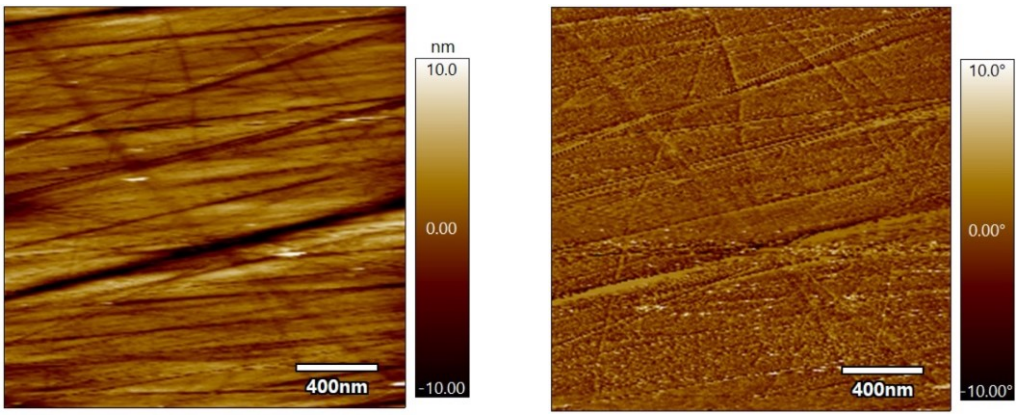

(B)

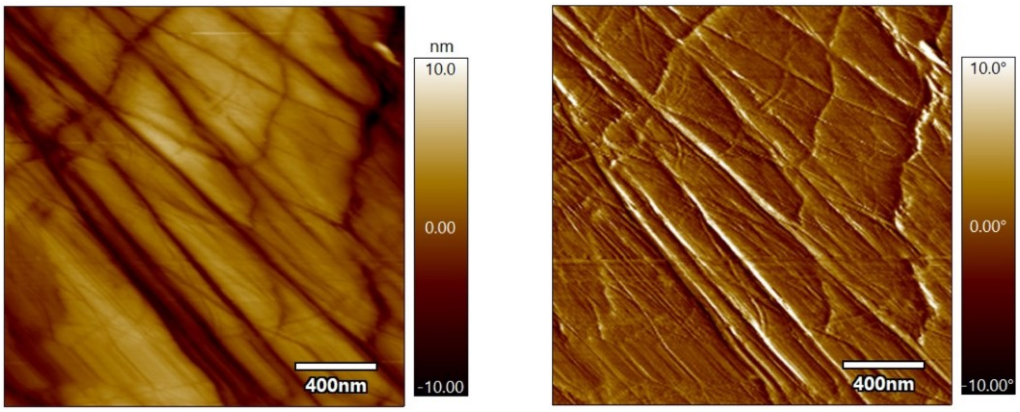

Figure 4.11 AFM height (left) and phase (right) images (2×2 μm^2) of chalcopyrite surface conditioned with (A) 0 ppm dextrin, (B) 10^{-4} M KEX and 10 ppm dextrin at pH 12.

4.3.7 Bulk Adsorption Test

4.3.7.1 Dextrin Adsorption Test versus pH with and without KEX

The adsorption kinetics of dextrin onto millerite and chalcopyrite was studied at pH 9 and pH 12. As shown in Figure 4.12, the adsorption of dextrin on millerite reached equilibrium faster at pH 12 than pH 9. Based on the results, it can be seen that dextrin's adsorption onto both minerals reached equilibrium within one hour. Hence, one hour was set as the optimal conditioning time for all adsorption tests.

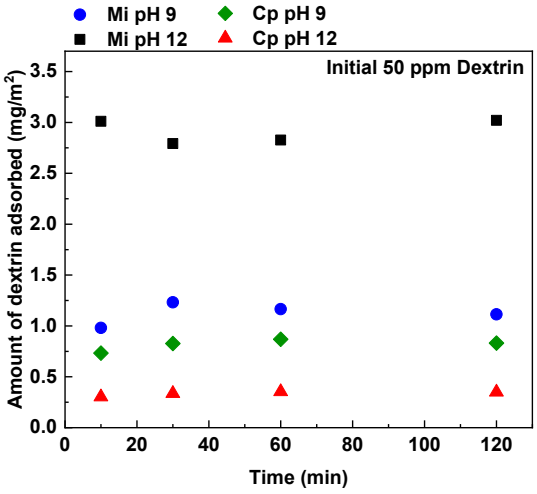

Figure 4.12 Adsorption kinetics of dextrin on millerite and chalcopyrite at pH 9 and pH 12.

The amount of dextrin's adsorption on millerite and chalcopyrite as a function of pH with and without KEX is shown in Figure 4.13 (A). Dextrin adsorbed more on millerite than

chalcopyrite over the pH ranged from 9 to 12 when only dextrin was present. For millerite, dextrin adsorption was strongly dependent on pH, where the maximum adsorption was around pH 11.5, dextrin adsorbed more on millerite at pH 12 than pH 9. For chalcopyrite, the adsorption was less pH-dependent and the maximum adsorption located around pH 9 and then gradually decreased as pH increased, which was consistent with previous findings (Q. Liu & Laskowski, 1989c). When the pulp was conditioned with KEX then dextrin was added, the adsorption of dextrin on millerite was inhibited by the presence of KEX, which implied dextrin and xanthate adsorbed through different surface sites, and the adsorption of xanthate reduced the sites available for dextrin adsorption. For chalcopyrite, dextrin adsorption was similar to the one without the KEX addition except at pH 12 where dextrin adsorption was nearly negligible if conditioned with KEX first, which supported the XPS analysis result. Even with the presence of KEX, the amount of dextrin adsorption on millerite was still higher than that on chalcopyrite. Adsorption of KEX was also studied in parallel to the dextrin adsorption tests. Figure 4.13 (B) shows the xanthate adsorption on millerite and chalcopyrite with and without dextrin as a function of solution pH. For both minerals, xanthate adsorption decreased as pH was increased; when conditioned with xanthate first then with dextrin, xanthate adsorption was not affected, indicating that xanthate that already adsorbed on the mineral surface did not desorb upon the addition of dextrin. To summarize, at pH 12, dextrin can adsorb on xanthate-treated millerite but not xanthate-treated chalcopyrite.

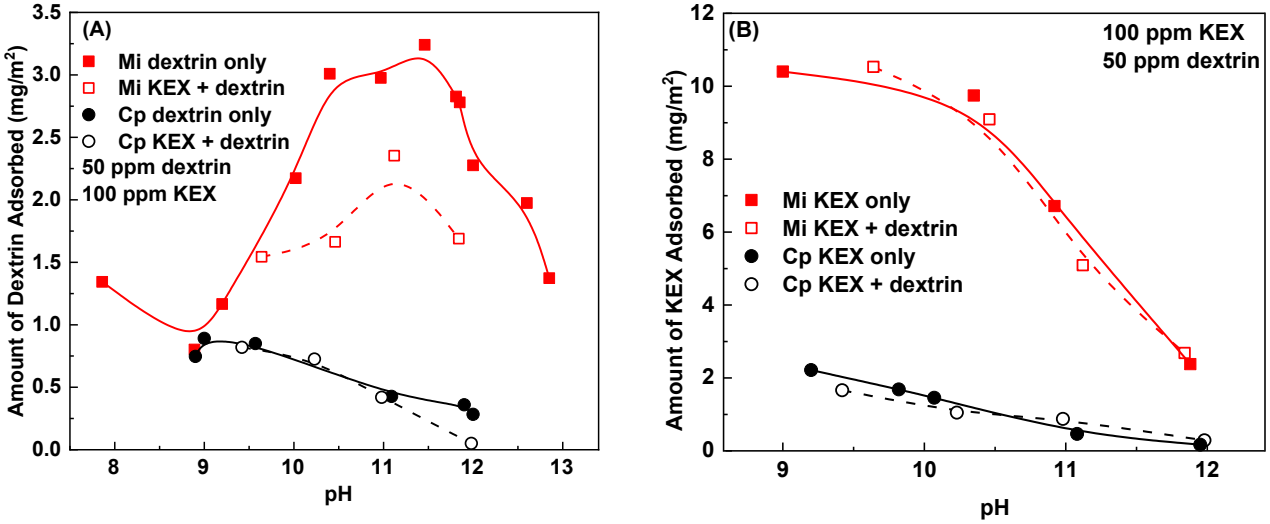

Figure 4.13 Amount of (A) dextrin and (B) KEX adsorbed on millerite and chalcopyrite as a function of pH; when both KEX and dextrin were present, mineral particle was first

conditioned with KEX for 30 minutes then conditioned with dextrin for 1 hour (initial dextrin concentration: 50 ppm; initial KEX concentration: 100 ppm).

4.3.7.2 Dextrin Adsorption Isotherm

Adsorption isotherm for dextrin adsorption on millerite and chalcopyrite at pH 9 and pH 12 were developed and shown in Figure 4.14. The isotherms were fitted with both Langmuir model (solid line) and Freundlich model (dashed line). Langmuir model is suitable for chemisorption process, which describes a monolayer homogeneous adsorption. According to the Langmuir model, a monolayer adsorption could be achieved at the maximum adsorption, the adsorption is homogenous on the localized adsorption sites on the surface while the adsorption energy between adsorbate and each of the adsorption sites on the adsorbent is the same; in addition, negligible interactions between the adsorbed species is assumed (Afenya, 1982; Langmuir, 1918; Raju et al., 1997; J. Wang & Guo, 2020). Langmuir isotherm is displayed in Equation (4.8), where the term q_e refers to amount of dextrin adsorbed, C_e is the dextrin concentration at equilibrium, q_{max} is the saturation amount that can be adsorbed, and K_L is the Langmuir equilibrium constant.

$$\mathrm{q_e} = \frac{\mathrm{q_{max} K_L C_e}}{1+\mathrm{K_L C_e}} \tag{4.8}$$

Freundlich model, shown in Equation (4.9), is an empirical model that characterize multilayer adsorptions on heterogeneous surfaces, where q_e refers to the amount of dextrin adsorbed, C_e refers to the dextrin concentration at equilibrium. Parameters K_F and n refer to as the Freundlich capacity factor and Freundlich intensity parameter (Li et al., 2019; Matias et al., 2015; Taffarel & Rubio, 2009).

$$\mathrm{q_e} = \mathrm{K_F C_e^{\frac{1}{n}}} \tag{4.9}$$

Table 4.5 shows the fitting parameters for both Langmuir and Freundlich models, and Figure 4.15 compares the determination coefficient R^2 of the Langmuir and Freundlich models. For millerite, two models yielded similar fitting results. For chalcopyrite, Freundlich model gave a better fitting, especially at pH 12.

For adsorption of dextrin, the Gibbs free energy of adsorption ΔG°_{abs} can be calculated using Equation (4.10), where K_a is the dimensionless thermodynamic equilibrium constant, R is the gas constant and T is the temperature (Gaudin & Fuerstenau, 1976). As dextrin is a non-ionic

polysaccharide that only carries weak charge in water, the activity coefficient of dextrin in water can be approximated to be unity. As a result, K_L can be used to estimate ΔG°_{abs} as shown in Equation (4.11) (Y. Liu, 2009), and the estimated results are shown in Table 4.5.

$$\Delta G^{\circ}_{abs} = -RTlnK_a \tag{4.10}$$

$$\Delta G^{\circ}_{abs} = -RTlnK_a \approx -RTln\left[K_L\left(1\frac{mol}{L}\right)\right] = -RTlnK_L \tag{4.11}$$

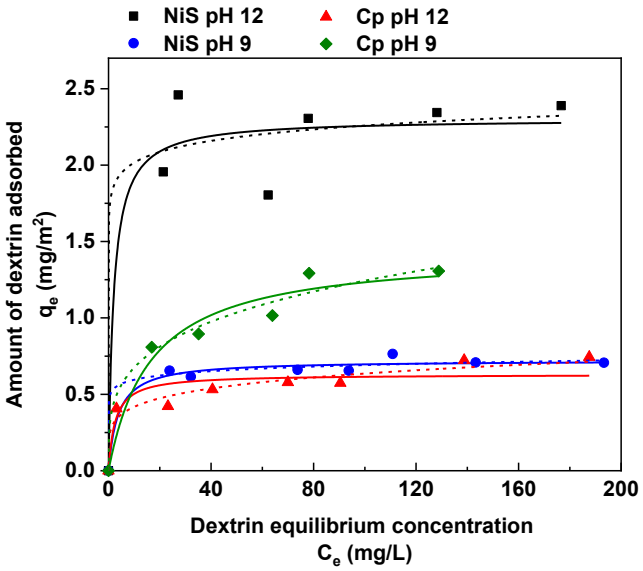

Figure 4.14 Dextrin adsorption isotherms for millerite and chalcopyrite at pH 9 and pH 12; solid line represent Langmuir isotherms and dashed line represent Freundlich isotherms.

Table 4.5 Fitted parameters of Langmuir model and Freundlich model of the dextrin adsorption isotherm for millerite and chalcopyrite at pH 9 and pH 12.

Isotherm	Langmuir model			Estimated free energy of adsorption based on K_L	Freundlich model		
	q_{max}	K_L	R^2	ΔG°_{abs}	K_F	n	R^2
	$(mg \cdot m^{-2})$	$(L \cdot m^{-1})$		$(kCal \cdot mol\ monomer^{-1})$	$(mg^{1-\frac{1}{n}} \cdot L^{\frac{1}{n}} \cdot m^{-2})$		
NiS pH 12	2.302	0.489	0.914	-6.62	1.799	20.241	0.918
NiS pH 9	0.722	0.269	0.976	-6.27	0.512	15.338	0.979
Cp pH 12	0.630	0.394	0.828	-6.49	0.274	5.481	0.954
Cp pH 9	1.436	0.061	0.954	-5.39	0.366	3.766	0.970

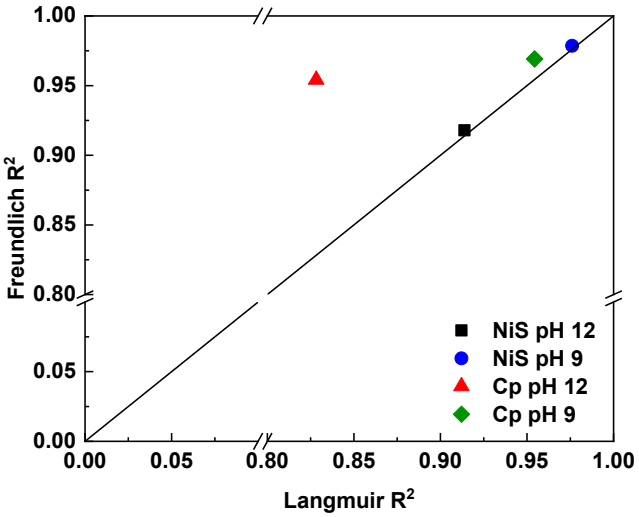

Figure 4.15 Comparison of the determination coefficient R^2 of Langmuir model and Freundlich model.

4.3.8 Electrokinetic Study

The zeta potential of millerite conditioned under various dextrin concentrations from pH 4 to pH 12 were examined and are shown in Figure 4.16 (A). Usually, for an non-oxidised sulphide mineral in the "pristine" state, the zeta potential should be negative as pH is greater than 2, where the IEP is located between pH 1 and pH 2 similar to that of an elemental sulfur (Fornasiero et al., 1992; Fullston et al., 1999; Gaudin & Fuerstenau, 1976). This is likely due to dissolution of metal ion under acidic pH, resulting in a metal-deficient, sulphur-rich surface.

However, two isoelectric points (IEP) were observed for millerite when no dextrin was added, first lied at pH 6.5 and the second was located at pH 11.7, which has a similar trend with the previous study carried out by Acar & Somasundaran (1992). The zeta potential that reversed from negative to positive at pH 6.5 indicated the formation of nickel oxide/hydroxide product on millerite's surface as the IEPs for nickel oxide and nickel hydroxide are located at both pH 10.3 and pH 11.5 (Acar & Somasundaran, 1992; Nyamekye & Laskowski, 1993). The IEP at pH 11.7 was very close to the IEP of nickel hydroxide implied the existence of a layer of nickel hydroxide on millerite surface under alkaline pH. Similar phenomenon was observed for zeta potential of pyrite and chalcopyrite conditioned with oxygen, for which an IEP was observed around pH 6 and pH 7 which resembled the existence of ferric hydroxide on the sulphide mineral surface (Fairthorne et al., 1997; Jin et al., 2021). Hence, the zeta-potential of millerite has a pattern for an oxidized sulphide mineral with metal hydroxide covering the surface (X. Wang et al., 1989b). The zeta potential of dextrin versus pH can be found in Appendix A. Although dextrin is a non-ionic polysaccharide, it carries slightly negative charge in water due to the dissociation of protons from the hydroxyl functional groups, the charge becomes more negative as pH increases (Moreira et al., 2017; Sedeva et al., 2010; Tang & Liu, 2012). Upon the addition of dextrin, the magnitude of the zeta potential of millerite decreased, and the decrease in the magnitude of millerite zeta potential was dependent on the dextrin's concentration. At 20 ppm dextrin, both IEPs disappeared and the millerite surface charge from pH 9 to pH 12 resembled that of dextrin. This confirms dextrin's adsorption onto millerite as the adsorption of macromolecule usually drives the Stern plane further away from the surface, thus lower the magnitude of the zeta potential (Nyamekye & Laskowski, 1993; Subramanian & Laskowski, 1993). The segments on dextrin that interacted with adsorbing sites on mineral surface can form "trains" and the rest part of dextrin formed "loops". This kind of conformation has an impact on the magnitude of mineral surface charge. As the concentration of dextrin is increased, the "loops" extend and lower the magnitude of mineral surface charge (Eirich, 1977; Gurumoorthy & Khan, 2011; Q. Liu et al., 1994). Furthermore, the presence of dextrin not only decreased the magnitude of the zeta potential of millerite, but also shifted the IEP at pH 11.7 towards more acidic pH, and the shift in IEP was dependent on dextrin's concentration. This might supported an interesting argument that dextrin adsorption on millerite at alkaline pH is a chemisorption

process through the nickel hydroxide on millerite surface (D. W. Fuerstenau & Pradip, 2005; Pradip, 1988; Pradip et al., 1994).

Zeta potential of chalcopyrite at different dextrin concentrations is shown in Figure 4.16 (B). Chalcopyrite surface charges were negative throughout the entire pH range investigated, originating from chalcopyrite dissolution in aqueous solutions and the formation of a meta-deficient and sulphur-rich layer (Fairthorne et al., 1997; Fullston et al., 1999). The sulphur-rich layer renders chalcopyrite surface more hydrophobic and is responsible for the floatability of chalcopyrite under collectorless condition. The trend of chalcopyrite's zeta-potential was similar to an elemental sulfur's surface charge with an IEP located around pH 2, indicating that the surface metal oxide/hydroxide on chalcopyrite is not enough to increase and even reverse the surface charge, which demonstrate that chalcopyrite is stable and not prone to oxidation in aqueous solutions (Fairthorne et al., 1997; Fullston et al., 1999; R. Liu et al., 2010; Rath et al., 2001). Upon the addition of dextrin, the zeta potential of chalcopyrite shifted toward less negative, indicating the adsorption of dextrin. Moreover, zeta potential of chalcopyrite in the presence of dextrin was independent with the dextrin concentration. With either 1 ppm or 20 ppm dextrin, the zeta potential of chalcopyrite remained similar, indicating dextrin adsorption on chalcopyrite was limited, which might be due to the insufficient surface oxidation species on chalcopyrite surface.

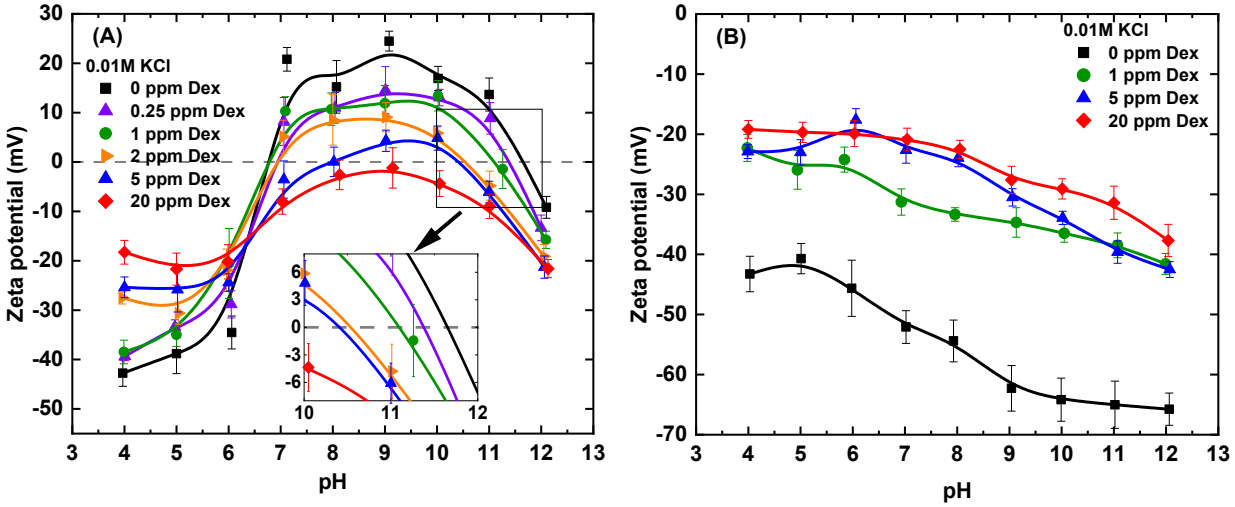

Figure 4.16 Zeta potential of (A) millerite and (B) chalcopyrite as a function of pH with various dextrin concentrations, inset of (A) amplifies the change in IEP at various dextrin concentrations.

4.3.9 Dextrin Adsorption on Millerite by QCM-D

QCM-D has been used to study the activation mechanism of sulphide minerals, adsorption of flotation reagent and interaction between nanoparticles and mineral surfaces using mineral-coated sensors for both sulphide and phosphate minerals (Deng et al., 2014; Deng, Liu, et al., 2013; Kou et al., 2010; Teng et al., 2012). In this study, a preliminary in-situ investigation by QCM-D on the dextrin adsorption on a millerite-coated sensor at pH 12 was carried out. The quartz crystal sensor coated with millerite (QSX999, Q-Sense) was custom-made with high purity millerite sample by Biolin Scientific (Gothenburg, Sweden). The sensor was preserved in a vacuum-sealed bag filled with argon gas to prevent any oxidation. The NiS sensor was characterized by XPS and details can be found in Appendix C. After 10 nm ion etching, the sensor surface exhibited an atomic ratio of Ni to S of 1.18 which was close to unity.

The frequency and dissipation changes of millerite sensor as a function of time in the presence of 10^{-4} M KEX and 100 ppm dextrin solution at pH 12 are shown in Figure 4.17, where only 3rd, 5th and 7th overtones were considered. As shown in Figure 4.17, the frequency dropped, and the dissipation factor increased as soon as pH 12 water was pumped into the flow module. The decrease in the frequency was mainly associated with the increasing thickness of millerite sensor, indicating an increase in the sensor mass. This might be because the nickel dissociated from the sensor surface formed nickel hydroxide and precipitated back on millerite surface as a passivation layer. Surface analysis by XPS indicated millerite surface can undergo oxidation in an aqueous solution; consequently, nickel hydroxide forms on millerite surface. When 10^{-4} M KEX solution was injected, there was no sudden drop in the observed frequency, indicating a negligible adsorption of KEX. The decrease in frequency and the increase in the dissipation factor at this stage might be due to the continued formation of nickel hydroxide on millerite surface. As discussed earlier, nickel hydroxide layer formed on the millerite sensor surface might inhibit xanthate adsorption. A sudden drop in frequency and an increase in dissipation were observed when 100 ppm dextrin was injected into the flow module, indicating dextrin adsorbed on millerite sensor covered with nickel hydroxide. The frequency initially dropped about 22 Hz in 2 minutes followed by another drop of 18 Hz in 50 minutes. The second phase of slower decrease in frequency may ascribe to the continued formation of nickel hydroxide passivation layer in addition to the dextrin adsorption. Finally, the millerite sensor was rinsed by background solution, the frequency and dissipation stayed the same, indicating no desorption of dextrin, and

the adsorption of dextrin on millerite was an irreversible chemisorption process. The surface hydrophobicity of millerite sensor was also characterized through the contact angle measurement. The contact angle of the sensor dropped from 43.1° to 17.7° after the QCM-D experiment. Millerite sensor became more hydrophilic after contacting with both KEX and dextrin solutions. The decrease in hydrophobicity confirmed dextrin adsorption.

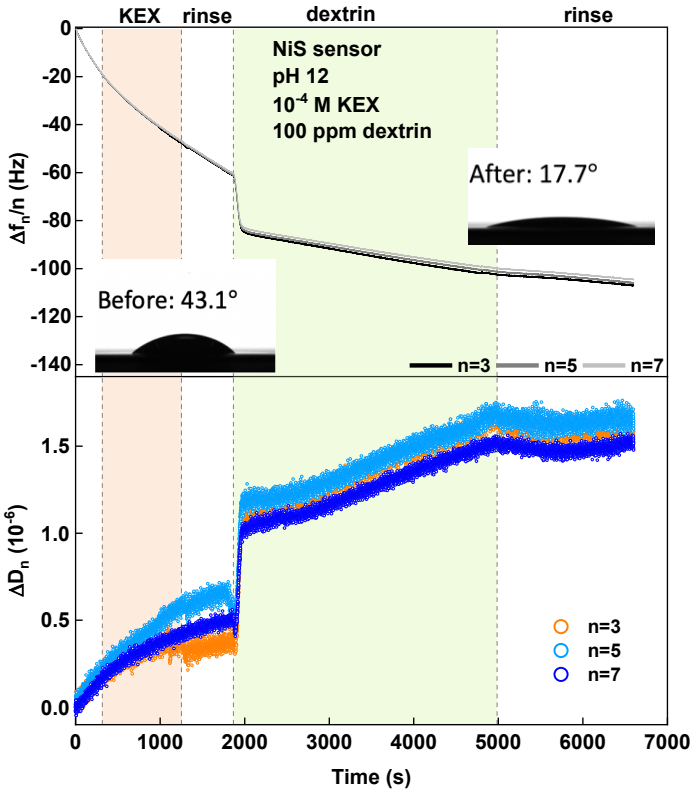

Figure 4.17 QCM-D monitoring of changes in frequency (Δf_n / n) and dissipation (ΔD_n) at 3rd, 5th and 7th overtones as a function of time for millerite sensor in the presence of 10^{-4} M KEX and 100 ppm dextrin at pH 12.

The change in dissipation per unit mass increase can be well described by plotting ΔD against Δf, so that information regarding the structure changes as well as the viscoelastic properties of the deposited layer can be obtained. For an adsorption process, if ΔD-Δf plot has a constant slope, there is no change in the conformation of the adsorbed layer. If ΔD-Δf plot shows discontinuities, that is, multiple slopes are observed on the ΔD-Δf plot, then the adsorption is a multiphase process and the adsorbed layer undergoes conformation change. Generally, a small

$\Delta D/\Delta f$ value implies a rigid and compact surface while a large $\Delta D/\Delta f$ value implies the sensor surface is relatively loose and soft (Kou et al., 2010; Rodahl et al., 1997; Sedeva et al., 2010).

Figure 4.18 (A) shows the ΔD-Δf plot for millerite sensor conditioned with pH 12 water and 10^{-4} M KEX solution, which yielded a constant slope, implying that there was no structural change on the millerite sensor. As discussed earlier, the frequency drop and the increase in dissipation at this stage was due to nickel dissolution and adsorption back to the sensor surface in the form of nickel hydroxide. The ΔD-Δf plot further confirmed the negligible xanthate adsorption as no conformation change was involved.

Figure 4.18 (B) shows the ΔD-Δf plot for millerite sensor conditioned with 100 ppm dextrin solution during the first 10 minutes as the adsorption kinetic tests indicated the dextrin adsorption on millerite at pH 12 reached equilibrium within 10 minutes. The plot contained two discontinuities and was divided into three different regions with different $\Delta D/\Delta f$ values, indicating there was a conformation rearrangement in the adsorbed layer. A smaller $\Delta D/\Delta f$ value in region I demonstrated the initial adsorbed layer was compact and rigid. In region II, the $\Delta D/\Delta f$ value became larger comparing with region I, indicating there was a conformation change in the adsorbed layer as the adsorption of dextrin continued. This might be due to the multi-layer adsorption of dextrin, where the "loops" of the dextrin extended outward and the adsorbed layer has a loose structure (Sedeva et al., 2010). In addition, trapped water might also contribute to the accelerated increase in dissipation in region II that resulted in a soft and loose layer of dextrin (Kou et al., 2010; Paul et al., 2008; Rodahl et al., 1997). Note that regions I and II occurred during the first 2 minutes of the adsorption, indicating that the dextrin adsorption on millerite at pH 12 was rapid and there was a conformation change involved in the adsorbed layer. The adsorption was split into two steps: an initial rapid adsorption of dextrin resulted in a compact and rigid layer followed by a loose and soft structure of a multi-layer adsorption, for which the adsorbed dextrin extended outward. The $\Delta D/\Delta f$ value decreased again in region III as the dextrin adsorption approached equilibrium, indicating that the adsorbed layer became more rigid and compact again. The decrease in the $\Delta D/\Delta f$ value might be due to the rearrangement of adsorbed layer as the dextrin continued to adsorb on millerite and gradually reached equilibrium, which might explain the decelerated increase in the dissipation. In addition to dextrin adsorption, the spontaneous formation of nickel hydroxide on the sensor surface was also possible, which might also contribute to the continued increase in the frequency in this region.

Although using QCM-D to study the adsorption of dextrin on millerite-coated sensor provided preliminary insights on the adsorption kinetics and the conformation change of dextrin adsorption at pH 12, the limitation was that the millerite-coated sensor did not have a stable baseline in the background solution due to the nickel dissolution and formation of nickel hydroxide on the surface, which interfered with the dextrin adsorption to a certain extent. Future work is required to investigate the system with a more stable baseline so that factors affecting frequency and dissipation such as hydration water and water content trapped among the adsorbed species on the sensor can be further examined.

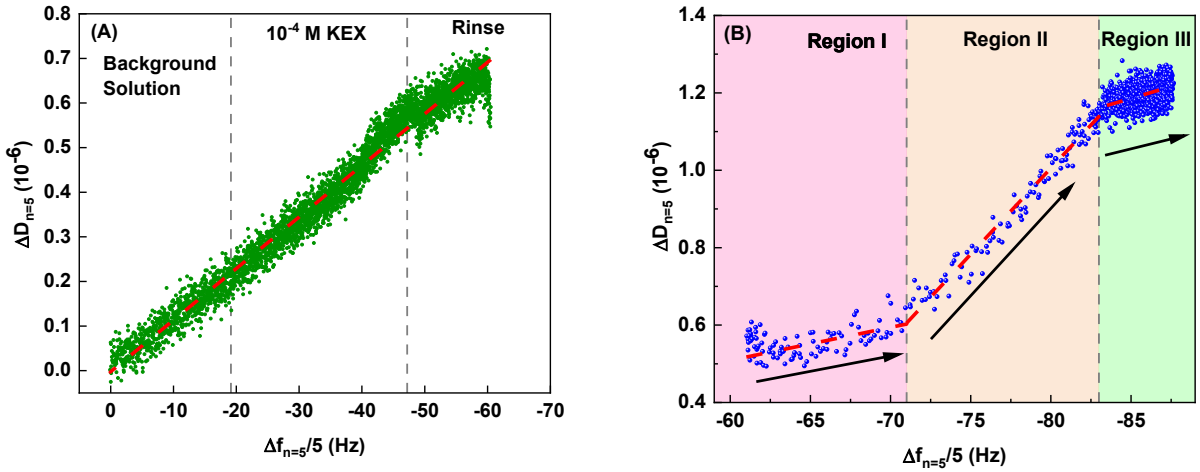

Figure 4.18 ΔD – Δf plots at the 5th overtone of (A) millerite sensor in pH 12 water and 10^{-4} M KEX, and (B) dextrin adsorption at pH 12.

4.4 Conclusions

In this chapter, the feasibility of using corn dextrin as a representative of polysaccharides to depress millerite in the differential flotation of chalcopyrite and millerite was investigated. Single mineral flotation tests indicated that dextrin's depressing effect on millerite was pH dependent. If adding dextrin after KEX, dextrin was efficient in depressing xanthate-treated millerite but not xanthate-treated chalcopyrite at alkaline pH. Mixed mineral flotation tests showed that Cu/Ni separation was significantly enhanced in the presence of dextrin without compromising Cu recovery. At pH 9, 2 ppm dextrin resulted in a Cu/Ni separation efficiency of 64%, which increased by 49.5% comparing with the baseline. At pH 12, a Cu/Ni separation efficiency of 79% that increased by 39% was achieved by 0.5 ppm dextrin. The underlying interaction mechanism was also studied. Static contact angle measurement indicated that dextrin

could lower the surface hydrophobicity of xanthate-treated millerite but not xanthate-treated chalcopyrite, which supported the micro-flotation test results. Millerite surface was dominated by a predominant nickel hydroxide passivation layer in alkaline solution with and without KEX that originated from severe surface oxidation. Dextrin adsorption on millerite was an irreversible chemisorption process, for which the hydroxyl functional group of dextrin interacted with the nickel hydroxide on millerite surface. QCM-D study indicated the conformation change in the adsorbed layer of dextrin on the millerite at pH 12. When adding dextrin after KEX, dextrin adsorbed less on xanthate-treated millerite surface, while KEX adsorption was not affected, indicating dextrin and KEX adsorbed through different surface sites. As the pH was increased from 9 to 12, the nickel hydroxide passivation layer gradually inhibited xanthate adsorption on millerite, which favoured dextrin adsorption. Compared with chalcopyrite, dextrin adsorbed more on millerite and displayed a higher affinity towards millerite. At pH 12, dextrin can still adsorb on xanthate-treated millerite but not on xanthate-treated chalcopyrite. XPS analysis, AFM imaging and bulk adsorption tests indicated a negligible adsorption of dextrin on xanthate-treated chalcopyrite at pH 12. Chalcopyrite was much less prone to surface oxidation in aqueous solutions, resulting in less sites available for dextrin adsorption than millerite, especially after conditioning with KEX.

Chapter 5 Effect of Copper (II) Ions on Millerite Flotation and Surface Properties in Alkaline Solutions

5.1 Introduction

The presence of copper ions (Cu^{2+}) is inevitable in the plant process water and the sources of copper ions might be mineral dissolution or chemical residuals. Numerous studies indicated that copper ions can promote floatability of xanthate treated pyrrhotite and pentlandite at alkaline environment (Allison & O'Connor, 2011; Gerson & Jasieniak, 2008; Malysiak et al., 2002; Nicol, 1984; Senior et al., 1994). The major theory was that some Cu (II) was reduced into Cu (I) upon adsorption on the mineral surface and both Cu (I) and Cu (II) co-exist on the mineral surface. Qi, Liu, et al. (2019) used time of flight – secondary ion mass spectroscopy (ToF-SIMS) to analyze rougher concentrate and tailing samples, and it was found that the amount of copper on polymorphic pyrrhotite surface was much greater in the rougher concentrate than rougher tails, indicating Cu has an activating effect on pyrrhotite flotation. Millerite was more abundant in the copper-rich ore and was found to be mainly associated with copper sulphide minerals such as chalcopyrite and bornite (Xu et al., 2011). Hence, millerite's flotation behavior can be greatly affected by the dissolution of copper sulphide minerals. However, to date, the effect of copper ions on millerite flotation in the presence of xanthate has not been studied or reported. Therefore, it is essential to understand the effect of copper ions on millerite surface chemistry in order to develop a depression strategy for millerite in the copper cleaner.

In this chapter, the effect of copper on millerite's flotation with xanthate at alkaline environment was studied. Micro-flotation tests were performed to examine millerite's floatability in the presence of Cu^{2+} at both pH 9 and pH 12 with potassium ethyl xanthate (KEX) as the collector. The effect of dextrin on Cu-treated millerite will also be tested using micro-flotation test. Millerite dissolution and surface chemistry in the presence of Cu^{2+} were investigated by mineral dissolution tests and EDTA extraction tests. X-ray photoelectron spectroscopy (XPS) analysis was used to study millerite surface oxidation by studying the surface species in the presence of copper and the activation mechanism.

5.2 Experimental

5.2.1 Micro-flotation Test

For a typical test, approximately 1.5 g of -75+38 μm fraction millerite was cleaned ultrasonically in Milli-Q water for 5 minutes to reduce surface oxidation. Then 150 mL pH-adjusted water with a specific amount of Cu^{2+} were added to the mineral achieve a desired Cu^{2+} concentration ranged from 10^{-6} M to 10×10^{-6} M, and the conditioning time with Cu^{2+} was 5 minutes. After conditioning with Cu^{2+}, KEX was added, and the pulp was conditioned for another 5 minutes. The pulp pH was adjusted constantly by sodium hydroxide to maintain at pH 9 or pH 12 during the conditioning stage and the pulp potential was constantly recorded during the conditioning stage. The procedure at the flotation stage was identical to the procedure described in Section 4.2.1. The recovery of millerite was calculated using Equation (4.1).

5.2.2 Copper Adsorption Test

Figure 5.1 shows the schematic of the experimental procedure for the millerite dissolution and EDTA extraction tests. For each test, approximately 1.5 g of -38 μm millerite was grounded with 5 mL pH 12 water with the desired Cu concentration using a McCrone Micronising Mill (Retsch, Germany) for 10 minutes to ensure the exposure of fresh mineral surface. The ground millerite was then conditioned with 50 mL pH 12 water for 5 minutes to allow sufficient Cu adsorption. The particles and water were then separated by a 0.22 μm membrane filter. The filtrate was then sent for ICP analysis to measure Cu, Ni and S content in the solution. Concentrations of Cu and Ni was analyzed by ICP-MS while the total dissolved sulphur content was analyzed by ICP-OES. The filtered mineral particles were freeze-dried under vacuum and analyzed by ethylenediaminetetraacetic acid (EDTA) extraction method to quantify oxidised species on mineral surface. The detailed procedure on the EDTA extraction can be found in section 4.2.4. After extraction, the EDTA solution was filtered and was sent for ICP-MS analysis. In the case that KEX was added to the system, KEX was added to the pulp after conditioned with Cu and the pulp was further conditioned with 3×10^{-4} M KEX for another 5 minutes. Residual Cu concentration was analyzed from the filtrate sample before KEX was added to avoid the interference of xanthate. All analysis results were normalized by the mass of the tested samples. The specific surface area (SSA) of millerite ground by micronizing mill was analyzed by a BET surface area analyzer (Autosorb – iQ, Quantachrome) which was determined to be 3.533 m^2/g.

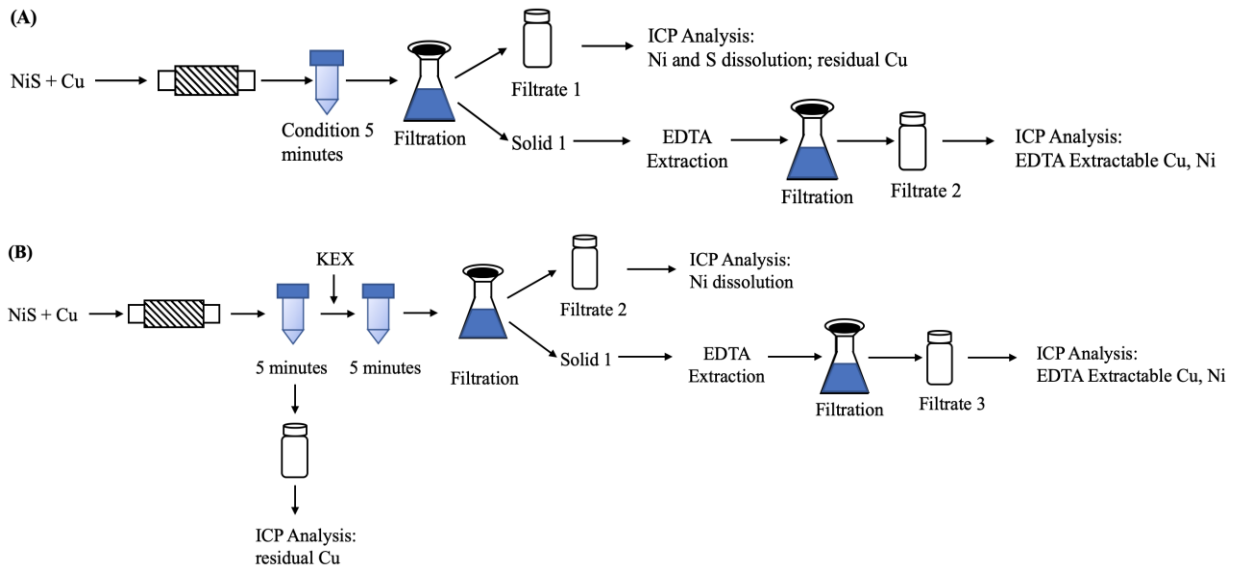

Figure 5.1 Schematic of experiment procedures of mineral dissolution and EDTA extraction tests for (A) collectorless condition, and (B) with 3×10^{-4} M KEX.

5.2.3 XPS Analysis

For each test, approximately 1 g of +38-75 µm millerite was cleaned by sonication for 5 minutes and then conditioned in 150 mL solution with Cu and KEX with desired concentrations. The conditioning order and time were identical to the flotation tests. After conditioning, the mineral particles were filtered and washed by Milli-Q water thoroughly to remove any residual Cu and/or KEX. After washing, the conditioned mineral sample was freeze-dried under vacuum until the test to prevent oxidation.

5.3 Results and Discussion

5.3.1 Millerite Flotation with Cu and KEX

Figure 5.2 (A) shows the millerite flotation recovery and average pulp potential as a function of Cu^{2+} concentration with 10^{-5} M KEX at pH 9 and pH 12. The Cu concentration was ranged from 10^{-6} M to 10×10^{-6} M, which was consistent with the Cu assay in the process streams based on the plant survey (Qi, Liu, et al., 2019). At pH 9, adding 10×10^{-6} M Cu^{2+} increased millerite recovery from 65.0% to 91.5%. For millerite flotation at pH 12, adding 10^{-6} M Cu^{2+} can increase millerite recovery from 29.5% to 50.1%; however, millerite's flotation was less activated when 10×10^{-6} M Cu^{2+} was added, and the recovery decreased from 50.1% to 34.4% as the Cu concentration was increased from 10^{-6} M to 10×10^{-6} M. The inconsistent activation effect

observed for 10×10^{-6} M Cu^{2+} at pH 9 and pH 12 might be due to different Cu species formed on millerite surface. Figure 5.2 (B) shows the pulp potential of millerite as a function of time during conditioning with Cu^{2+} and KEX at various Cu^{2+} concentrations. The pulp potential increased if Cu^{2+} was present in the system. The increase in the pulp potential indicated that activation of millerite flotation by Cu^{2+} involved electrochemical reactions. Thus, solution and surface analyses were then conducted to supplement the flotation results.

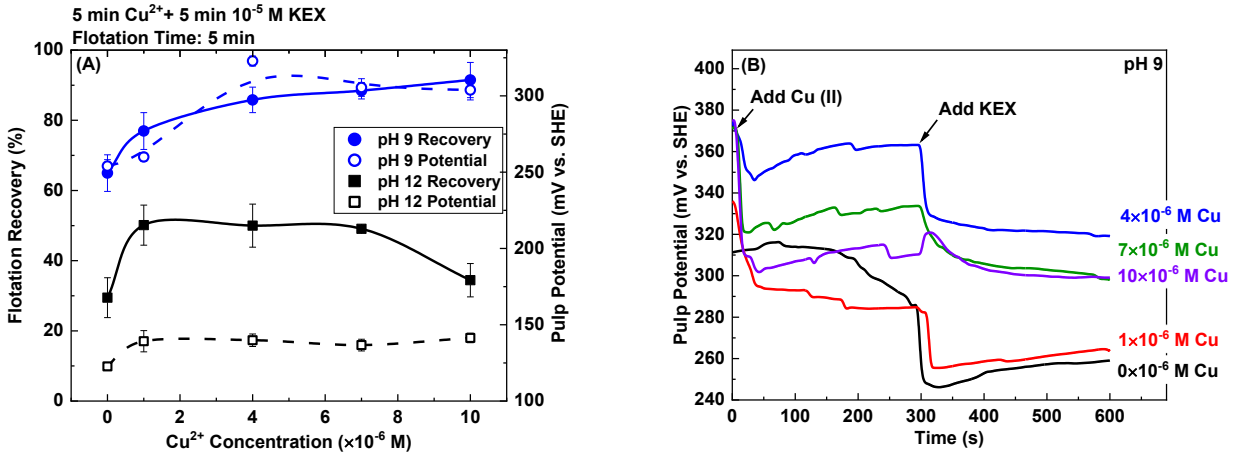

Figure 5.2 (A) The flotation recovery and pulp potential of millerite as a function of Cu(II) with 10^{-5} M KEX at pH 9 and pH 12; (B) the pulp potential of millerite as a function of time during conditioning with Cu (II) and KEX with various Cu (II) concentrations at pH 9.

The speciation diagrams of 10^{-6} M and 10×10^{-6} M Cu corresponding to the flotation conditions from pH 3 to pH 13 are shown in Figure 5.3, which are consistent with the literature. (Acar & Somasundaran, 1992; X. Wang et al., 1989b) At pH 9, $Cu(OH)_{2(s)}$ precipitation is dominant while a small amount of $CuOH^{+}$ is present. As pH continues to increase, negatively charge species $Cu(OH)_3^-$ and $Cu(OH)_4^{2-}$ begin to appear in the system. At pH 12, $Cu(OH)_{2(s)}$ is only dominant for 10×10^{-6} M Cu while not for 10^{-6} M Cu. According to the speciation diagrams, negatively charged Cu (II) species $Cu(OH)_3^-$ and $Cu(OH)_4^{2-}$ are dominant for 10^{-6} M Cu. At pH 12, the inactivation observed at 10×10^{-6} M Cu compared with that of 10^{-6} M Cu may be due to the excess adsorption of $Cu(OH)_{2(s)}$ on millerite surface, which required further surface analyses.

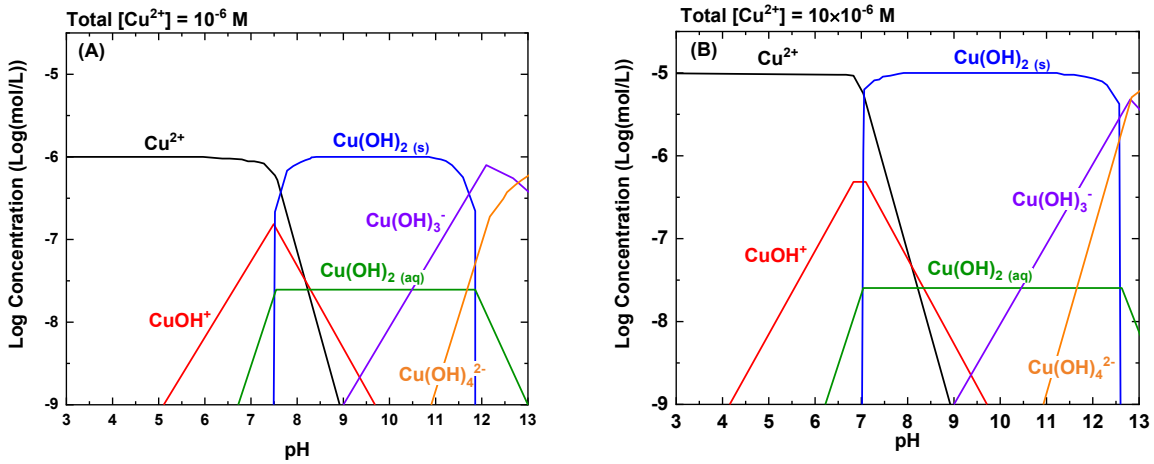

Figure 5.3 Speciation diagrams of (A) 10^{-6} M Cu^{2+} and (B) 10×10^{-6} M Cu^{2+} at room temperature (diagrams were generated using Hydra and MEDUSA software).

More flotation tests were carried out to examine whether dextrin Cu-activated millerite. The conditioning order was: 10^{-6} M Cu^{2+}, 10^{-5} M KEX and then with 1 ppm or 5 ppm dextrin. The conditioning time for each reagent was 5 minutes. The flotation results are shown in Figure 5.4. At pH 9, 1 ppm dextrin was less-efficient in depressing Cu-activated millerite compared with non-activated millerite; yet Cu-activated millerite can be depressed as dextrin's concentration was raised to 5 ppm. For pH 12, 1 ppm dextrin was sufficient enough to depress Cu-activated millerite.

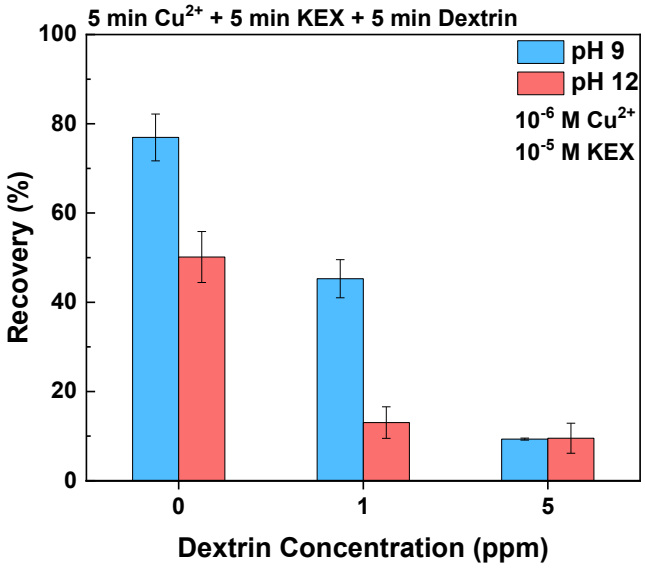

Figure 5.4 Flotation recovery of Cu-activated millerite ([Cu^{2+}]=10^{-6} M) as a function of dextrin concentration in the presence of 10^{-5} M KEX after 5 minutes of flotation at both pH 9 and pH 12.

5.3.2 Effect of Cu on Millerite Dissolution and Oxidation

To gain a better understanding on copper ion's effect on millerite flotation, EDTA extraction combined with ICP analysis were used to investigate the effect of Cu on millerite dissolution as well as surface oxidation with and without KEX at pH 12. For the collectorless condition, five parameters were studied: Cu adsorption, Cu oxidation on millerite surface, nickel dissolution, sulphur dissolution as well as nickel oxidation species on millerite surface, and the results are shown in Figure 5.5 (A) as a function of Cu added. The amount of Cu adsorbed were identical to the amount of Cu added, which implied all Cu has adsorbed on millerite surface within 5 minutes. Meanwhile, Cu oxidation species extracted from millerite surface increased as well as the Cu concentration increased. On the other hand, total sulphur dissolutions decreased when Cu was present in the system, implying that millerite surface oxidation was affected and less sulphoxy species were formed. In addition, there was no increase in the nickel dissolution and nickel oxidation species after conditioning with Cu, indicating that nickel dissolution and the subsequent formation of nickel hydroxide passivation layer was not promoted by Cu, and Cu adsorption on millerite was not a simple ion exchange process between Cu and Ni at the lattice.

Figure 5.5 (B) shows the ICP analysis results with the addition of 3×10^{-4} M KEX. Note that the amount of Cu adsorbed here was determined by analyzing the residual Cu in the solution right before the addition of xanthate, so that the reported amount of Cu adsorption contained no contribution of residual Cu forming complex with xanthate and adsorb on millerite. In addition, the amount of residual Cu forming complex with free xanthate can be assumed negligible as the Cu concentration was much lower than KEX concentration. The sulphur dissolution was not considered when KEX was added, this was due to that free residual xanthate ion in the filtrate may interfere the measurement of sulphur content in the filtrate. Similar to collectorless condition, all Cu was adsorbed on millerite during the 5 minutes conditioning and the amount of Cu oxidation species increased on millerite surface as the Cu dosage increased. The increase in Cu oxidation species can lower the surface hydrophobicity, which explained the decrease in millerite's recovery at 10×10^{-6} M Cu addition at pH 12. Again, the changes in Ni dissolution and

the oxidised Ni seems to not have a direct relationship with the amount of Cu adsorbed. Therefore, the Cu adsorption tests confirmed Cu adsorbed on millerite and the existence of Cu oxidation species on millerite surface. In the meanwhile, the adsorbed Cu modified millerite surface by affecting the sulphur oxidation and reduced sulphur dissolution. Ni dissolution and the surface passivation layer formed by $Ni(OH)_2$ were not increased upon the adsorption of Cu, indicating the adsorption is not a simple ion exchange process. To examine the underlying mechanism of the phenomenon observed in the copper adsorption test, the surface chemistry of millerite was then further studied by XPS analysis.

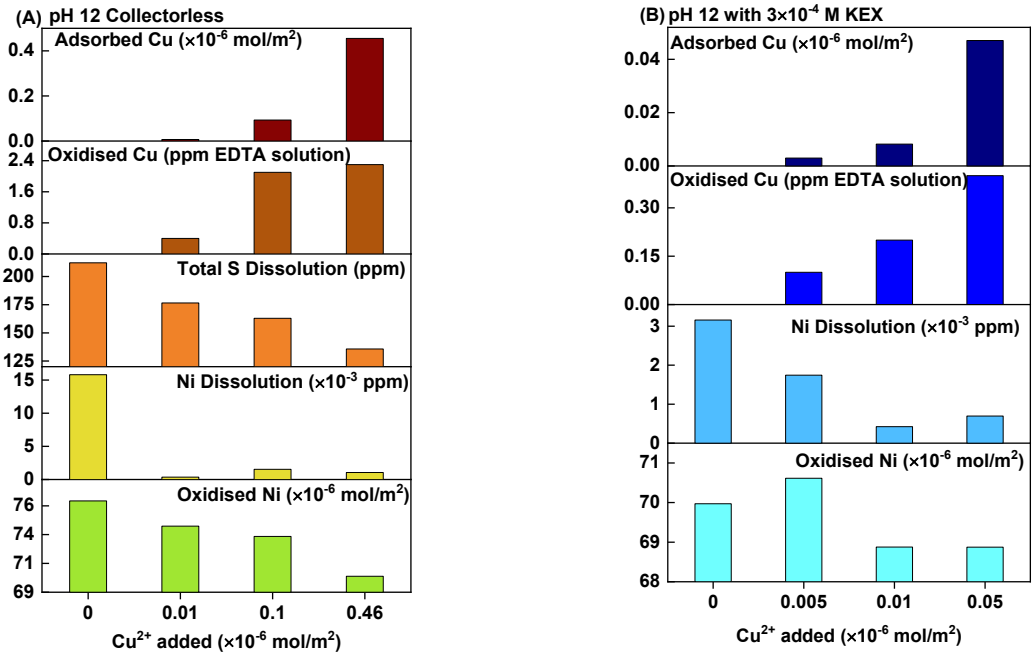

Figure 5.5 Effect of Cu (II) on Cu adsorption, Cu oxidation on surface, total sulfur dissolution, nickel dissolution and Ni surface oxidation for (A) collectorless condition and (B) with 3×10^{-4} M KEX at pH 12.

5.3.3 XPS Analysis

Millerite surfaces conditioned with Cu^{2+} and KEX at pH 9 and pH 12 were analyzed by XPS to further understand the impact of copper on the millerite surface chemistry. Millerite was conditioned with no Cu, 10^{-6} M Cu, 10×10^{-6} M Cu, KEX, and both Cu and KEX. The conditioning time for each reagent was 5 minutes. For "Cu+KEX" condition, millerite was first conditioned with copper for 5 minutes and then conditioned with KEX for another 5 minutes. To

better examine the effect of KEX on millerite surface chemistry, the KEX concentration used for pH 9 and pH 12 were 2×10^{-5} M and 10^{-4} M, respectively.

Figure 5.6 shows the ratio of atomic proportions of oxygen to sulphur (O/S) based on the survey scan. For each condition, the O/S value at pH 12 was higher than pH 9, indicating more severe oxidation at pH 12 than pH 9. Upon the addition of 10^{-6} M Cu, the O/S value dropped compared with baseline. The O/S value increased as the Cu concentration increased to 10×10^{-6} M, indicating that at higher copper concentration, more oxide/hydroxide formed on millerite surface. The addition of KEX or Cu with KEX lowered the O/S value, which implied KEX can hinder millerite surface oxidation. At pH 9, when adding Cu and KEX together, the O/S value reached minimum, indicating a synergistic effect of these two reagents on affecting millerite surface oxidation. Other XPS studies also revealed that xanthate can hinder severe surface oxidation thus render the surface less hydrophilic (Deng, Karpuzov, et al., 2013; Legrand et al., 2005b).

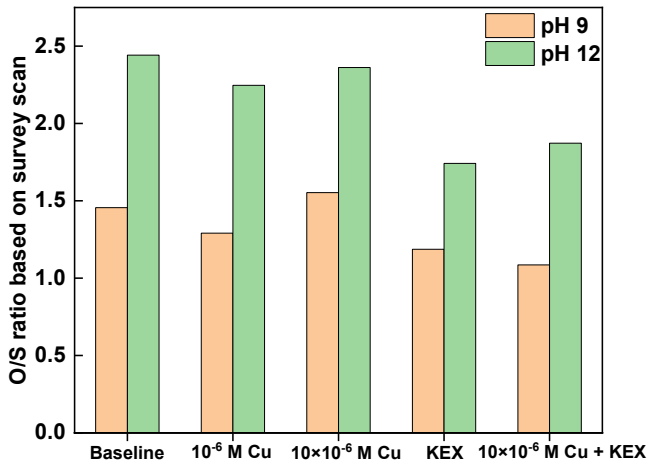

Figure 5.6 The ratio of oxygen to sulphur based on XPS survey scan of millerite surface conditioned under various conditions at pH 9 and pH 12. (KEX concentration was 2×10^{-5} M at pH 9 and 10^{-4} M at pH 12)

High resolution spectra of Cu 2p $_{3/2}$, S 2p and Ni 2p $_{3/2}$ were also analyzed. Table 5.1 shows the peak parameters used for the fitting of the XPS narrow scans, including binding energy, FWHM and the corresponding chemical species.

Table 5.1 XPS fitting peaks binding energy, FWHM and the corresponding chemical state for Cu 2p $_{3/2}$, S 2p and Ni 2p $_{3/2}$ spectra.

Peak	Binding Energy (eV)	FWHM (eV)	Chemical State
Cu 2p $_{3/2}$	931.93 – 932.15	1.2	Cu (I) – S
Cu 2p $_{3/2}$	933.26	1.2	Cu (II) – S
	941.0	*1.3*	*Cu (II) – S shake-up satellite*
	942.41	*0.7*	*Cu (II) – S shake-up satellite*
	944.01	*0.9*	*Cu (II) – S shake-up satellite*
Cu 2p $_{3/2}$	934.67	2.8	Cu (II) – O
	939.30	*2.8*	*Cu (II) – O shake-up satellite*
	942.20	*3.7*	*Cu (II) – O shake-up satellite*
	944.12	*1.8*	*Cu (II) – O shake-up satellite*
S 2p $_{3/2}$	160.9	0.62	Surface S^{2-}
S 2p $_{3/2}$	161.5	0.62	Bulk S^{2-}
S 2p $_{3/2}$	162.1	1.0	Surface S_2^{2-}
S 2p $_{3/2}$	163.7	1.6	Polysulphide, S_n^{2-}
S 2p $_{3/2}$	166.8	1.6	Thiosulfate, $S_2O_3^{2-}$
S 2p $_{3/2}$	168.3	1.6	Sulfate, SO_4^{2-}
Ni 2p $_{3/2}$	852.93 – 853.2	1.2	NiS
	859.6 – 859.7	3.5	NiS satellite
Ni 2p $_{3/2}$	855.25 – 855.45	1.8	$Ni(OH)_2$
	860.5 – 860.6	3.2	$Ni(OH)_2$ satellite
Ni 2p $_{3/2}$	856.3 – 856.5	1.5	NiS_2O_3
	862.1	3.0	NiS_2O_3 satellite
Ni 2p $_{3/2}$	857.4 – 857.6	1.6	$NiSO_4$
	863.1 – 863.2	3.0	$NiSO_4$ satellite

5.3.3.1 Cu 2p $_{3/2}$ Spectra

Figure 5.7 (A) and (B) show the fitted spectra of Cu 2p $_{3/2}$ for millerite conditioned with Cu and KEX at both pH 9 and pH 12; the surface species proportions as well as the ratio of Cu – S to Cu – O at pH 9 and pH 12 are shown in Figure 5.7 (C) and (D). The most intense peak was identified to be Cu (I) sulphide, which might have a similar valence state as covellite CuS (Biesinger, 2017; Cabrera-German et al., 2019; Fairthorne et al., 1997; Nakai et al., 1978). The copper in CuS is actually in monovalent state and the chemical state of Cu and S in CuS can be

best described as $Cu_3^+S^{2-}S_2^{2-}$, where monovalent Cu bonded to both monosulphide and disulphide species (Goh et al., 2006; Bingqiao Yang et al., 2019). Hence, the majority of Cu (II) adsorbed on millerite was reduced to Cu (I) state (Leppinen, 1990; Leppinen et al., 1995). The peak next to Cu (I) sulphide located at 933.3 eV was identified as Cu (II) sulphide, which was accompanied by satellite peaks in the Cu (II) shake-up area (Cabrera-German et al., 2019; Kundu et al., 2008), indicating the existence of Cu (II) – S on millerite surface in addition to Cu (I) – S species. The proportion of Cu (II) sulphide remained similar for either 10^{-6} M Cu or 10×10^{-6} M Cu. In addition to copper sulphide species, the main peak for Cu (II) – O was also identified at 934.67 eV along with the corresponding satellite peaks in the Cu (II) shake-up area (Biesinger, 2017; Biesinger et al., 2010; Cabrera-German et al., 2019). As Cu concentration increased from 10^{-6} M Cu to 10×10^{-6} M Cu, the intensities of Cu (II) – O peak and the shake-up area increased, yet the dominant species was still Cu (I) sulphide. The copper oxidation product on millerite surface increased as copper concentration increased was also observed through the EDTA extraction tests. However, after xanthate was added, proportions of Cu (I) sulphide and Cu (II) sulphide was significantly increased, especially at pH 9, where the Cu (II) hydroxyl species was significantly depressed accompanied by the disappearance of the Cu (II) shake-up area. Hence, the Cu – S to Cu – O ratio for millerite conditioned with both Cu and KEX was much higher at pH 9 than at pH 12. For millerite conditioned with both Cu and KEX at pH 9, a new peak at 932.9 eV yielded a better fit. The new peak at 932.9 eV might attribute to the existence Cu (I) ethyl xanthate species (Deng, Karpuzov, et al., 2013; Mikhlin, Vorobyev, et al., 2016) that contributed to the intensity increase of the main Cu (I) peak. As Cu (II) and KEX both present in a system with near equivalent concentrations, an unstable Cu (II) xanthate first formed which then quickly decomposed to Cu (I) xanthate and dixanthogen (Donaldson, 1976; Mikhlin, Vorobyev, et al., 2016; Pohlandt et al., 1969; Sparrow et al., 1977). Furthermore, the Cu – S to Cu – O ratio at pH 12 was very sensitive towards the Cu concentration. Increasing Cu concentration from 10^{-6} M to 10×10^{-6} M resulted in a significant increase in the proportion of Cu (II) – O species even in the presence of KEX, thus the ratio Cu (I)/Cu (II) decreased dramatically as a result. A relatively high Cu dosage (10×10^{-6} M) resulted in a relatively high proportion of Cu (II) – O, rendering the surface more hydrophilic that has a negative effect on the copper activation of millerite flotation. The XPS analysis justified the flotation result that millerite's flotation was less activated with 10×10^{-6} M Cu than with 10^{-6} M Cu at pH 12. The existence of

the Cu (II) – O peak indicated that it is possible to have precipitation and adsorption Cu (II) hydroxide on millerite surface at alkaline pH in addition to the reduction of Cu (II) to Cu (I) and formed Cu (I) sulphide (Voigt et al., 1994; Weisener & Gerson, 2000a, 2000b; Bo Yang et al., 2016). The Cu (II) – O might also originate from the oxidation of the copper sulphide formed on millerite surface as previous XPS study suggested the existence of copper hydroxide for oxidized covellite (Fullston et al., 1999).

As a summary of what has been discussed, the dominant copper species formed on millerite at alkaline environment was Cu (I) sulphide, which originated from the reduction of Cu (II) adsorbed on millerite surface. In the meantime, Cu (II) sulphide as well as Cu (II) hydroxide species also existed. The Cu (II) – O species might be attributable to the precipitation and adsorption of Cu (II) from the bulk and/or because of the oxidation of copper sulphide formed on the millerite surface.

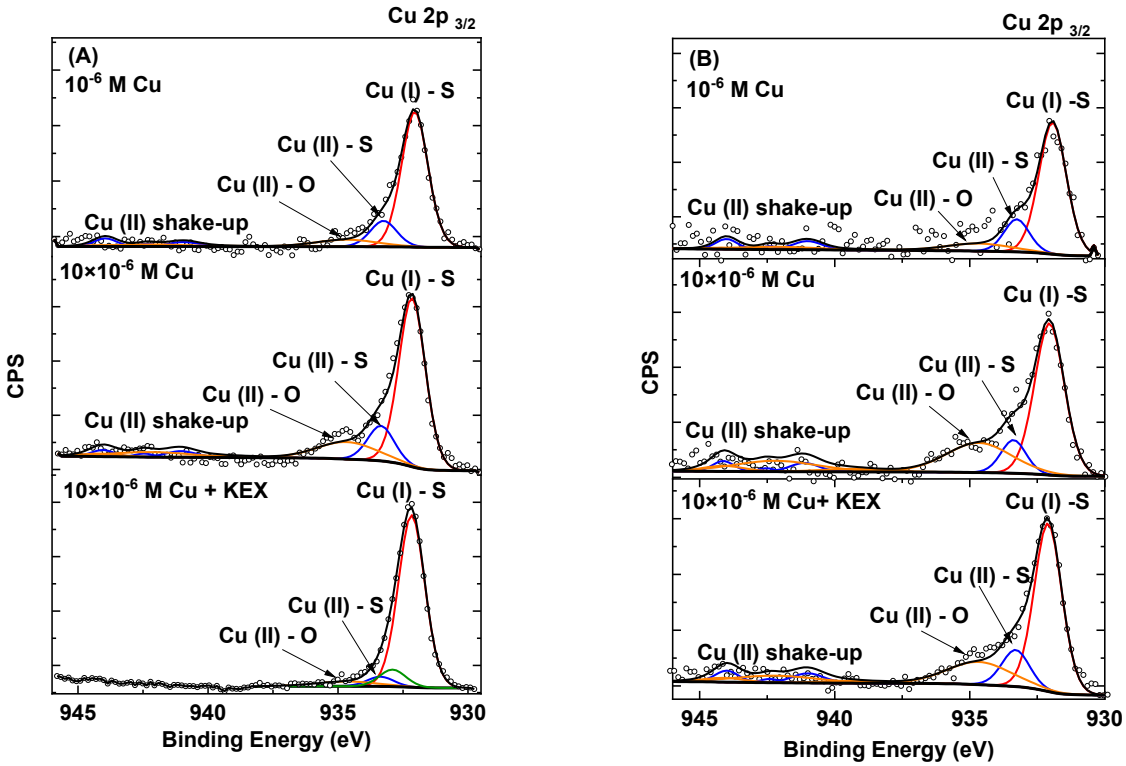

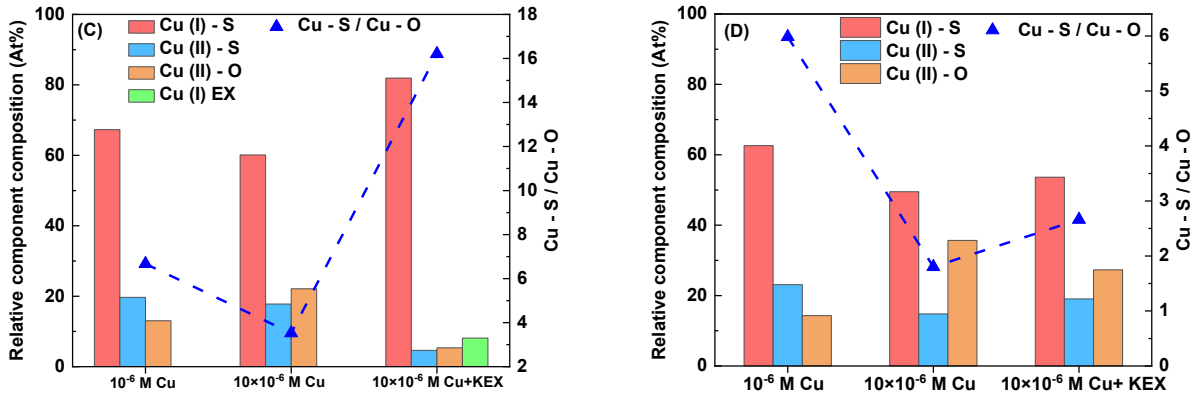

Figure 5.7 XPS Cu 2p $_{3/2}$ spectra of millerite at (A) pH 9 and (B) pH 12 conditioned with (i) 10^{-6} M Cu, (ii) 10×10^{-6} M Cu and (iii) 10×10^{-6} M Cu and KEX, and the corresponding species proportions and the ratio of Cu sulphide to Cu hydroxide at (C) pH 9 and (D) pH 12. (KEX concentration was 2×10^{-5} M at pH 9 and 10^{-4} M at pH 12)

5.3.3.2 S 2p Spectra

Fitted sulphur 2p narrow scans at pH 9 and pH 12 are shown in Figure 5.8 (A) and (B). All fitted sulphur peaks are doublets with a binding energy difference of 1.18 eV. Doublets have equal full width at half maximum (FWHM) values and the intensity of S 2p $_{1/2}$ peak is half of that of S 2p $_{3/2}$ peak (Legrand et al., 1998). Only S 2p$_{3/2}$ peak will be referred and discussed. The peak at 161.5 eV was identified as fully coordinated monosulphide (S^{2-}) for bulk millerite (Legrand et al., 1998; Nesbitt et al., 2001). Another peak at a slightly lower binding energy at 160.9 eV was observed, and was identified as surface monosulphide species (surface S^{2-}) that represented a lower coordinated surface sites than bulk monosulphide, which should be the first sulphur species to react (Nesbitt et al., 2001). The peaks at 162.1 eV and 163.7 eV represented surface disulphide species (S_2^{2-}) and polysulphide (S_n^{2-}), respectively (Legrand et al., 1998, 2005a; Leiro et al., 1998; Nesbitt et al., 2001; Nesbitt, Scaini, et al., 2000; Qi, Khalkhali, et al., 2019; Qi, Liu, et al., 2019). The observation of disulphide peak might be due to reconstruction of millerite surface (Nesbitt et al., 2001). Thiosulfate and sulfate species were assigned at peaks with binding energies of 166.8 eV and 168.3 eV, respectively (Descostes et al., 2000; Legrand et al., 1998, 2005a; Qi, Khalkhali, et al., 2019; Qi, Liu, et al., 2019; Y. Sun et al., 2018; Swartz et al., 1971). The sulphur species proportions, and ratios of sulphoxy species to disulphide species

($S_xO_y^{2-}/S_2^{2-}$) as well as surface monosulphide species to disulphide species (surface S^{2-}/S_2^{2-}) are shown in Figure 5.8 (C) and (D). Regarding the surface S^{2-} species, at alkaline environment, nickel dissociated from lattice might be hydroxylated and then precipitate back to millerite surface forming the nickel hydroxide passivation layer that prevent the surface S^{2-} species beneath the passivation layer from being further oxidized. Upon the addition of Cu, the proportion of surface S^{2-} was reduced while an increase in S_2^{2-} was observed. Meanwhile, the proportions of sulphoxy species also decreased. The ratios of $S_xO_y^{2-}/S_2^{2-}$ and surface S^{2-}/S_2^{2-} decreased in the presence of Cu. For sulphur oxidation process, surface S^{2-} can be oxidized into S_2^{2-} and/or S_n^{2-}, which are responsible for the surface hydrophobicity, followed by the oxidation of the bulk fully-coordinated S^{2-}; and excess oxidation will result in formation of hydrophilic sulphoxy species such as thiosulfate and sulfate species. As suggested in Cu $2p_{3/2}$ spectra, the adsorbed Cu (II) was reduced to Cu (I) state and formed a covellite-like structure, where Cu (I) bonded to both S^{2-} and S_2^{2-}. In response to this reduction process, the surface S^{2-} was oxidized into S_2^{2-}, which justified the decrease in surface $S^{2-}$and the increase in S_2^{2-}. In the meantime, the adsorption of copper also resulted in less sulphoxy species. Upon the adsorption and reduction of Cu (II), surface active S^{2-} was oxidized to S_2^{2-}, the formation of Cu (I) sulphide inhibited S^{2-} contacting oxygen and being excessively oxidized, the formation of sulpoxy species was reduced as a result. The addition of xanthate inhibited excessive sulphur oxidation of millerite, resulted in less sulphoxy when comparing with baseline. Millerite conditioned with both copper and xanthate has even less surface S^{2-} and more S_2^{2-} existing, the excessive sulphur oxidation was inhibited while the mild oxidation to disulphide was promoted with Cu to render surface more hydrophobic. The XPS analysis of S 2p narrow scans was consistent with ICP analysis, which suggested that sulphur oxidation was affected upon the adsorption of Cu, the interaction between Cu and surface S^{2-} resulted in an increase in S_2^{2-} and S_n^{2-} while reduced the sulphoxy species generated.

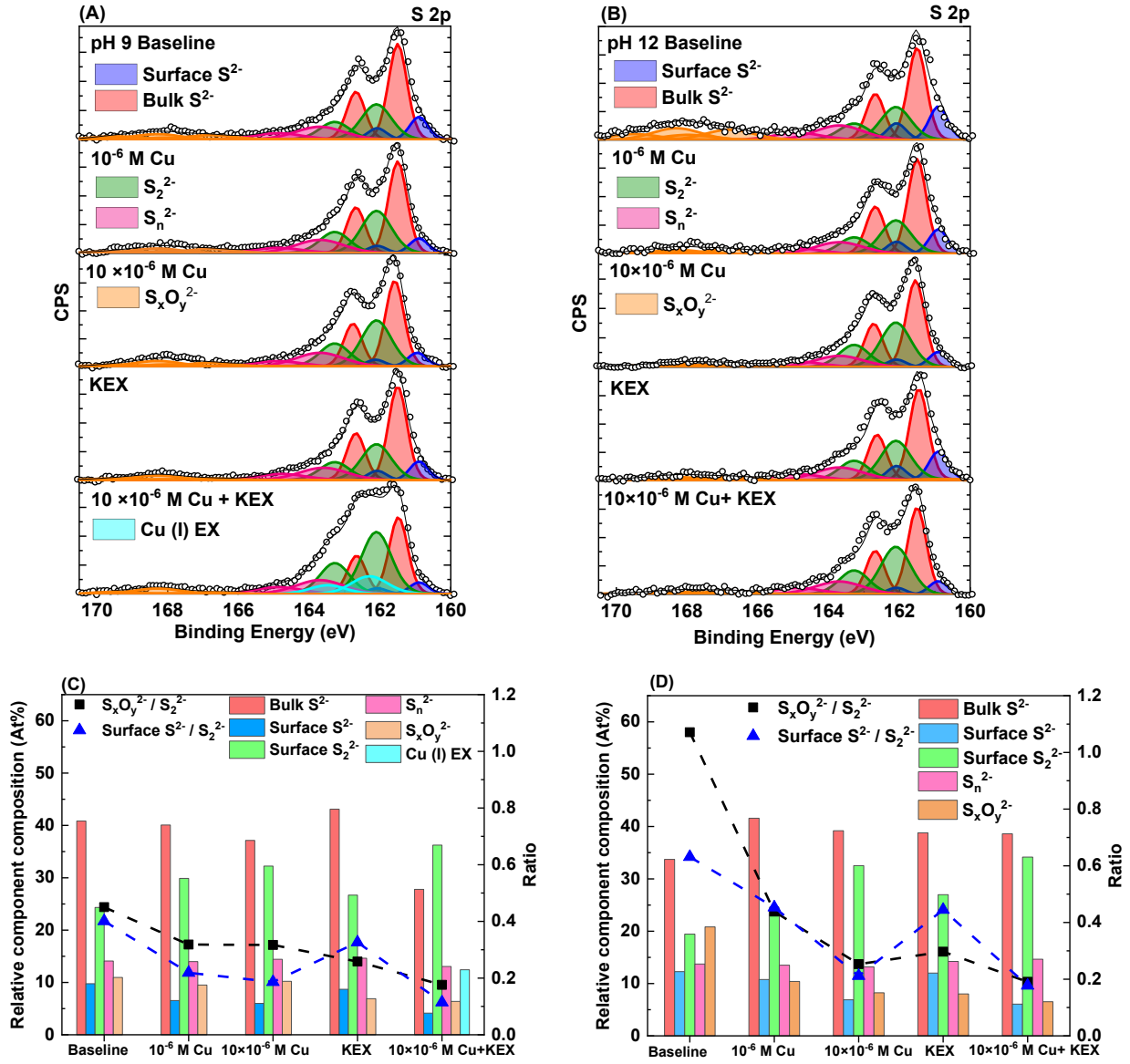

Figure 5.8 XPS S 2p spectra of millerite at (A) pH 9 and (B) pH 12 conditioned with (i) collectorless condition, (ii) 10^{-6} M Cu, (iii) 10×10^{-6} M Cu, (iv) KEX and (v) 10×10^{-6} M Cu and KEX, and the corresponding species proportions and ratios of surface monosulphide and sulphoxy species to disulphide species at (C) pH 9 and (D) pH 12. (KEX concentration was 2×10^{-5} M at pH 9 and 10^{-4} M at pH 12)

Note that upon the addition of xanthate, the peaks for dixanthogen, chemisorbed xanthate or metal xanthate were not identified. Previous study using infrared spectroscopy suggested that

both dixanthogen (X_2) and nickel (II) ethyl xanthate (NiX_2) can form on millerite at pH 9 and pH 12 upon xanthate adsorption through oxidation (Zhao, 2019), as shown in the Equations (5.1) and (5.2) (Hepel & Pomianowski, 1977; L. K. Smith et al., 2011).

$$NiS + 2X^- \rightleftharpoons NiX_2 + S + 2e^- \quad E_h = -0.11 - 0.0591\log[X^{-1}] \tag{5.1}$$

$$2X^- \rightleftharpoons X_2 + 2e^- \quad E_h = -0.07 - 0.0591\log[X^{-1}] \tag{5.2}$$

As a result, the formation potential for NiX_2 and X_2 at 2×10^{-5} M KEX are calculated to be 0.167 V and 0.207 V, and the formation potential for NiX_2 and X_2 at 10^{-4} M KEX are 0.126 V and 0.166 V. Hence, it can be speculated that both NiX_2 and X_2 can form at the open circuit potentials shown in Figure 5.2. However, the peak at 164.4 eV featuring the bridging S in dixanthogen was not observed for millerite conditioned with KEX. For XPS analysis conducted at room temperature under ultra-high vacuum, dixanthogen usually cannot be detected as dixanthogen is unstable and will desorb from mineral surface under such a condition (Deng, Karpuzov, et al., 2013; Kartio et al., 1992; Legrand et al., 2005b). Therefore, cryo-XPS can be used to identify dixanthogen and other xanthate product on millerite. Furthermore, the S $2p_{3/2}$ peak position of the doublet for chemisorbed xanthate, metal xanthate or the terminal S in dixanthogen (~162.3 eV) overlaps with that of surface S_2^{2-} species (Buckley & Woods, 1995; Deng, Karpuzov, et al., 2013; Mikhlin, Karacharov, et al., 2016a, 2016b), and no increase in the spectrum intensity was observed for KEX-treated millerite compared with baseline at 162.3 eV, it was difficult to identify whether there was a peak for xanthate.

For Cu-KEX-treated millerite at pH 9, a new low-intensity doublet was identified at 162.3 eV, which contributed to the increase in the spectrum intensity around 162.3 eV comparing with KEX-treated millerite. The new doublet might be due to the presence of Cu (I) ethyl xanthate or chemisorbed xanthate species on millerite surface (Deng, Karpuzov, et al., 2013; Kartio et al., 1992; J. Mielczarski et al., 1983; Mikhlin, Karacharov, et al., 2016a, 2016b; Mikhlin, Vorobyev, et al., 2016; Szargan et al., 1992). As discussed in Cu $2p_{3/2}$ spectra, both Cu (I) ethyl xanthate and dixanthogen can form upon the reaction of Cu (II) and free xanthate ions, and Cu (I) ethyl xanthate is stable until pH 12 at room temperature (Sheikh & Leja, 1974). To further examine the existence of Cu (I) ethyl xanthate at pH 9, C 1s and O 1s spectra of millerite conditioned at pH 9 were fitted and shown in Figure 5.9. For millerite baseline and KEX-treated millerite, C 1s mainly showed peaks for adventitious carbon. Upon the addition of both Cu and

KEX, the intensity of R-C-O peak at 286.3 eV increased and a new peak at 287.7 eV appeared that featured the $-O-C-SS^-$ in xanthate, which implied the existence of xanthate on millerite surface (Ihs et al., 1994; J. A. Mielczarski et al., 1998; Mikhlin, Vorobyev, et al., 2016; Szargan et al., 1992). The O 1s spectra of millerite and millerite conditioned with KEX were fitted by three peaks located at 531.2 eV, 532 eV and 533 eV, which were assigned to nickel hydroxide, sulphate and adsorbed water (Biesinger et al., 2009, 2011; Ejtemaei & Nguyen, 2017b; Legrand et al., 1998; Qi, Liu, et al., 2019; Richardson & Vaughan, 1989). The intensity of the peak at 533 eV clearly increased if millerite was conditioned with Cu and KEX, which might ascribe to the xanthate species (Ihs et al., 1994; Mikhlin, Karacharov, et al., 2016b; Szargan et al., 1992), yet it was difficult to differentiate between the adsorbed water or xanthate species as the peak locations overlapped. Although the analysis of S 2p, C 1s and O 1s spectrum suggested the existence of Cu (I) xanthate species on Cu-activated millerite at pH 9, it was difficult to discern between the chemisorbed xanthate or metal xanthate species and the surface sulphur species due to the peak overlapping. It was inconclusive whether there was dixanthogen or not since the XPS analysis that conducted under ultra-high vacuum at room temperature failed to detect dixanthogen. Further studies are required to identify whether dixanthogen exists or not.

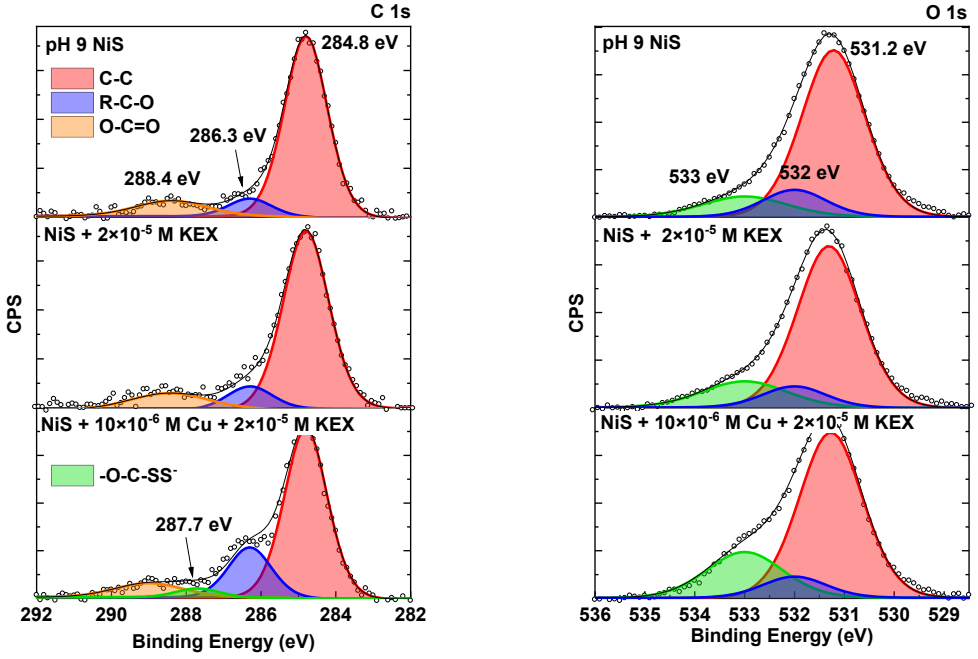

Figure 5.9 XPS (A) C 1s and (B) O 1s spectra of millerite conditioned with (i) collectorless condition, (ii) 2×10^{-5} M KEX and (iii) 10×10^{-6} Cu and 2×10^{-5} M KEX at pH 9.

5.3.3.3 Ni 2p $_{3/2}$ Spectra

In addition to Cu and S spectra, Ni 2p $_{3/2}$ spectra were also analyzed to provide complementary information on millerite surface chemistry. The fitted spectra are shown in Figure 5.10 (A) and (B). For Ni 2p $_{3/2}$ spectrum, each main peak was accompanied by a satellite peak (Biesinger et al., 2009, 2011; Legrand et al., 1998; Mansour, 1994a, 1994b; Mansour & Melendres, 1994; Richardson & Vaughan, 1989), and nickel sulphide (NiS), nickel hydroxide ($Ni(OH)_2$) as well as nickel sulphoxy species (NiS_xO_y) had been identified. Species proportions and the ratio of NiS_xO_y to NiS at pH 9 and pH 12 are shown in Figure 5.10 (C) and (D), respectively. Millerite surface was more dominated by $Ni(OH)_2$ species at pH 12 than at pH 9. Upon the addition of copper and/or xanthate, the ratio of nickel sulphoxy species to nickel sulphide decreased, suggested that millerite surface oxidation was affected and less sulphoxy species were formed. The reduction in nickel sulphoxy species also supported the findings based on S 2p spectra and the solution analysis result. In addition, there was no obvious increase in the proportion of $Ni(OH)_2$ upon the adsorption of Cu, suggesting that Ni dissolution was not affected by the adsorption of Cu, and Cu adsorption on millerite was not a not a simple ion exchange process between Cu and Ni at the lattice sites. This finding agreed with the Cu adsorption test result.

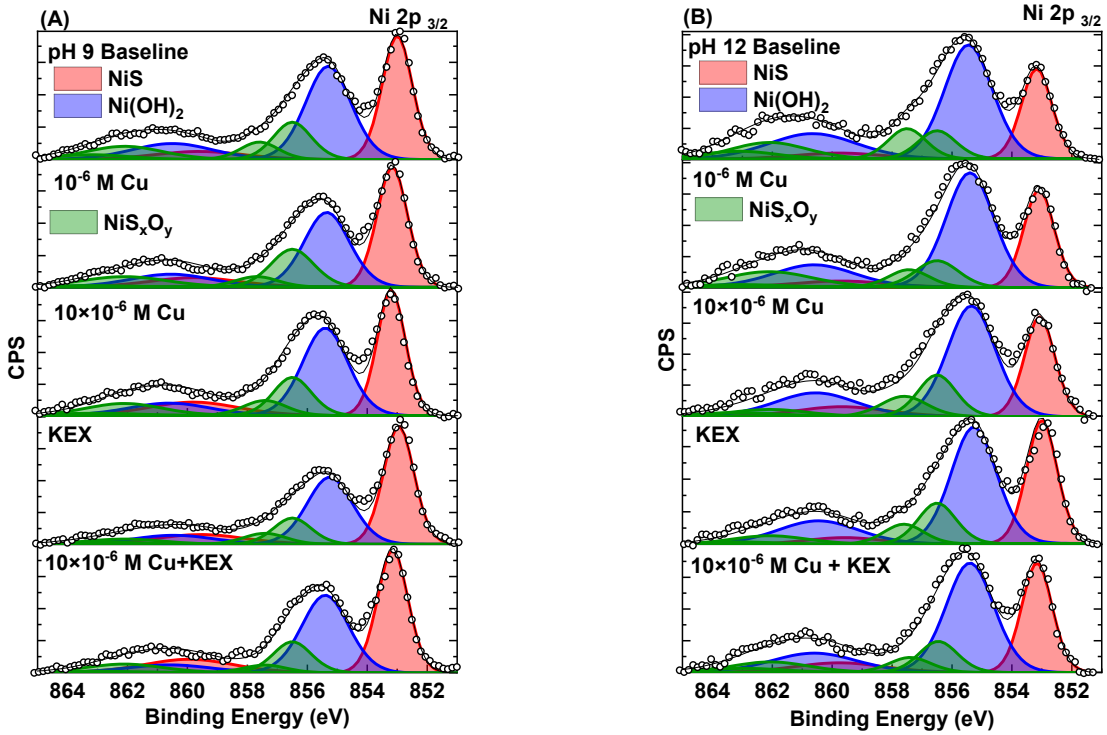

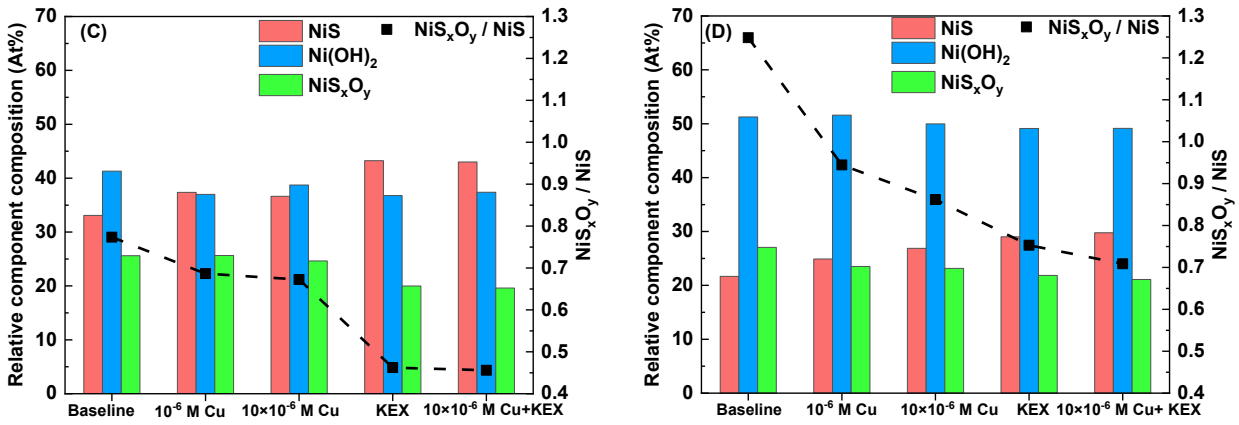

Figure 5.10 XPS Ni 2p $_{3/2}$ spectra of millerite at (A) pH 9 and (B) pH 12 conditioned with (i) collectorless condition, (ii) 10^{-6} M Cu, (iii) 10×10^{-6} M Cu, (iv) KEX and (v) 10×10^{-6} M Cu and KEX, and the corresponding species proportions, and ratio of nickel sulphoxy species to nickel sulphide at (C) pH 9 and (D) pH 12. (KEX concentration was 2×10^{-5} M at pH 9 and 10^{-4} M at pH 12)

5.4 Conclusions

Copper ions were found to be able to activate millerite flotation at both pH 9 and pH 12 if millerite was conditioned with Cu prior to KEX. The activation effect depended on the concentration of copper. At pH 9, adding 10×10^{-6} M Cu^{2+} increased millerite recovery from 65.0% to 91.5%, while adding 10^{-6} M Cu^{2+} can increase millerite recovery from 29.5% to 50.1% at pH 12. A relatively high copper dosage (10×10^{-6} M) at pH 12 had a negative effect on the copper activation of millerite flotation, with the recovery only increased to 34.4%. Cu-activated millerite can still be depressed by dextrin in the presence of KEX at both pH 9 and pH 12. Copper adsorption test revealed that Cu uptake by millerite was rapid, almost all Cu were consumed by millerite within 5 minutes. The addition of copper ions resulted in less sulphur dissolution, and copper (II) oxidation species was also detected on millerite surface. There was no obvious increase in Ni dissolution and nickel hydroxide on millerite surface upon the adsorption of Cu. Surface analysis by XPS revealed the main copper species formed on millerite surface is Cu (I) sulphide that might have a similar valence state as covellite ($Cu_3^+S^{2-}S_2^{2-}$) with minor Cu (II) sulphide and Cu (II) oxide/hydroxide. The Cu (I) sulphide arose from the reduction of Cu (II) that adsorbed on millerite surface. The Cu (II) – O species might attribute to the

precipitation and adsorption of Cu (II) from the bulk and/or because of the oxidation of copper sulphide formed on the millerite surface. The ratio of Cu – S to Cu – O increased significantly for millerite conditioned with Cu and KEX at pH 9, where copper hydroxide species reduced considerably. As the concentration of Cu (II) was increased from 10^{-6} M to 10×10^{-6} M, the ratio of Cu – S to Cu – O dropped significantly at pH 12, indicating a substantial increase in Cu (II) hydroxide species that rendered the surface more hydrophilic, which supported the flotation results at pH 12 with 10×10^{-6} M Cu. Surface monosulphide species (surface S^{2-}) was identified based on S 2p spectrum of millerite, which might be due to the nickel hydroxide passivation layer covering the metal-deficient sulphur-rich layer, preventing monosulphide from further oxidation. In response to the reduction of Cu (II) to Cu (I), sulphur oxidation was affected, where surface $S^{2-}$was oxidized to disulphide S_2^{2-}. As a result, the proportion of disulphide S_2^{2-} increased with less sulphoxy species generated. In conclusion, copper ion activated millerite flotation by affecting the surface oxidation.

Chapter 6 Conclusions and Future Work

6.1 Major Conclusions

This dissertation investigated the flotation chemistry of millerite, a less common nickel sulphide mineral, at alkaline environment with pure minerals using potassium ethyl xanthate (KEX) as the collector. The depression of millerite by natural polysaccharide in the Cu-Ni sulphide flotation as well as the activation of millerite by copper (II) ions were fundamentally studied. The major findings are summarized below:

- Single mineral flotation tests indicated that dextrin's depressing effect on millerite was pH dependent. If adding dextrin after KEX, dextrin was efficient in depressing xanthate-treated millerite but not xanthate-treated chalcopyrite at alkaline pH.
- Mixed mineral flotation tests showed that dextrin was efficient in depressing xanthate-treated millerite while not compromising chalcopyrite's recovery under alkaline environment. At pH 9, 2 ppm dextrin resulted in a Cu/Ni separation efficiency of 64%, which increased by 49.5% compared with the baseline. At pH 12, a Cu/Ni separation efficiency of 79% that increased by 39% was achieved by 0.5 ppm dextrin.
- Static contact angle measurement indicated that dextrin could lower the surface hydrophobicity of xanthate-treated millerite but not xanthate-treated chalcopyrite, which supported the micro-flotation test results.
- Millerite surface was dominated by a nickel hydroxide passivation layer in alkaline solution with and without KEX that originated from severe surface oxidation.
- Dextrin adsorption on millerite was an irreversible chemisorption process, for which the hydroxyl functional group of dextrin interacted with the nickel hydroxide on millerite surface. When adding dextrin after KEX, dextrin adsorbed less on xanthate-treated millerite surface, while KEX adsorption was not affected, indicating dextrin and KEX adsorbed through different surface sites. As pH was increased from pH 9 to pH 12, the nickel hydroxide passivation layer gradually inhibited xanthate adsorption on millerite, which favoured dextrin adsorption.
- Dextrin displayed a higher affinity toward millerite than chalcopyrite accompanied by a higher free energy of adsorption. At pH 12, dextrin can still adsorb on xanthate-treated millerite but not on xanthate-treated chalcopyrite. XPS analysis, AFM imaging and bulk

adsorption tests indicated a negligible adsorption of dextrin on xanthate-treated chalcopyrite at pH 12. Chalcopyrite was much less prone to surface oxidation in aqueous solutions, resulting in less sites available for dextrin adsorption than millerite, especially after conditioning with KEX.

- Copper ions were found to be able to activate millerite flotation at both pH 9 and pH 12 if millerite was conditioned with Cu prior to KEX. At pH 9, adding 10×10^{-6} M Cu^{2+} increased millerite recovery from 65.0% to 91.5%, while adding 10^{-6} M Cu^{2+} can increase millerite recovery from 29.5% to 50.1% at pH 12. However, adding 10×10^{-6} M Cu^{2+} at pH 12 had a negative effect on the activation, the recovery only increased to 34.4% comparing with the baseline.
- Copper adsorption tests revealed that Cu uptake by millerite was rapid, almost all Cu were consumed by millerite within 5 minutes, copper hydroxide was the dominant adsorption species at alkaline pH. The addition of copper ions resulted in less sulphur dissolution while copper (II) oxidation species was also detected on millerite surface. Meanwhile, Ni dissolution and nickel hydroxide passivation layer on millerite surface were not increased.
- The main copper species that existed on millerite surface under alkaline pH was Cu (I) sulphide that might have a similar valence as covellite ($Cu_3^+S^{2-}S_2^{2-}$) with minor Cu (II) sulphide and Cu (II) hydroxide. The Cu (I) sulphide originated from the reduction of Cu (II) that adsorbed on millerite surface. The Cu (II) – O species might be attributable to the precipitation and adsorption of Cu (II) from the bulk and/or because of the oxidation of copper sulphide formed on the millerite surface.
- The ratio of Cu – S to Cu – O increased significantly for millerite conditioned with Cu and KEX at pH 9, where copper hydroxide species reduced considerably.
- As the concentration of Cu (II) was increased from 10^{-6} M to 10×10^{-6} M, the ratio of Cu – S to Cu – O dropped significantly at pH 12, indicating a substantial increase in Cu (II) hydroxide species that rendered the surface more hydrophilic, which supported the flotation results at pH 12 with 10×10^{-6} M Cu.
- A surface monosulphide species (surface S^{2-}) was identified that was less coordinated than the bulk monosulphide, which might be due to the nickel hydroxide passivation

layer covering the metal-deficient sulphur-rich layer, preventing surface monosulphide from further oxidation.

- In response to the reduction of Cu (II) to Cu (I), sulphur oxidation was affected. Surface monomeric sulphur species $S^{2-}$was oxidized to surface disulphide species S_2^{2-} with less sulphoxy species generated.

6.2 Suggestions for Future Work

- In this study, dextrin was chosen as a representative of natural polysaccharide to examine its depression performance on millerite in Cu-Ni flotation. As it was found that dextrin adsorption was strongly related to the metal hydroxide species on mineral surface, surface oxidation thus played a key role. There are numerous studies on the combination use of polysaccharide depressants with a secondary regulator in sulphide mineral flotation to enhance separation in sulphide mineral flotation (B. Feng et al., 2021; Q. Liu & Zhang, 2000; R. Z. Liu et al., 2016; C. Wang et al., 2020). Hence, it is worthy to explore the use of an oxidising reagent such as hypochlorite, hydrogen peroxide and ammonium persulfate as a secondary regulator in combination with the use of dextrin. The synergistic effect can then be studied.
- The possibility of using other polysaccharides such as chitosan, starch or cellulose and their derivatives as millerite depressant should be investigated to provide the most cost-efficient depression strategy for the plant operations. The depression performance can be compared based on factors such as different functional groups or molecular weight of the polysaccharide.
- In this study, only micro-flotation tests using pure mineral were carried out to study the flotation chemistry of millerite. In order to be more practical, batch flotation tests using plant samples (real ore samples) and process water should be conducted with Denver flotation cell under the optimal conditions obtained from this study on the millerite flotation chemistry; and the results should be evaluated and compared with micro-flotation tests.
- Copper ion's effect on xanthate uptake by millerite can be studied to elucidate whether the adsorption of Cu promotes xanthate adsorption or not. Surface characterization techniques such as FTIR and cryo-XPS can be powerful in identifying the xanthate

species adsorbed on millerite in the presence of Cu and the adsorption mechanism (Deng, Karpuzov, et al., 2013; Kartio et al., 1992).

- This work explored the effect of copper ions on the flotation of millerite and it was observed that copper ion has an activation effect on the flotation of millerite. Qi, Liu, et al. (2019) studied divalent cations' effect on pyrrhotite flotation at alkaline environment and it was found that copper and nickel ions have an activation effect while calcium and magnesium ions have a depression effect. Hence, divalent cations such as nickel, calcium and magnesium's effect on millerite flotation can be investigated, especially calcium ions as lime instead of caustic is usually used as pH regulator in the plant operations.

Bibliography

Acar, S., & Somasundaran, P. (1992). Effect of dissolved mineral species on the electrokinetic behaviour of sulphides. *Minerals Engineering*, *5*(1), 27–40.

Acres, R. G., Harmer, S. L., & Beattie, D. A. (2010). Synchrotron XPS, NEXAFS, and ToF-SIMS studies of solution exposed chalcopyrite and heterogeneous chalcopyrite with pyrite. *Minerals Engineering*, *23*(11–13), 928–936. https://doi.org/10.1016/j.mineng.2010.03.007

Afenya, P. M. (1982). Adsorption of xanthate and starch on synthetic graphite. *International Journal of Mineral Processing*, *9*, 303–319.

Agar, G. E. (1991). Flotation of chalcopyrite, pentlandite, pyrrhotite ores. *International Journal of Mineral Processing*, *33*(1–4), 1–19. https://doi.org/10.1016/0301-7516(91)90039-L

Allison, S. A. (1982). Interactions between sulphide minerals and metal ions in the activation, deactivation, and depression of mixed sulphide ores during the flotation process. In *Report No.M 29*. Council for Mineral Technology.

Allison, S. A., & O'Connor, C. T. (2011). An investigation into the flotation behaviour of pyrrhotite. *International Journal of Mineral Processing*, *98*(3–4), 202–207. https://doi.org/10.1016/j.minpro.2010.12.003

Amais, R. S., Donati, G. L., & Nóbrega, J. A. (2012). Interference standard applied to sulfur determination in biodiesel microemulsions by ICP-QMS. *Journal of the Brazilian Chemical Society*, *23*(5), 797–803. https://doi.org/10.1590/S0103-50532012000500002

Amaral, I. F., Granja, P. L., & Barbosa, M. A. (2005). Chemical modification of chitosan by phosphorylation: An XPS, FT-IR and SEM study. *Journal of Biomaterials Science, Polymer Edition*, *16*(12), 1575–1593. https://doi.org/10.1163/156856205774576736

Avotins, P. V., Wang, S. S., & Nagaraj, D. R. (1994). Recent advances in sulfide collector development. In P. S. Mulukutla (Ed.), *Reagents for better metallurgy* (pp. 47–56).

Balajee, S. R., & Iwasaki, I. (1969). Adsorption mechanism of starches in flotation and

flocculation of iron ores. *Trans. SME/AIME*.

Beamson, G., & Briggs, D. (1993). High resolution XPS of organic polymers: The Science ESCA 300 Database. *Journal of Chemical Education*, *70*(1), A25.

Beattie, D. A., Huynh, L., Kaggwa, G. B. N., & Ralston, J. (2006). The effect of polysaccharides and polyacrylamides on the depression of talc and the flotation of sulphide minerals. *Minerals Engineering*, *19*, 598–608. https://doi.org/10.1016/j.mineng.2005.09.011

Beaussart, A., Mierczynska-Vasilev, A., & Beattie, D. A. (2009). Adsorption of dextrin on hydrophobic minerals. *Langmuir*, *25*(17), 9913–9921. https://doi.org/10.1021/la9010778

Berg, J. C. (2009). Electrical Properties of Interfaces. In *Introduction To Interfaces And Colloids: The Bridge To Nanoscience* (pp. 455–524). World Scientific Publishing Company.

Bertin, E. P. (1975). Principles and Practice of X-Ray Spectrometric Analysis. In *NASPA Journal* (2nd ed., Vol. 42, Issue 4). Springer US. https://doi.org/10.1017/CBO9781107415324.004

Biesinger, M. C. (2017). Advanced analysis of copper X-ray photoelectron spectra. *Surface and Interface Analysis*, *49*(13), 1325–1334. https://doi.org/10.1002/sia.6239

Biesinger, M. C., Lau, L. W. M., Gerson, A. R., & Smart, R. S. C. (2010). Resolving surface chemical states in XPS analysis of first row transition metals, oxides and hydroxides: Sc, Ti, V, Cu and Zn. *Applied Surface Science*, *257*(3), 887–898. https://doi.org/10.1016/j.apsusc.2010.07.086

Biesinger, M. C., Payne, B. P., Grosvenor, A. P., Lau, L. W. M., Gerson, A. R., & Smart, R. S. C. (2011). Resolving surface chemical states in XPS analysis of first row transition metals, oxides and hydroxides: Cr, Mn, Fe, Co and Ni. *Applied Surface Science*, *257*(7), 2717–2730. https://doi.org/10.1016/j.apsusc.2010.10.051

Biesinger, M. C., Payne, B. P., Lau, L. W. M., Gerson, A., & Smart, R. S. C. (2009). X-ray photoelectron spectroscopic chemical state Quantification of mixed nickel metal, oxide and

hydroxide systems. *Surface and Interface Analysis*, *41*(4), 324–332. https://doi.org/10.1002/sia.3026

Bolin, N. J., & Laskowski, J. S. (1991). Polysaccharides in flotation of sulphides. Part II. Copper/lead separation with dextrin and sodium hydroxide. *International Journal of Mineral Processing*, *33*(1–4), 235–241. https://doi.org/10.1016/0301-7516(91)90055-N

Bozkurt, V., Xu, Z., & Finch, J. A. (1998). Pentlandite/pyrrhotite interaction and xanthate adsorption. *International Journal of Mineral Processing*, *52*(4), 203–214. https://doi.org/10.1016/s0301-7516(97)00072-0

Bozkurt, V., Xu, Z., & Finch, J. A. (1999). Effect of Depressants on Xanthate Adsorption on Pentlandite and Pyrrhotite: Single vs Mixed Minerals. *Canadian Metallurgical Quarterly*, *38*(2), 105–112. https://doi.org/10.1179/cmq.1999.38.2.105

Bryson, L. J., Hofirek, Z., Collins, M. J., Stiksma, J., & Berezowsky, R. M. (2008). New matte leaching developments at anglo platinum's base metal refinery. *Hydrometallurgy 2008: Proceedings of the 6th International Symposium*, 570–579.

Buckley, A. N., & Woods, R. (1995). Identifying chemisorption in the interaction of thiol collectors with sulfide minerals by XPS: adsorption of xanthate on silver and silver sulfide. *Colloids and Surfaces A: Physicochemical and Engineering Aspects*, *104*, 295–305. https://doi.org/10.1016/0927-7757(95)03279-1

Bulatovic, S. M. (2007). Flotation of Nickel and Nickel-Copper Ores. In *Handbook of Flotation Reagents: chemistry, theory and practice:flotation of sulfide ores* (pp. 401–442). Elsevier. https://doi.org/10.1016/B978-0-444-53082-0.00023-8

Butt, H. J., Cappella, B., & Kappl, M. (2005). Force measurements with the atomic force microscope: Technique, interpretation and applications. *Surface Science Reports*, *59*(1–6), 1–152. https://doi.org/10.1016/j.surfrep.2005.08.003

Cabrera-German, D., García-Valenzuela, J. A., Martínez-Gil, M., Suárez-Campos, G., Montiel-González, Z., Sotelo-Lerma, M., & Cota-Leal, M. (2019). Assessing the chemical state of chemically deposited copper sulfide: A quantitative analysis of the X-ray photoelectron

spectra of the amorphous-to-covellite transition phases. *Applied Surface Science*, *481*(November 2018), 281–295. https://doi.org/10.1016/j.apsusc.2019.03.054

Cao, M., & Liu, Q. (2006). Reexamining the functions of zinc sulfate as a selective depressant in differential sulfide flotation-The role of coagulation. *Journal of Colloid and Interface Science*, *301*(2), 523–531. https://doi.org/10.1016/j.jcis.2006.05.036

Chachula, F., & Liu, Q. (2003). Upgrading a rutile concentrate produced from athabasca oil sands tailings. *Fuel*, *82*(8), 929–942. https://doi.org/10.1016/S0016-2361(02)00401-5

Chander, S. (1991). Electrochemistry of sulfide flotation: Growth characteristics of surface coatings and their properties, with special reference to chalcopyrite and pyrite. *International Journal of Mineral Processing*, *33*(1–4), 121–134. https://doi.org/10.1016/0301-7516(91)90047-M

Chen, Q., Xu, S., Liu, Q., Masliyah, J., & Xu, Z. (2016). QCM-D study of nanoparticle interactions. *Advances in Colloid and Interface Science*, *233*, 94–114. https://doi.org/10.1016/j.cis.2015.10.004

Clarke, P., Fornasiero, D., Ralston, J., & Smart, R. S. C. (1995). A study of the removal of oxidation products from sulfide mineral surfaces. *Minerals Engineering*, *8*(11), 1347–1357. https://doi.org/10.1016/0892-6875(95)00101-U

Crundwell, F. K., Moats, M. S., Ramachandran, V., Robinson, T. G., & Davenport, W. G. (2011). Production of Nickel Concentrate from Ground Sulfide Ore. In *Extractive Metallurgy of Nickel, Cobalt and Platinum Group Metals* (pp. 171–189). Elsevier. https://doi.org/10.1016/b978-0-08-096809-4.10015-2

de Wet, J. R., Pistorius, P. C., & Sandenbergh, R. F. (1997). The influence of cyanide on pyrite flotation from gold leach residues with sodium isobutyl xanthate. *International Journal of Mineral Processing*, *49*(3–4), 149–169. https://doi.org/10.1016/s0301-7516(96)00031-2

Deng, M., Karpuzov, D., Liu, Q., & Xu, Z. (2013). Cryo-XPS study of xanthate adsorption on pyrite. *Surface and Interface Analysis*, *45*(4), 805–810. https://doi.org/10.1002/sia.5165

Deng, M., Liu, Q., & Xu, Z. (2013). Impact of gypsum supersaturated water on the uptake of copper and xanthate on sphalerite. *Minerals Engineering*, *49*, 165–171. https://doi.org/10.1016/j.mineng.2013.05.014

Deng, M., Xu, Z., & Liu, Q. (2014). Impact of gypsum supersaturated process water on the interactions between silica and zinc sulphide minerals. *Minerals Engineering*, *55*, 172–180. https://doi.org/10.1016/j.mineng.2013.09.017

Descostes, M., Mercier, F., Thromat, N., Beaucaire, C., & Gautier-Soyer, M. (2000). Use of XPS in the determination of chemical environment and oxidation state of iron and sulfur samples: Constitution of a data basis in binding energies for Fe and S reference compounds and applications to the evidence of surface species of an oxidized py. *Applied Surface Science*, *165*(4), 288–302. https://doi.org/10.1016/S0169-4332(00)00443-8

Dixon, M. C. (2008). Quartz crystal microbalance with dissipation monitoring: Enabling real-time characterization of biological materials and their interactions. *Journal of Biomolecular Techniques*, *19*(3), 151–158.

Donaldson, E. M. (1976). Solvent extraction of metal xanthates. *Talanta*, *23*(6), 417–426. https://doi.org/10.1016/0039-9140(76)80121-X

Dubois, M., Gilles, K. A., Hamilton, J. K., Rebers, P. A., & Smith, F. (1956). Colorimetric Method for Determination of Sugars and Related Substances. *Analytical Chemistry*, *28*, 350–356. https://doi.org/10.1021/ac60111a017

Eirich, F. R. (1977). The conformational states of macromolecules adsorbed at solid-liquid interfaces. *Journal of Colloid And Interface Science*, *58*(2), 423–436. https://doi.org/10.1016/0021-9797(77)90152-7

Ejtemaei, M., & Nguyen, A. V. (2017a). Characterisation of sphalerite and pyrite surfaces activated by copper sulphate. *Minerals Engineering*, *100*, 223–232. https://doi.org/10.1016/j.mineng.2016.11.005

Ejtemaei, M., & Nguyen, A. V. (2017b). Kinetic studies of amyl xanthate adsorption and bubble attachment to Cu-activated sphalerite and pyrite surfaces. *Minerals Engineering*, *112*(July),

36–42. https://doi.org/10.1016/j.mineng.2017.07.005

Fairthorne, G., Fornasiero, D., & Ralston, J. (1997). Effect of oxidation on the collectorless flotation of chalcopyrite. *International Journal of Mineral Processing*, *49*, 31–48. https://doi.org/10.1016/s0301-7516(96)00039-7

Fan, H., Yu, H., Wu, X., Zhang, Y., Luo, Z., Wang, H., Guo, Y., Madhavi, S., & Yan, Q. (2016). Controllable Preparation of Square Nickel Chalcogenide (NiS and NiSe2) Nanoplates for Superior Li/Na Ion Storage Properties. *ACS Applied Materials and Interfaces*, *8*, 25261–25267. https://doi.org/10.1021/acsami.6b07300

Feng, B., Jiao, X., Wang, H., Peng, J., & Yang, G. (2021). Improving the separation of chalcopyrite and galena by surface oxidation using hydroxyethyl cellulose as depressant. *Minerals Engineering*, *160*(October 2020), 106657. https://doi.org/10.1016/j.mineng.2020.106657

Feng, L. (2019). *Understanding surface forces and interaction mechanisms in mineral flotation by atomic force microscopy*. University of Alberta.

Fornasiero, D., Eijt, V., & Ralston, J. (1992). An electrokinetic study of pyrite oxidation. *Colloids and Surfaces*, *62*(1–2), 63–73. https://doi.org/10.1016/0166-6622(92)80037-3

Fuerstenau, D. W., & Pradip. (2005). Zeta potentials in the flotation of oxide and silicate minerals. *Advances in Colloid and Interface Science*, *114–115*, 9–26. https://doi.org/10.1016/j.cis.2004.08.006

Fuerstenau, M. C., Jameson, G. J., & Yoon, R. H. (2007). *Froth Flotation: A centruy of innovation*. Society for Mining, Metallurgy, and Exploration.

Fullston, D., Fornasiero, D., & Ralston, J. (1999). Zeta potential study of the oxidation of copper sulfide minerals. *Colloids and Surfaces A: Physicochemical and Engineering Aspects*, *146*, 113–121. https://doi.org/10.1016/S0927-7757(98)00725-0

Gardner, J. R., & Woods, R. (1979). An electrochemical investigation of the natural flotability of chalcopyrite. *International Journal of Mineral Processing*, *6*(1), 1–16.

https://doi.org/10.1016/0301-7516(79)90028-0

Gaudin, A. M., & Fuerstenau, M. C. (1976). *Flotation: A.M. Gaudin Memorial Volume*. American Institute of Mining, Metallurgical, and Petroleum Engineers.

Gerson, A. R., & Jasieniak, M. (2008). The effect of surface oxidation on the Cu activation of pentlandite and pyhrrotite.pdf. *XXIV International Minerals Processing Congress IMPC*, 1054–1063.

Glencore. (n.d.). *Welcome to Sudbury Integrated Nickel Operations*. Retrieved August 17, 2020, from https://www.sudburyino.ca/en/Pages/home.aspx

Goh, S. W., Buckley, A. N., & Lamb, R. N. (2006). Copper(II) sulfide? *Minerals Engineering*, *19*(2), 204–208. https://doi.org/10.1016/j.mineng.2005.09.003

Guo, B., Peng, Y., & Espinosa-Gomez, R. (2014). Cyanide chemistry and its effect on mineral flotation. *Minerals Engineering*, *66*, 25–32. https://doi.org/10.1016/j.mineng.2014.06.010

Gurumoorthy, A. V. P., & Khan, K. H. (2011). Polymers at interfaces: Biological and non-biological applications. *Recent Research in Science and Technology*, *3*(2), 80–86.

Haldar, S. K. (2017). Introduction. In *Platinum-Nickel-Chromium Deposits: Geology, Exploration and Reserve Base* (pp. 1–35). https://doi.org/10.1016/b978-0-12-802041-8.00001-8

Haung, H. H., Calara, J. V., Bauer, D. L., & Miller, J. D. (1978). Adsorption reactions in the depression of coal by organic colloids. *Recent Development in Separation Science*, *4*, 115–133.

Hepel, T., & Pomianowski, A. (1977). Diagrams of electrochemical equilibria of the system copper-potassium ethylxanthate-water at 25°C. *International Journal of Mineral Processing*, *4*(4), 345–361. https://doi.org/10.1016/0301-7516(77)90013-8

Hodgson, M., & Agar, G. E. (1989). Electrochemical investigations into the flotation chemistry of pentlandite and pyrrhotite: process water and xanthate interactions. *Canadian*

Metallurgical Quarterly, *28*(3), 189–198.

Huang, P., Cao, M., & Liu, Q. (2012). Adsorption of chitosan on chalcopyrite and galena from aqueous suspensions. *Colloids and Surfaces A: Physicochemical and Engineering Aspects*, *409*, 167–175. https://doi.org/10.1016/j.colsurfa.2012.06.016

Ihs, A., Uvdal, K., & Liedberg, B. (1994). Infrared Study of Ethyl and Octyl Xanthate Ions Adsorbed on Metallic and Sulfidized Copper and Silver Surfaces. *Langmuir*, *10*(3), 734–740. https://doi.org/10.1021/la00015a023

Iwasaki, I., & Lai, R. W. (1965). Starches and starch products as depressatns in soap flotation of activated silica from iron ores. *Trans. AIME*, *232*, 364–371.

Jiang, N., Tang, Q., Sheng, M., You, B., Jiang, D. E., & Sun, Y. (2016). Nickel sulfides for electrocatalytic hydrogen evolution under alkaline conditions: A case study of crystalline NiS, NiS2, and Ni3S2 nanoparticles. *Catalysis Science and Technology*, *6*, 1077–1084. https://doi.org/10.1039/c5cy01111f

Jin, J., Wang, X., Gao, P., Liu, J., Zhu, Y., & Han, Y. (2021). Selective adsorption behavior and mechanism of a high-performance depressant in the flotation separation of pyrite from talcum. *Journal of Molecular Liquids*, *325*, 114707. https://doi.org/10.1016/j.molliq.2020.114707

Kalegowda, Y., Chan, Y. L., Wei, D. H., & Harmer, S. L. (2015). X-PEEM, XPS and ToF-SIMS characterisation of xanthate induced chalcopyrite flotation: Effect of pulp potential. *Surface Science*, *635*, 70–77. https://doi.org/10.1016/j.susc.2014.12.012

Kandil, A. A. E. H. A. (2016). *Understanding the Effect of Non-starch Grain Components on the Amylolysis of Starch in Whole Grains*. University of Alberta.

Kartio, I., Laajalehto, K., Suoninen, E., Karthe, S., & Szargan, R. (1992). Technique for XPS Measurements of Volatile Adsorbed Layers: Application to Studies of Sulphide Flotation. *Surface and Interface Analysis*, *18*, 807–810.

Kelebek, S., Fekete, S. O., & Wells, G. W. (1995). Selective depression of pyrrhotite using

sulphur dioxide-diethylenetriamine reagent combination. *Proceedings XIX Int. Mineral Processing Congress, Vol. 3*, 181–187.

Kelebek, S., & Tukel, C. (1999). The effect of sodium metabisulfite and triethylenetetramine system on pentlandite-pyrrhotite separation. *International Journal of Mineral Processing*, *57*(2), 135–152. https://doi.org/10.1016/S0301-7516(99)00012-5

Kelebek, S., Wells, P. F., & Fekete, S. O. (1996). Differential flotation of chalcopyrite, pentlandite and pyrrhotite in Ni-Cu Fe, Ni9S8 sulphide ores. *Canadian Metallurgical Quarterly*, *35*(4), 329–336. https://doi.org/10.1016/S0008-4433(96)00017-1

Keleşoğlu, S., Volden, S., Kes, M., & Sjöblom, J. (2012). Adsorption of naphthenic acids onto mineral surfaces studied by quartz crystal microbalance with dissipation monitoring (QCM-D). *Energy and Fuels*, *26*(8), 5060–5068. https://doi.org/10.1021/ef300612z

Kerr, A. (2002). An overview of recent developments in flotation technology and plant practice for nickel ores. In A. L. Mular, D. N. Halbe, & D. J. Barratt (Eds.), *Mineral processing, plant design, practice and control proceedings, Vol. 1* (pp. 1142–1158). SME.

Khosla, N. K., Bhagat, R. P., Gandhi, K. S., & Biswas, A. K. (1984). Calorimetric and other interaction studies on mineral-starch adsorption systems. *Colloids and Surfaces*, *8*, 321–336. https://doi.org/10.1016/0166-6622(84)80127-4

Kibel, M. H. (2003). X-Ray Photoelectron Spectroscopy. In D. J. O'Connor, B. A. Sexton, & R. S. C. Smart (Eds.), *Surface Analysis Methods in Materials Science* (2nd ed.). Springer Berlin Heidelberg. https://doi.org/https://doi-org.login.ezproxy.library.ualberta.ca/10.1007/978-3-662-05227-3

Kou, J., Tao, D., & Xu, G. (2010). Fatty acid collectors for phosphate flotation and their adsorption behavior using QCM-D. *International Journal of Mineral Processing*, *95*(1–4), 1–9. https://doi.org/10.1016/j.minpro.2010.03.001

Krasowska, M., Zawala, J., Bradshaw-Hajek, B. H., Ferri, J. K., & Beattie, D. A. (2018). Interfacial characterisation for flotation: 1. Solid-liquid interface. *Current Opinion in Colloid and Interface Science*, *37*(May), 61–73. https://doi.org/10.1016/j.cocis.2018.06.004

Kullerud, G., & Yund, R. A. (1962). The Ni - S System and Related Minerals. *Journal of Petrology*, *3*(1), 126–175.

Kundu, M., Hasegawa, T., Terabe, K., Yamamoto, K., & Aono, M. (2008). Structural studies of copper sulfide films: Effect of ambient atmosphere. *Science and Technology of Advanced Materials*, *9*(3). https://doi.org/10.1088/1468-6996/9/3/035011

Kydros, K. A., Gallios, G. P., & Matis, K. A. (1994). Modification of Pyrite and Sphalerite Flotation by Dextrin. *Separation Science and Technology*, *29*(17), 2263–2275. https://doi.org/10.1080/01496399408003178

Langmuir, I. (1918). The adsorption of gases on plane surfaces of glass, mica and platinum. *Journal of the American Chemical Society*, *9*, 1361–1403.

Laskowski, J. S., Liu, Q., & O'Connor, C. T. (2007). Current understanding of the mechanism of polysaccharide adsorption at the mineral/aqueous solution interface. *International Journal of Mineral Processing*, *84*, 59–68. https://doi.org/10.1016/j.minpro.2007.03.006

Laskowski, J. S., & Nyamekye, G. A. (1994). Adsorption studies in flotation research: differential flotation of Cu–Ni sulfides using dextrin. In S. Castro & J. Alvarez (Eds.), *IV Meeting of the Southern Hemisphere on Mineral Technology and III Latin American Congress on Froth Flotation* (pp. 15–28). Conception.

Lawson, V., Kerr, A. N., Shields, Y., Wells, P. W., Xu, M., & Dai, Z. (2005). Improving pentlandite pyrrhotite separation at INCO's Clarabelle Mill. *Centenary of Flotation Symposium*, 875–885.

Legrand, D. L., Bancroft, G. M., & Nesbitt, H. W. (2005a). Oxidation/alteration of pentlandite and pyrrhotite surfaces at pH 9.3: Part 1. Assignment of XPS spectra and chemical trends. *American Mineralogist*, *90*(7), 1042–1054. https://doi.org/10.2138/am.2005.1691

Legrand, D. L., Bancroft, G. M., & Nesbitt, H. W. (2005b). Oxidation of pentlandite and pyrrhotite surfaces at pH 9.3: Part 2. Effect of xanthates and dissolved oxygen. *American Mineralogist*, *90*(7), 1055–1061. https://doi.org/10.2138/am.2005.1692

Legrand, D. L., Nesbitt, H. W., & Bancroft, G. M. (1998). X-ray photoelectron spectroscopic study of a pristine millerite (NiS) surface and the effect of air and water oxidation. *American Mineralogist*, *83*, 1256–1265. https://doi.org/10.2138/am-1998-11-1214

Leiro, J. A., Laajalehto, K., Kartio, I., & Heinonen, M. H. (1998). Surface core-level shift and phonon broadening in PbS(100). *Surface Science*, *412–413*, 3–8. https://doi.org/10.1016/S0039-6028(98)00479-8

Lekki, J., & Drzymala, J. (1990). Flotometric analysis of the collectorless flotation of sulphide materials. *Colloids and Surfaces*, *44*, 179–190. https://doi.org/10.1016/0166-6622(90)80195-A

Leppinen, J. (1990). FTIR and flotation investigation of the adsorption of ethyl xanthate on activated and non-activated sulfide minerals. *International Journal of Mineral Processing*, *30*, 245–263. https://doi.org/10.1016/0301-7516(90)90018-T

Leppinen, J., Basilio, C. I., & Yoon, R. H. (1989). In-situ FTIR study of ethyl xanthate adsorption on sulfide minerals under conditions of controlled potential. *International Journal of Mineral Processing*, *26*(3–4), 259–274. https://doi.org/10.1016/0301-7516(89)90032-X

Leppinen, J., Laajalehto, K., Kartio, I., & Souninenm, E. (1995). FTIR and XPS studies of surface chemistry of pyrite in flotation. *XIX Int. Miner. Process. Congress*, 35–38.

Li, Y., Taggart, M. A., McKenzie, C., Zhang, Z., Lu, Y., Pap, S., & Gibb, S. (2019). Utilizing low-cost natural waste for the removal of pharmaceuticals from water: Mechanisms, isotherms and kinetics at low concentrations. *Journal of Cleaner Production*, *227*, 88–97. https://doi.org/10.1016/j.jclepro.2019.04.081

Liu, Q., & Laskowski, J. S. (1989a). The interactions between dextrin and metal hydroxides in aqueous solutions. *Journal of Colloid And Interface Science*, *130*, 101–111. https://doi.org/10.1016/0021-9797(89)90081-7

Liu, Q., & Laskowski, J. S. (1989b). The role of metal hydroxides at mineral surfaces in dextrin adsorption, I. Studies on modified quartz samples. *International Journal of Mineral*

Processing, *26*, 297–316. https://doi.org/10.1016/0301-7516(89)90035-5

Liu, Q., & Laskowski, J. S. (1989c). The role of metal hydroxides at mineral surfaces in dextrin adsorption, II. Chalcopyrite-galena separations in the presence of dextrin. *International Journal of Mineral Processing*, *27*, 147–155. https://doi.org/10.1016/0301-7516(89)90012-4

Liu, Q., & Laskowski, J. S. (2006). Polysaccharide applications in mineral processing. In P. Somasundaran (Ed.), *Encyclopedia of Surface and Colloid Science* (2nd ed., pp. 5035–5055). Taylor & Francis.

Liu, Q., Laskowski, J. S., Li, Y., & Wang, D. (1994). Synergistic effect of mineral surface constituents in dextrin adsorption. *International Journal of Mineral Processing*, *42*, 251–266. https://doi.org/10.1016/0301-7516(94)00033-6

Liu, Q., & Zhang, Y. (2000). Effect of calcium ions and citric acid on the flotation separation of chalcopyrite from galena using dextrin. *Minerals Engineering*, *13*(13), 1405–1416. https://doi.org/10.1016/S0892-6875(00)00122-9

Liu, Q., Zhang, Y., & Laskowski, J. S. (2000). The adsorption of polysaccharides onto mineral surfaces: An acid/base interaction. *International Journal of Mineral Processing*, *60*, 229–245. https://doi.org/10.1016/S0301-7516(00)00018-1

Liu, R., Sun, W., Hu, Y., & Wang, D. (2010). Surface chemical study of the selective separation of chalcopyrite and marmatite. *Mining Science and Technology*, *20*, 542–545. https://doi.org/10.1016/S1674-5264(09)60240-4

Liu, R. Z., Qin, W. Q., Jiao, F., Wang, X. J., Pei, B., Yang, Y. J., & Lai, C. H. (2016). Flotation separation of chalcopyrite from galena by sodium humate and ammonium persulfate. *Transactions of Nonferrous Metals Society of China (English Edition)*, *26*(1), 265–271. https://doi.org/10.1016/S1003-6326(16)64113-4

Liu, S., Huang, B., Chai, L., Liu, Y., Zeng, G., Wang, X., Zeng, W., Shang, M., Deng, J., & Zhou, Z. (2017). Enhancement of As(v) adsorption from aqueous solution by a magnetic chitosan/biochar composite. *RSC Advances*, *7*(18), 10891–10900.

https://doi.org/10.1039/c6ra27341f

Liu, Y. (2009). Is the free energy change of adsorption correctly calculated? *Journal of Chemical and Engineering Data*, *54*, 1981–1985. https://doi.org/10.1021/je800661q

López-Valdivieso, A., Cervantes, T. C., Song, S., Cabrera, A. R., & Laskowski, J. S. (2004). Dextrin as a non-toxic depressant for pyrite in flotation with xanthates as collector. *Minerals Engineering*, *17*(9–10), 1001–1006. https://doi.org/10.1016/j.mineng.2004.04.003

López-Valdivieso, A., Sánchez López, A. A., Song, S., García Martínez, H. A., & Licón Almada, S. (2007). Dextrin as a regulator for the selective flotation of chalcopyrite, galena and pyrite. *Canadian Metallurgical Quarterly*, *46*(3), 301–310. https://doi.org/10.1179/cmq.2007.46.3.301

Lotter, N. O., Kormos, L. J., Oliveira, J., Fragomeni, D., & Whiteman, E. (2011). Modern process mineralogy: Two case studies. *Minerals Engineering*, *24*(7), 638–650. https://doi.org/10.1016/j.mineng.2011.02.017

Luttrell, G. H., & Yoon, R. H. (1984). Surface studies of the collectorless flotation of chalcopyrite. *Colloids and Surfaces*, *12*(C), 239–254. https://doi.org/10.1016/0166-6622(84)80103-1

Ma, H.-W., & Deng, M. (2017). An Optimized Procedure for Determining the Amylase/Amylopectin Ratio in Common Wheat Grains Based on the Dual Wavelength Iodine-Binding Method. *Journal of Genetics and Genetic Engineering*, *1*(1), 23–30.

Malysiak, V., O'Connor, C. T., Ralston, J., Gerson, A. R., Coetzer, L. P., & Bradshaw, D. J. (2002). Pentlandite-feldspar interaction and its effect on separation by flotation. *International Journal of Mineral Processing*, *66*(1–4), 89–106. https://doi.org/10.1016/S0301-7516(02)00007-8

Mansour, A. N. (1994a). Characterization of α-Ni(OH)2 by XPS. *Surface Science Spectra*, *3*(3), 279–286. https://doi.org/10.1116/1.1247757

Mansour, A. N. (1994b). Characterization of β-Ni(OH)2 by XPS. *Surface Science Spectra*, *3*(3),

279–286. https://doi.org/10.1116/1.1247757

Mansour, A. N., & Melendres, C. A. (1994). Characterization of Slightly Hydrated Ni(OH)2 by XPS. *Surface Science Spectra*, *3*(3), 247–254. https://doi.org/10.1116/1.1247753

Masliyah, J. H., & Bhattacharjee, S. (2005). Chapter 5: Electric Double Layer. In *Electrokinetic and Colloid Transport Phenomena* (pp. 105–178). Wiley-Interscience. https://doi.org/10.1002/0471799742.ch5

Masliyah, J. H., Jan, C., & Xu, Z. (2011). *Handbook on Theory and Practice of Bitumen Recovery from Athabasca Oil Sands Volume I: Theoretical Basis*. Kingsley Knowledge Pub.

Matias, T., Marques, J., Quina, M. J., Gando-Ferreira, L., Valente, A. J. M., Portugal, A., & Durães, L. (2015). Silica-based aerogels as adsorbents for phenol-derivative compounds. *Colloids and Surfaces A: Physicochemical and Engineering Aspects*, *480*, 260–269. https://doi.org/10.1016/j.colsurfa.2015.01.074

McNeil, M., Rao, S. R., & Finch, J. A. (1994). Oxidation of amyl xanthate by pentlandite. *Canadian Metallurgical Quarterly*, *33*(2), 165–167.

Mendiratta, N. K. (2000). *Kinetic Studies of Sulfide Mineral Oxidation and Xanthate Adsorption*. Virginia Polytechnic Institute and State University.

Mielczarski, J. A., Cases, J. M., Alnot, M., & Ehrhardt, J. J. (1996). XPS characterization of chalcopyrite, tetrahedrite, and tennantite surface products after different conditioning. 1. aqueous solution at pH 10. *Langmuir*, *12*(10), 2519–2530. https://doi.org/10.1021/la9505881

Mielczarski, J. A., Mielczarski, E., & Cases, J. M. (1998). Influence of chain length on adsorption of xanthates on chalcopyrite. *International Journal of Mineral Processing*, *52*(4), 215–231. https://doi.org/10.1016/s0301-7516(97)00074-4

Mielczarski, J., Werfel, F., & Suoninen, E. (1983). XPS studies of interaction of xanthate with copper surfaces. *Applications of Surface Science*, *17*(2), 160–174.

https://doi.org/10.1016/0378-5963(83)90031-4

Mikhlin, Y., Karacharov, A., Tomashevich, Y., & Shchukarev, A. (2016a). Cryogenic XPS study of fast-frozen sulfide minerals: Flotation-related adsorption of n-butyl xanthate and beyond. *Journal of Electron Spectroscopy and Related Phenomena*, *206*, 65–73. https://doi.org/10.1016/j.elspec.2015.12.003

Mikhlin, Y., Karacharov, A., Tomashevich, Y., & Shchukarev, A. (2016b). Interaction of sphalerite with potassium n-butyl xanthate and copper sulfate solutions studied by XPS of fast-frozen samples and zeta-potential measurement. *Vacuum*, *125*, 98–105. https://doi.org/10.1016/j.vacuum.2015.12.006

Mikhlin, Y., Vorobyev, S., Saikova, S., Tomashevich, Y., Fetisova, O., Kozlova, S., & Zharkov, S. (2016). Preparation and characterization of colloidal copper xanthate nanoparticles. *New Journal of Chemistry*, *40*(4), 3059–3065. https://doi.org/10.1039/c6nj00098c

Miller, J. D., Laskowski, J. S., & Chang, S. S. (1983). Dextrin adsorption by oxidized coal. *Colloids and Surfaces*, *8*, 137–151. https://doi.org/10.1016/0166-6622(83)80081-X

Moreira, G. F., Peçanha, E. R., Monte, M. B. M., Leal Filho, L. S., & Stavale, F. (2017). XPS study on the mechanism of starch-hematite surface chemical complexation. *Minerals Engineering*, *110*, 96–103. https://doi.org/10.1016/j.mineng.2017.04.014

Multani, R. S., Williams, H., Johnson, B., Li, R., & Waters, K. E. (2018). The effect of superstructure on the zeta potential, xanthate adsorption, and flotation response of pyrrhotite. *Colloids and Surfaces A: Physicochemical and Engineering Aspects*, *551*(April), 108–116. https://doi.org/10.1016/j.colsurfa.2018.04.057

Nagaoka, T., Ohmura, N., & Saiki, H. (1999). A novel mineral processing by flotation using Thiobacillus ferrooxidans. *Applied and Environmental Microbiology*, *65*(8), 3588–3593. https://doi.org/10.1016/S1572-4409(99)80123-0

Nagaraj, D. R., & Ravishankar, S. A. (2007). Flotation reagents - a critical reviewfrom an industry perspective. In M. C. Fuerstenau (Ed.), *Froth flotation: A century of innovation* (pp. 375–423). SME.

Nakai, I., Sugitani, Y., Nagashima, K., & Niwa, Y. (1978). X-ray photoelectron spectroscopic study of copper minerals. *Journal of Inorganic and Nuclear Chemistry*, *40*(5), 789–791. https://doi.org/10.1016/0022-1902(78)80152-3

Nesbitt, H. W., Legrand, D., & Bancroft, G. M. (2000). Interpretation of Ni2p XPS spectra of Ni conductors and Ni insulators. *Physics and Chemistry of Minerals*, *27*, 357–366. https://doi.org/10.1007/s002690050265

Nesbitt, H. W., & Reinke, M. (1999). Properties of As and S at NiAs, NiS, and Fe(1-X)S surfaces, and reactivity of niccolite in air and water. *American Mineralogist*, *84*, 639–649. https://doi.org/10.2138/am-1999-0417

Nesbitt, H. W., Scaini, M., Höchst, H., Bancroft, G. M., Schaufuss, A. G., & Szargan, R. (2000). Synchrotron XPS evidence for Fe2+-S and Fe3+-S surface species on pyrite fracture-surfaces, and their 3D electronic states. *American Mineralogist*, *85*(5–6), 850–857. https://doi.org/10.2138/am-2000-5-628

Nesbitt, H. W., Schaufuss, A. G., Scaini, M., Bancroft, G. M., & Szargan, R. (2001). XPS measurement of fivefold and sixfold coordinated sulfur in pyrrhotites and evidence for millerite and pyrrhotite surface species. *American Mineralogist*, *86*, 318–326. https://doi.org/10.2138/am-2001-2-315

Neumann, G. W., & Schnarr, J. R. (1971). Concentrator Operation at Brunswick Mining and Smelting Corporation's No. 2 Mine. *C.I.M. Bulletin*, *Sept. Ed.*, 51.

Nicol, M. J. (1984). An electrochemical study of hte interaction of Cu (II) ions with sulphide minerals. In P. E. Richardson, S. Srinivan, & R. Woods (Eds.), *Proceedings of the International Symposium on Electrochemistry in Mineral and Metal Processing* (pp. 152–168). Electrochemical Society.

Nyamekye, G. A. (1993). *Adsorption of dextrin onto sulphide minerals and its effect on the differential flotation of the inco matte*. The University of British Columbia.

Nyamekye, G. A., & Laskowski, J. S. (1993). Adsorption and electrokinetic studies on the dextrin-sulfide mineral interactions. *Journal of Colloid And Interface Science*, *157*(1), 160–

167. https://doi.org/10.1006/jcis.1993.1171

Nyamekye, G. A., & Laskowski, J. S. (1991). The differential flotation of INCO matte with the use of polysaccharides. In G. S. Dobby, S. A. Argyropoulos, & S. R. Rao (Eds.), *Copper '91 Int. Symp vol.2* (pp. 231–243). Pergamon.

Paul, S., Paul, D., Basova, T., & Ray, A. K. (2008). Studies of adsorption and viscoelastic properties of proteins onto liquid crystal phthalocyanine surface using quartz crystal microbalance with dissipation technique. *Journal of Physical Chemistry C*, *112*(31), 11822–11830. https://doi.org/10.1021/jp800975t

Perkampus, H.-H. (1992). *UV-VIS Spectroscopy and Its Application* (H. C. Grinter & T. L. Threlfall (eds.)). Springer Berlin Heidelberg.

Pohlandt, C., Cook, E. B. T., & Steele, T. W. (1969). Determination of small quantities of xanthate. *Talanta*, *16*, 1129–1135.

Pomianowski, A., & Leja, J. (1963). SPECTROPHOTOMETRIC STUDY OF XANTHATE AND DIXANTHOGEN SOLUTIONS. *Canadian Journal of Chemistry*, *41*, 2219–2230. https://doi.org/10.1139/v63-322

Power, R. F. (2003). Enzymatic conversion of starch to fermentable sugars. In K. A. Jacques, T. P. Lyons, & D. R. Kelsall (Eds.), *The Alcohol Textbook: A reference for the beverage, fuel and industrial alcohol industries* (4th ed., pp. 23–32). Nottingham University Press.

Pradip. (1988). On the interpretation of electrokinetic behavior of chemisorbing surfactant systems. *Trans. Indian Institute of Metals*, *41*(1), 15–25.

Pradip, Premachandran, R. S., & Malghan, S. G. (1994). Electrokinetic behaviour and dispersion characteristics of ceramic powders with cationic and anionic polyelectrolytes. *Bull. Mater. Sci.*, *17*(6), 911–920. https://doi.org/10.1016/0032-5910(93)02793-A

Pugh, R. J. (1989). Macromolecular organic depressants in sulphide flotation-A review, 1. Principles, types and applications. *International Journal of Mineral Processing*, *25*, 101–130. https://doi.org/10.1016/0301-7516(89)90059-8

Qi, C., Khalkhali, M., Grundy, J. S., Liu, J., Malainey, J., & Liu, Q. (2019). Unraveling Polymorphic Pyrrhotite Electrochemical Oxidation by Underlying Electronic Structures. *Journal of Physical Chemistry C*, *123*(43), 26442–26449. https://doi.org/10.1021/acs.jpcc.9b08005

Qi, C., Liu, J., Malainey, J., Kormos, L. J., Coffin, J., Deredin, C., Liu, Q., & Fragomeni, D. (2019). The role of Cu ion activation and surface oxidation for polymorphic pyrrhotite flotation performance in Strathcona Mill. *Minerals Engineering*, *134*(November 2018), 87–96. https://doi.org/10.1016/j.mineng.2019.01.025

Rajamani, R., & Prewitt, C. T. (1974). The Crystal Structure of Millerite. *Canadian Mineralogist*, *12*, 253–257.

Raju, G. B., Holmgren, A., & Forsling, W. (1997). Adsorption of dextrin at mineral/water interface. *Journal of Colloid and Interface Science*, *193*(2), 215–222. https://doi.org/10.1006/jcis.1997.5004

Rath, R. K., & Subramanian, S. (1999). Adsorption, electrokinetic and differential flotation studies on sphalerite and galena using dextrin. *International Journal of Mineral Processing*, *57*(4), 265–283. https://doi.org/10.1016/S0301-7516(99)00028-9

Rath, R. K., Subramanian, S., Sivanandam, V., & Pradeep, T. (2001). Studies on the interaction of guar gum with chalcopyrite. *Canadian Metallurgical Quarterly*, *40*(1), 1–12. https://doi.org/10.1179/cmq.2001.40.1.1

Rhodes, M. K. (1979). The effect of the physical variables of carboxymethyl cellulose reagents on the depression of magnesia bearing minerals in Western Australian nickel-sulfide ores. In J. S. Laskowski (Ed.), *Proceedings of the 13th International Mineral Processing Congress* (pp. 346–366). PWN-Elsevier.

Richardson, S., & Vaughan, D. J. (1989). Surface alteration of pentlandite and spectroscopic evidence for secondary violarite formation. *Mineralogical Magazine*, *53*(370), 213–222. https://doi.org/10.1180/minmag.1989.053.370.08

Rodahl, M., Höök, F., Fredriksson, C., Keller, C. A., Krozer, A., Brzezinski, P., Voinova, M., &

Kasemo, B. (1997). Simultaneous frequency and dissipation factor QCM measurements of biomolecular adsorption and cell adhesion. *Faraday Discussions*. https://doi.org/10.1039/a703137h

Rodahl, M., Höök, F., Krozer, A., Brzezinski, P., & Kasemo, B. (1995). Quartz crystal microbalance setup for frequency and Q-factor measurements in gaseous and liquid environments. *Review of Scientific Instruments*, *66*(7), 3924–3930. https://doi.org/10.1063/1.1145396

Rumball, J. A., & Richmond, G. D. (1996). Measurement of oxidation in a base metal flotation circuit by selective leaching with EDTA. *International Journal of Mineral Processing*, *48*, 1–20. https://doi.org/10.1016/s0301-7516(96)00010-5

Santhiya, D., Subramanian, S., & Natarajan, K. A. (2002). Surface chemical studies on sphalerite and galena using extracellular polysaccharides isolated from Bacillus polymyxa. *Journal of Colloid and Interface Science*, *256*, 237–248. https://doi.org/10.1006/jcis.2002.8681

Sauerbrey, G. (1959). Use of crystal oscillators for weighing thin films and for microweighing. *Zeitschrift Fuer Physik*, 206–222.

Sedeva, I. G., Fetzer, R., Fornasiero, D., Ralston, J., & Beattie, D. A. (2010). Adsorption of modified dextrins to a hydrophobic surface: QCM-D studies, AFM imaging, and dynamic contact angle measurements. *Journal of Colloid and Interface Science*, *345*(2), 417–426. https://doi.org/10.1016/j.jcis.2010.01.075

Senior, G. D., Shannon, L. K., & Trahar, W. J. (1994). The flotation of pentlandite from pyrrhotite with particular reference to the effects of particle size. *International Journal of Mineral Processing*, *42*(3–4), 169–190. https://doi.org/10.1016/0301-7516(94)00031-X

Shackleton, N. J., Malysiak, V., & O'Connor, C. T. (2003). The use of amine complexes in managing inadvertent activation of pyroxene in a pentlandite-pyroxene flotation system. *Minerals Engineering*, *16*(9), 849–856. https://doi.org/10.1016/S0892-6875(03)00215-2

Shea, D., & Helz, G. R. (1989). Solubility product constants of covellite and a poorly crystalline copper sulfide precipitate at 298 K. *Geochimica et Cosmochimica Acta*, *53*(2), 229–236.

https://doi.org/10.1016/0016-7037(89)90375-X

Sheikh, N., & Leja, J. (1974). Precipitation and stability of copper ethyl xanthate in hot acid and alkaline solutions. *Journal of Colloid And Interface Science*, *47*(2), 300–308. https://doi.org/10.1016/0021-9797(74)90261-6

Shen, W. Z., Fornasiero, D., & Ralston, J. (2001). Flotation of sphalerite and pyrite in the presence of sodium sulfite. *International Journal of Mineral Processing*, *63*(1), 17–28. https://doi.org/10.1016/S0301-7516(00)00067-3

Shombe, G. B., Khan, M. D., Zequine, C., Zhao, C., Gupta, R. K., & Revaprasadu, N. (2020). Direct solvent free synthesis of bare α-NiS, β-NiS and α-β-NiS composite as excellent electrocatalysts: Effect of self-capping on supercapacitance and overall water splitting activity. *Scientific Reports*, *10*, 1–14. https://doi.org/10.1038/s41598-020-59714-9

Shrimali, K., Yin, X., Wang, X., & Miller, J. D. (2017). Fundamental issues on the influence of starch in amine adsorption by quartz. *Colloids and Surfaces A: Physicochemical and Engineering Aspects*, *522*, 642–651. https://doi.org/10.1016/j.colsurfa.2017.03.031

Singh, A. K. (2016). Experimental Methodologies for the Characterization of Nanoparticles. In *Engineered Nanoparticles* (pp. 125–170). Academic Press, Elsevier. https://doi.org/10.1016/b978-0-12-801406-6.00004-2

Smart, R. S. C., Amarantidis, J., Skinner, W. M., Prestidge, C. A., La Vanier, L., & Grano, S. R. (2003). Surface Analytical Studies of Oxidation and Collector Adsorption in Sulfide Mineral Flotation. *Solid-Liquid Interfaces, Topics Appl. Phys.*, *85*, 3–62. https://doi.org/10.1007/3-540-44817-9_1

Smith, E. M., Nestola, F., Pasqualetto, L., Zorzi, F., Secco, L., & Wang, W. (2021). The new mineral crowningshieldite: A high-temperature NiS polymorph found in a type IIa diamond from the Letseng mine, Lesotho. *American Mineralogist*, *106*(2), 301–308. https://doi.org/10.2138/am-2020-7567

Smith, L. K., Senior, G. D., Bruckard, W. J., & Davey, K. J. (2011). The flotation of millerite - A single mineral study. *International Journal of Mineral Processing*, *99*, 27–31.

https://doi.org/10.1016/j.minpro.2011.02.004

Solari, J. A., Araujo, A. C. D., & Laskowski, J. S. (1986). The effect of carboxymethyl cellulose on the flotation and surface properties of graphite. *Coal Preparation*, *3*, 15–31. https://doi.org/10.1080/07349348608905271

Somasundaran, P. (1969). Adsorption of starch and oleate and interaction between them on calcite in aqueous solutions. *Journal of Colloid And Interface Science*, *31*(4), 557–565. https://doi.org/10.1016/0021-9797(69)90056-3

Sowa, H., Klein, H., & Raue, L. (2010). Determination of the orientation relations between the low- and high-temperature phases of NiS. *Solid State Phenomena*, *160*(2), 177–182. https://doi.org/10.4028/www.scientific.net/SSP.160.177

Sparrow, G., Pomianowski, A., & Leja, J. (1977). Soluble Copper Xanthate Complexes. *Separation Science*, *12*(1), 87–102. https://doi.org/10.1080/00372367708058066

Speight, J. (2005). 1.18. solubility and equilibrium constant. In *Lange's Handbook of Chemistry* (16th ed.). McGraw-Hill Education LLC.

Stamboliadis, E. (1978). *The surface chemistry of the flotation of millerite, pyrrhotite and pentlandite with dialkyl-dithiophosphates* [McGill University]. https://doi.org/10.1017/CBO9781107415324.004

Steenberg, E., & Harris, P. J. (1984). Adsorption of carboxymethyl cellulose, guar gum, and starch onto talc, sulfides, oxides, and salt-type mienrals. *S. Afr. J. Chem.*, *37*, 85–90.

Stevens, J. S., & Schroeder, S. L. M. (2009). Quantitative analysis of saccharides by X-ray photoelectron spectroscopy. *Surface and Interface Analysis*, *41*(6), 453–462. https://doi.org/10.1002/sia.3047

Subramanian, S., & Laskowski, J. S. (1993). Adsorption of Dextrin onto Graphite. *Langmuir*, *9*, 1330–1333. https://doi.org/10.1021/la00029a029

Subramanian, S., & Natarajan, K. A. (1988). Some studies on the adsorption behaviour of an

oxidised starch onto haematite. *Minerals Engineering*, *1*(3), 241–254. https://doi.org/10.1016/0892-6875(88)90046-5

Sun, X., Lu, Q., Boluk, Y., & Liu, Y. (2014). The impact of cellulose nanocrystals on the aggregation and initial adhesion of Pseudomonas fluorescens bacteria. *Soft Matter*, *10*(44), 8923–8931. https://doi.org/10.1039/c4sm00946k

Sun, Y., Wu, S., Xia, D. H., Xu, L., Wang, J., Song, S., Fan, H., Gao, Z., Zhang, J., Wu, Z., & Hu, W. (2018). Temperature dependence of passivity degradation on UNS N08800 in near neutral crevice chemistries containing thiosulphate. *Corrosion Science*, *140*(May), 260–271. https://doi.org/10.1016/j.corsci.2018.05.038

Swartz, W. E., Wynne, K. J., & Hercules, D. M. (1971). X-Ray Photoelectron Spectroscopic Investigation of Group VI-A Elements. *Analytical Chemistry*, *43*(13), 1884–1887. https://doi.org/10.1021/ac60307a044

Szargan, R., Karthe, S., & Suoninen, E. (1992). XPS studies of xanthate adsorption on pyrite. *Applied Surface Science*, *55*(4), 227–232. https://doi.org/10.1016/0169-4332(92)90173-U

Taffarel, S. R., & Rubio, J. (2009). On the removal of Mn2+ ions by adsorption onto natural and activated Chilean zeolites. *Minerals Engineering*, *22*(4), 336–343. https://doi.org/10.1016/j.mineng.2008.09.007

Tang, M., & Liu, Q. (2012). The acidity of caustic digested starch and its role in starch adsorption on mineral surfaces. *International Journal of Mineral Processing*, *112–113*, 94–100. https://doi.org/10.1016/j.minpro.2012.06.001

Teng, F., Liu, Q., & Zeng, H. (2012). In situ kinetic study of zinc sulfide activation using a quartz crystal microbalance with dissipation (QCM-D). *Journal of Colloid and Interface Science*, *368*(1), 512–520. https://doi.org/10.1016/j.jcis.2011.10.048

Thompson, M., & Walsh, J. N. (1989). *Handbook of Inductively Coupled plasma spectrometry* (2nd ed.). Champan and Hall. https://doi.org/10.1017/CBO9781107415324.004

Tukel, C., & Kelebek, S. (2010). Modulation of xanthate action by sulphite ions in pyrrhotite

deactivation/depression. *International Journal of Mineral Processing*, *95*(1–4), 47–52. https://doi.org/10.1016/j.minpro.2010.04.001

Voigt, S., Szargan, R., & Suoninen, E. (1994). Interaction of copper(II) ions with pyrite and its influence on ethyl xanthate adsorption. *Surface and Interface Analysis*, *21*(8), 526–536. https://doi.org/10.1002/sia.740210804

Voinova, M. V, Rodahl, M., Jonson, M., & Kasemo, B. (1999). Viscoelastic Acoustic Response of Layered Polymer Films at Fluid-Solid Interfaces: Continuum Mechanics Approach. *Physica Scripta*, *59*(5), 391–396. https://doi.org/10.1238/physica.regular.059a00391

Wang, C., Liu, R., Ahmed Khoso, S., Lu, H., Sun, W., Ni, Z., & Lyu, F. (2020). Combined inhibitory effect of calcium hypochlorite and dextrin on flotation behavior of pyrite and galena sulphides. *Minerals Engineering*, *150*(September 2019), 106274. https://doi.org/10.1016/j.mineng.2020.106274

Wang, D., & Hu, Y. (1987). Appendix 1. In *浮选溶液化学 (Solution Chemistry of Flotation)* (p. 345). Hunan Science & Technology Press Co., Ltd.

Wang, J., & Guo, X. (2020). Adsorption isotherm models: Classification, physical meaning, application and solving method. *Chemosphere*, *258*. https://doi.org/10.1016/j.chemosphere.2020.127279

Wang, X., Forssberg, E., & Bolin, N. J. (1989a). The Aqueous and Surface Chemistry of Activation in the Flotation of Sulphide Minerals—A Review. Part I: An Electrochemical Model. *Mineral Processing and Extractive Metallurgy Review*, *4*(3–4), 135–165. https://doi.org/10.1080/08827508908952635

Wang, X., Forssberg, E., & Bolin, N. J. (1989b). The Aqueous and Surface Chemistry of Activation in the Flotation of Sulphide Minerals—A Review. Part II: A Surface Precipitation Model. *Mineral Processing and Extractive Metallurgy Review*, *4*(3–4), 167–199. https://doi.org/10.1080/08827508908952636

Wang, X. H., & Forssberg, K. S. E. (1996). The solution electrochemistry of sulfide-xanthate-

cyanide systems in sulfide mineral flotation. *Minerals Engineering*, *9*(5), 527–546. https://doi.org/10.1016/0892-6875(96)00041-6

Weisener, C., & Gerson, A. (2000a). Cu(II) adsorption mechanism on pyrite: An XAFS and XPS study. *Surface and Interface Analysis*, *30*(1), 454–458. https://doi.org/10.1002/1096-9918(200008)30:1<454::AID-SIA807>3.0.CO;2-1

Weisener, C., & Gerson, A. (2000b). Investigation of the Cu(II) adsorption mechanism on pyrite by ARXPS and SIMS. *Minerals Engineering*, *13*(13), 1329–1340. https://doi.org/10.1016/S0892-6875(00)00116-3

Weissenborn, P. K., Warren, L. J., & Dunn, J. G. (1995). Selective flocculation of ultrafine iron ore. 1. Mechanism of adsorption of starch onto hematite. *Colloids and Surfaces A: Physicochemical and Engineering Aspects*, *99*, 11–27. http://linkinghub.elsevier.com/retrieve/pii/0927775795033548

Wie, J. M., & Fuerstenau, D. W. (1974). The effect of dextrin on surface properties and the flotation of molybdenite. *International Journal of Mineral Processing*, *1*, 17–32.

Wills, B. A., & Finch, J. A. (2016). Froth Flotation. In *Wills' Mineral Processing Technology* (8th ed., pp. 265–380). Butterworth-Heinemann, Oxford, UK. https://doi.org/10.1016/b978-0-08-097053-0.00012-1

Xu, M., Ford, F. D., Dai, Z., Lawson, V., Mill, C., & Cliff, C. (2011). Millerite and Its Impact on Cu / Ni Separation. *43rd Annual Meeting of the Canadian Mineral Processors*, *January 2011*, 319–330.

Yang, Bingqiao, Wang, D., Wang, T., Zhang, H., Jia, F., & Song, S. (2019). Effect of Cu2+ and Fe3+ on the depression of molybdenite in flotation. *Minerals Engineering*, *130*(August 2018), 101–109. https://doi.org/10.1016/j.mineng.2018.10.012

Yang, Bo, Tong, X., Deng, Z., & Lv, X. (2016). The adsorption of Cu species onto pyrite surface and its effect on pyrite flotation. *Journal of Chemistry*, *2016*, 2–9. https://doi.org/10.1155/2016/4627929

Yin, Q., Vaughan, D. J., England, K. E. R., Kelsall, G. H., & Brandon, N. P. (2000). Surface Oxidation of Chalcopyrite (CuFeS[sub 2]) in Alkaline Solutions. *Journal of The Electrochemical Society*, *147*(8), 2945–2951. https://doi.org/10.1149/1.1393629

Yuan, D., Cadien, K., Liu, Q., & Zeng, H. (2019). Adsorption characteristics and mechanisms of O-Carboxymethyl chitosan on chalcopyrite and molybdenite. *Journal of Colloid and Interface Science*, *552*, 659–670. https://doi.org/10.1016/j.jcis.2019.05.023

Zhang, M. (2015). *Investigation of Chalcopyrite and Pyrite Flotation in High Salinity Water*. University of Alberta.

Zhao, H. R. (2019). *Fundamental Studies of the Surface Properties of Millerite under Different Pulp Potentials and Water Chemistry*. Unviersity of Alberta.

Appendix A: Dextrin Characterization Data

A.1 Molecular weight distribution of dextrin

The molecular weight distribution of dextrin was characterized by Gel Permeation Chromatography (GPC, Agilent Technologies, 1260 Infinity). For the analysis, 1000 ppm dextrin was prepared using 0.2 M sodium nitrate solution. Two GPC columns (TKS gel G6000PW XL-CP) were connected in series for higher resolution. Prior to the test, the GPC was calibrated using polyethylene oxide (PEO) standards provided by Agilent Technologies. An aqueous solution of 0.2 M sodium nitrate was used as the mobile phase for the analyses. The calibration data is shown in Figure A1, where the log of the molecular weights of the PEO standards was plotted against the corresponding retention times of peak maximum.

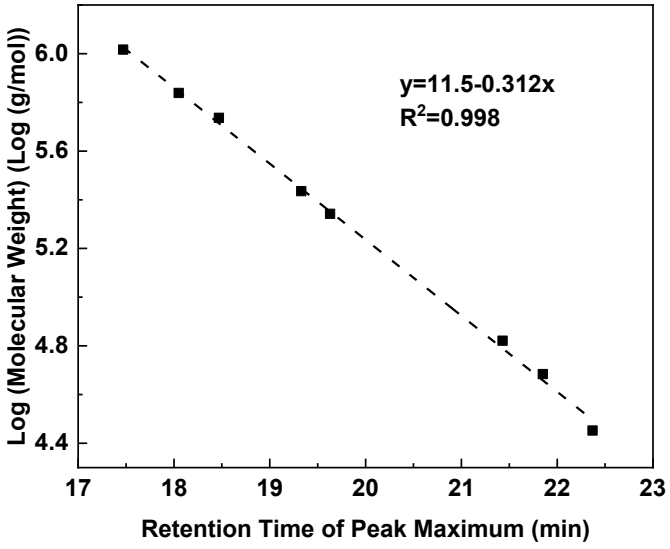

Figure A1. GPC calibration curve using PEO standards.

A.2 Diffuse reflectance infrared Fourier transform (DRIFT) spectrum of dextrin

Diffuse reflectance infrared Fourier transform (DRIFT) spectrum was used to identify dextrin's structure. The DRIFT spectrum of dextrin was obtained by Fourier Transform Infrared (FTIR) spectrometer (Agilent Technologies, Cary 670) with a number of scans of 32 and a resolution of 2 cm^{-1}. To acquire the dextrin's spectrum, dextrin powder was mixed with potassium bromide (KBr) in a mass ratio of 1 to 10. The spectrum was obtained by subtracting the background of pure KBr powder.

A.3 Zeta potential of dextrin as a function of pH

Figure A2 shows the zeta potential of 1000 ppm colloidal dextrin as a function of pH.

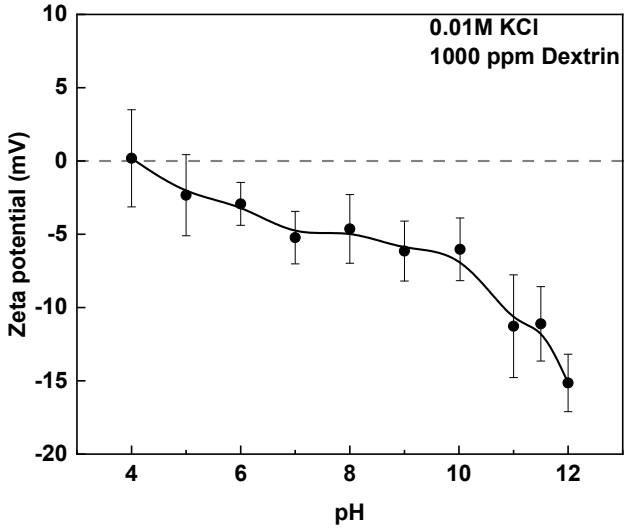

Figure A2. Zeta potential of 1000 ppm dextrin as a function of pH.

Appendix B: Detailed Peak Parameters for XPS Analysis

Detailed peak parameters for XPS analysis in Chapter 4, including binding energy, full width at half maximum (FWHM), and the corresponding chemical state (peak assignment) for each peak are shown in

Table B1 to Table B3, and the corresponding fitted spectra are shown in Figure 4.3, Figure 4.7 and Figure 4.8.

Table B1. Detailed peak parameters for XPS C 1s and O 1s spectra of dextrin.

Peak	Binding Energy (eV)	FWHM (eV)	Peak Assignment
C 1s	284.8	1.0	C-C
C 1s	286.3	1.1	C-O
C 1s	287.7	1.1	O-C-O
O 1s	532.46	1.3	C-O
O 1s	533.2	1.3	O-C-O

Table B2. Detailed peak parameters for XPS C 1s and O 1s spectra of chalcopyrite.

Peak	Cp Baseline		Cp + 10 ppm dextrin		Cp + 10^{-4} M KEX + 10 ppm dextrin		Peak Assignment
	Binding Energy (eV)	FWHM (eV)	Binding Energy (eV)	FWHM (eV)	Binding Energy (eV)	FWHM (eV)	
C 1s	284.8	1.4	284.8	1.4	284.8	1.3	C-C
C 1s	286.3	1.4	286.3	1.4	286.3	1.3	C-O
C 1s	-	-	287.7	1.4	-	-	O-C-O
C 1s	288.4	2.5	288.7	2.5	288.4	2.5	O-C=O
O 1s	529.9	1.2	530	1.2	530.1	1.2	Oxide
O 1s	531.6	1.9	531.5	1.9	531.9	1.9	Hydroxide
O 1s	-	-	532.7	1.4	-	-	C-O
O 1s	533.0	1.8	533.0	1.7	533.0	1.8	Adsorbed Water
O 1s	-	-	533.5	1.4	-	-	O-C-O

Table B3. Detailed peak parameters for XPS C 1s, O 1s and Ni 2p $_{3/2}$ spectra of millerite and $Ni(OH)_2$ – dextrin complex.

Peak	Mi Baseline		Mi + 10 ppm dextrin		Mi + 10^{-4} M KEX + 10 ppm dextrin		Ni(OH)2 – dextrin complex		Peak Assignment
	B.E. (eV)	FWHM (eV)	B.E. (eV)	FWHM (eV)	B.E. (eV)	FWHM (eV)	B.E. (eV)	FWHM (eV)	
C 1s	284.8	1.2	284.8	1.4	284.8	1.3	284.8	1.4	C-C
C 1s	286.3	1.2	286.4	1.1	286.4	1.1	286.4	1.4	C-O
C 1s	-	-	287.8	1.4	287.6	1.3	287.7	1.4	O-C-O
C 1s	288.4	2.2	288.7	2.2	288.7	2.0	288.7	2.2	O-C=O
O 1s	531.2	1.5	531.1	1.5	531.3	1.5	531.0	1.4	$Ni(OH)_2$
O 1s	532.0	1.7	532	1.6	532	1.7	-	-	$SO4^{2-}$
O 1s	-	-	532.7	1.5	532.7	1.4	532.7	1.6	C-O
O 1s	533.0	2.0	-	-	-	-	-	-	Adsorbed water
O 1s	-	-	533.5	1.3	533.5	1.4	533.5	1.6	O-C-O

Ni $2p_{3/2}$	853.1	1.2	853.1	1.2	853.1	1.2	-	-	NiS
Ni $2p_{3/2}$	859.7	3.5	859.7	3.5	859.7	3.5	-	-	NiS satellite
Ni $2p_{3/2}$	855.4	1.9	855.5	2.1	855.5	2.1	855.8	2.6	$Ni(OH)_2$
Ni $2p_{3/2}$	860.6	3.5	860.7	3.9	860.7	3.9	861.2	3.5	$Ni(OH)_2$ satellite
Ni $2p_{3/2}$	856.5	1.7	856.4	1.7	856.5	1.7	-	-	NiS_2O_3
Ni $2p_{3/2}$	862.1	3.3	862.0	3.4	862.1	3.4	-	-	NiS_2O_3 satellite
Ni $2p_{3/2}$	857.7	1.7	857.4	1.7	857.7	1.6	-	-	$NiSO_4$
Ni $2p_{3/2}$	863.3	3.4	863.0	3.4	863.3	3.2	-	-	$NiSO_4$ satellite

Appendix C: Mineral Characterization Data

C.1 Bulk Mineral Surface Characterization by SEM

Bulk millerite and chalcopyrite samples used in this study were from the same batch as the grounded mineral particles. The purities of the bulk mineral samples were determined using scanning electron microscopy (SEM) coupled with energy dispersive X-ray spectroscopy (EDS) analysis. Back-scattered electron (BSE) detector was utilized to observe any contrast in a grayscale SEM images in order to examine the sample purity. A Quanta 250 scanning electron microscope (FEI, USA) was used.

Figure C1and Figure C2 show both the SEM and BSE images of bulk millerite and chalcopyrite surface under different magnifications. Both samples had negligible impurities as no obvious contrast was observed in the BSE images. EDS analysis were conducted at three different spots on the mineral surface to obtain the average elemental composition. Table C1 shows the average elemental composition of the millerite and chalcopyrite samples. Millerite contains 62.43 wt% Ni with insignificant amounts of Cu and Fe as impurities, while chalcopyrite contains 34.1 wt% Cu and 31.7 wt% Fe with insignificant amounts of Ni and Zn as impurities. The EDS results were similar to the XRF analysis on the powder samples.

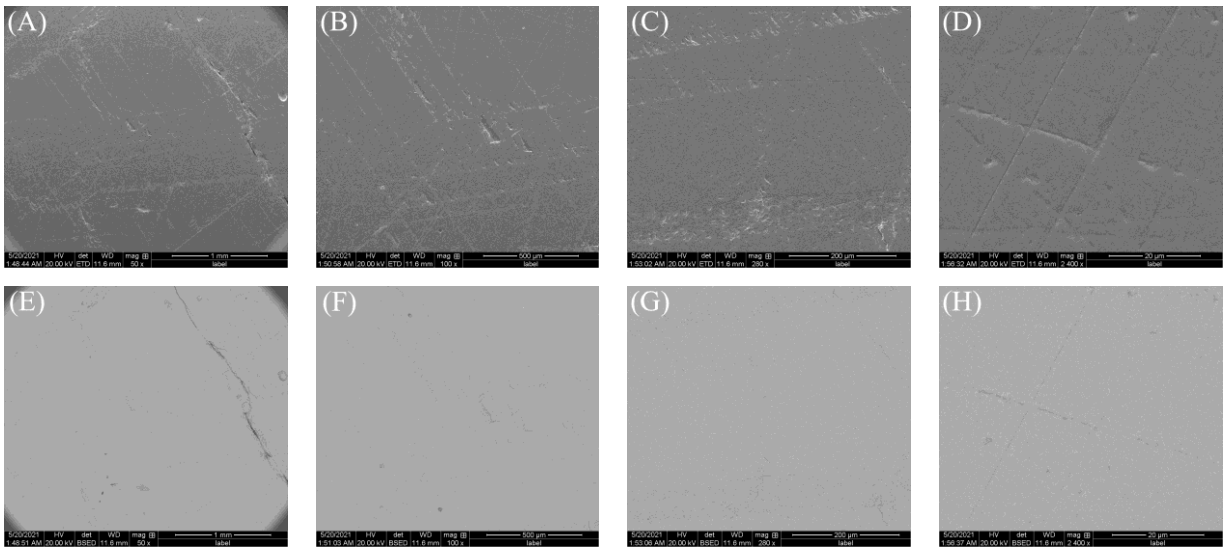

Figure C1. SEM and the corresponding BSE images of bulk chalcopyrite surface under 50× (A, E), 100× (B, F), 280× (C, G) and 2400× (D, H) magnifications; top – SEM images, bottom – BSE images.

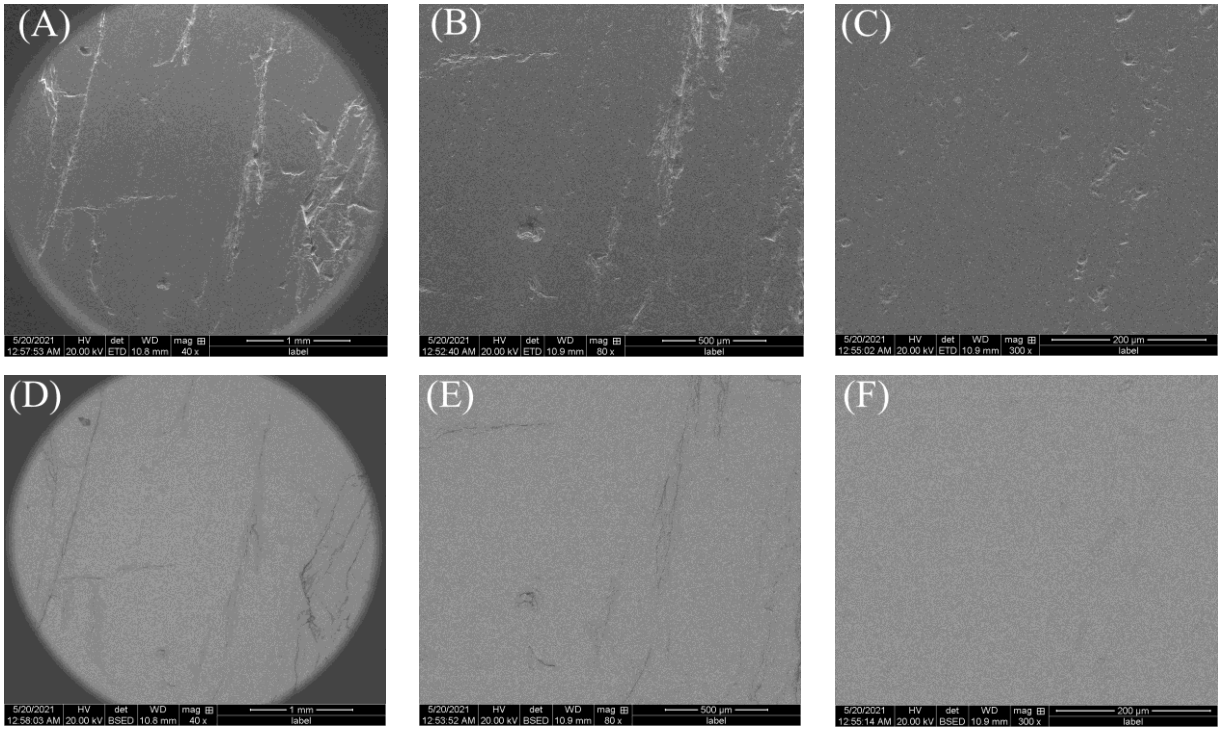

Figure C2. SEM and the corresponding BSE images of bulk chalcopyrite surface under 40× (A, D), 80× (B, E) and 300× (C, F) magnifications; top – SEM images, bottom – BSE images.

Table C1. Elemental composition of bulk millerite and chalcopyrite samples by EDS analysis.

Element	Composition (wt%)				
	S	Fe	Ni	Cu	Zn
Millerite	36.9	0.24	62.4	0.45	-
Chalcopyrite	33.9	31.7	0.06	34.1	0.23

C.2 Millerite QCM-D Sensor Characterization

The quartz crystal sensor coated with millerite (QSX999, Q-Sense) was characterized by XPS (PHI5000 VersaProbe III Scanning XPS Microprobe) by Biolin Scientific. The data was displayed here with the permission of Biolin Scientific. The binding energy was calibrated using C 1s at 285.0 eV as the reference. Argon ion sputtering was used to remove surface oxidation and contaminants, the etch rate is approximately 2.5 nm per minute. Figure C3 Shows the Ni 2p and S 2p narrow scans of the upmost sensor surface and the sensor surface after 5 nm and 10 nm etchings. Based on the XPS narrow scans, after ion etching, the Ni 2p3/2 peak at 852.8 eV and the S 2p doublet at 161.9 eV featured bulk nickel monosulphide. Table C2 shows the atomic concentrations of elements of the upmost surface millerite sensor, millerite sensor surface after 5 nm ion etching and 10 nm ion etching based on the XPS survey scans. With a 34.2% O and only 9.8% S, the upmost surface was oxidized, and the detection of C might be due to the adventitious carbon. As nitrogen gas was used to fill the container when the sample was sent to Q-sense, nitrogen was also detected. For the etched surface, the oxygen, nitrogen and carbon content dropped significantly. After 10 nm ion etching, the atomic ratio of Ni to S was 1.18, which was close to unity.

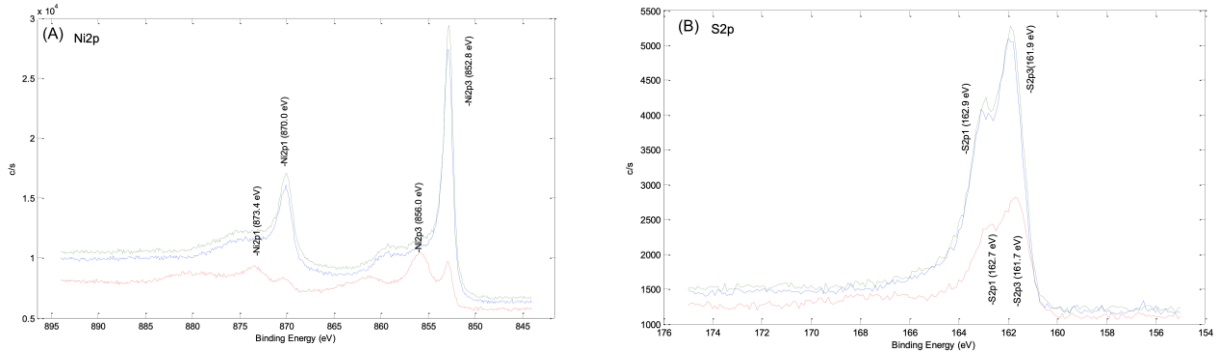

Figure C3. High resolution scans of (A) Ni 2p and (B) S 2p of (i) the upmost surface of NiS sensor (red), (ii) the NiS sensor after 5 nm ion etching (blue) and (iii) the NiS sensor after 10 nm ion etching (green).

Table C2. Atomic concentrations of elements of the NiS sensor on the upmost surface and on the etched surface by XPS.

	Atomic Concentration (%)				
	Ni	O	N	C	S
Upmost surface	15.8	34.2	15.8	31.0	9.8
5 nm ion etching	43.6	4.6	7.5	5.8	38.5
10 nm ion etching	44.5	7.6	10.2	-	37.7

Appendix D: Sample Calibration Curves for Adsorption Tests

The calibration of UV-Vis spectrophotometer was conducted using a series of dextrin and KEX samples with known concentrations. A calibration curve was always acquired for each series of measurements. Figure D1 shows the sample calibration curves for both dextrin and KEX solutions, a linear relationship was obtained between the absorbance and the sample concentrations, which can be used to calculate the residual concentrations of dextrin or KEX based on the measured absorbance.

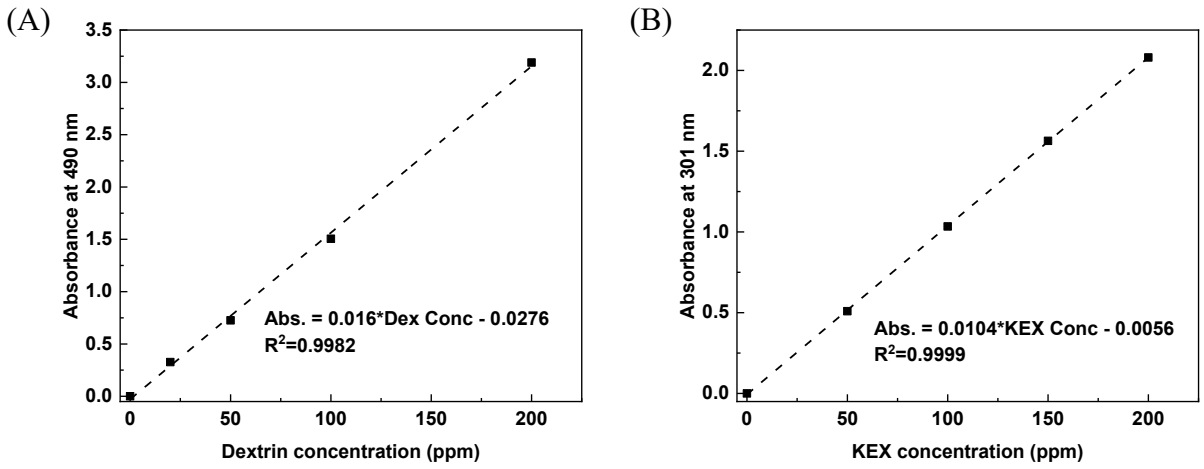

Figure D1. Sample calibration curves for (A) dextrin solution and (B) KEX solution.

Appendix E: Ultrasonication Treatment of Mineral Samples

Ultrasonication was found to be an effective physical method to reduce surface oxidation (Clarke et al., 1995). In this research, ultrasonication was used in mineral sample preparation and various tests to reduce surface oxidation. An ultrasonic bath was used for the sonication process. In order to verify whether sonication can reduce surface oxidation, an air-oxidized millerite sample (exposed to air for over 1 year in the fridge) was sonicated in the ultrasonic batch for 5 minutes and was sent for XPS analysis to examine the surface species and compared with the untreated oxidized sample. Figure E1 shows the high-resolution scans of S 2p of untreated and sonicated samples. The air-oxidized millerite showed significant proportions of polysulphide and sulfate, indicating a severe oxidation on millerite surface. After the 5 minutes sonication, the sonicated sample contained less sulfate and polysulphide while more bulk and surface monosulphide were observed, indicating that the surface became less oxidized after the ultrasonication treatment.

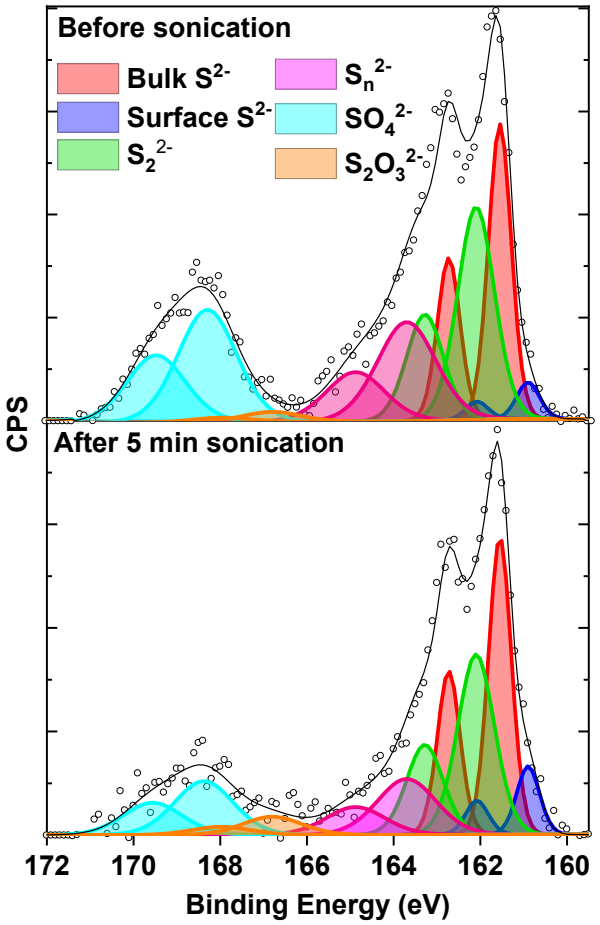

Figure E1. XPS S 2p spectra of oxidized millerite sample before and after 5 minutes sonication treatment.